Development and application of mass-spectrometric methods for the quantification and characterization of organic compounds in ice cores

Dissertation

zur Erlangung des Grades

„Doktor der Naturwissenschaften"

im Promotionsfach Chemie

am Fachbereich Chemie, Pharmazie und Geowissenschaften

der Johannes Gutenberg-Universität Mainz

vorgelegt von

Christina Müller-Tautges

geboren in Prüm

Mainz, 2014

Dekan:

1. Gutachter:
2. Gutachter:

Tag der mündlichen Prüfung: 12.09.2014

Darin besteht das Wesen der Wissenschaft. Zuerst denkt man an etwas, das wahr sein könnte.

Dann sieht man nach, ob es der Fall ist und im Allgemeinen ist es nicht der Fall.

Bertrand Russell (1872-1970),

brit. Philosoph u. Mathematiker, 1950 Nobelpr. f. Lit.

ZUSAMMENFASSUNG

Um sowohl durch den Menschen verursachte als auch natürliche Umwelt- und Klimaveränderungen zu untersuchen, sind Informationen über die Zusammensetzung der Atmosphäre in der Vergangenheit unerlässlich. Verständnis vergangener Klimaänderungen kann zudem dazu beitragen, Modelle zur Vorhersage des Klimawandels zu erstellen und zu verbessern. Eisbohrkerne stellen in diesem Zusammenhang wertvolle Umweltarchive dar, da sie atmosphärisches Aerosol konservieren, welches mit dem Schneefall deponiert wird. Die Analyse chemischer Verbindungen als Bestandteil atmosphärischer Aerosole im Eis liefert somit wichtige Informationen über Umweltbedingungen und Klima der Vergangenheit. Gletscher aus Hochgebirgsregionen der gemäßigten Breiten, wie zum Beispiel den Alpen, dienen als Klimaarchive für regionale Klimaveränderungen und erlauben eine Rückverfolgung der chemischen Verbindungen in der Atmosphäre über mehrere Dekaden bis einige hundert Jahre. Neben der Untersuchung anorganischer Spurenstoffe gibt es bisher nur sehr wenige Studien, die sich mit der Analyse organischer Verbindungen in Eisbohrkernen befassen. Diese spielen jedoch eine wichtige Rolle als Bestandteil von sekundärem organischem Aerosol (SOA), welches einen Großteil des atmosphärischen Aerosols darstellt. In diesem Zusammenhang wichtige organische Substanzklassen sind z. B. α-Dicarbonyle, die eine Rolle bei Bildung und Wachstum von SOA-Partikeln spielen, sowie Dicarbonsäuren, die als ubiquitäre Verbindungen in der Atmosphäre maßgeblich zur SOA-Masse beitragen.

Um die α-Dicarbonyle Glyoxal (G) und Methylglyoxal (MG) in Eis- und Schneeproben zu untersuchen, wurde eine neue, sensitive Methode entwickelt, bei der die *Stir Bar Sorptive Extraction* (SBSE) mit anschließender Flüssigkeitsdesorption (*liquid desorption*, LD) zum Einsatz kommt. Hierbei werden Extraktion, Anreicherung und Derivatisierung des Analyten simultan durchgeführt. Eine Derivatisierung der Analyten mittels *O*-Benzylhydroxylamin ermöglicht eine effiziente Extraktion und verbessert zudem die chromatographischen Eigenschaften und die Ionisierbarkeit. Die hochselektiven Messungen der resultierenden Analyt-Derivate wurden unter Anwendung von Hochleistungs-Flüssigchromatographie gekoppelt mit Elektrospray Tandem Massenspektrometrie (HPLC-ESI-MS/MS) durchgeführt. Im Rahmen der Methodenentwicklung wurden Parameter wie z.B. Extraktionszeit, Derivatisierungsmittel, Desorptionszeit und -lösungsmittel, der Effekt von NaCl Zugabe auf den Extraktionsprozess sowie Messparameter des HPLC-ESI-MS Systems optimiert. Die Kalibrierung erfolgte mit Hilfe von dotierten Reinstwasserproben und umfasste somit die gesamte Probenaufarbeitung. Die zu Beginn der Methodenentwicklung sehr hohen Hintergrundwerte konnten durch Aufreinigung des Derivatisierungsmittels mit Festphasenextraktion (*solid phase extraction*, SPE) und Ausheizen aller verwendeten Glasgeräte vermindert werden, wodurch niedrige Nachweisgrenzen erzielt wurden. Die optimierte Methode wurde zunächst zur Analyse von Schneeproben aus Hohenpeißenberg (Bayern) sowie Eisbohrkernproben des oberen Grenzgletschers (Schweizer Alpen) angewendet. Die ermittelten Konzentrationen der α-Dicarbonyle in den Schneeproben lagen ein bis zwei Größenordnungen über denen der Eisbohrkernproben. Die beschriebene Methode stellt eine einfache, gegenüber anderen

Extraktionsverfahren ressourcenschonende und sensitive analytische Vorgehensweise zur Quantifizierung von Glyoxal und Methylglyoxal in wässrigen Proben wie Schnee und Eis dar.

Zur Analyse von Dicarbonsäuren in Eisbohrkernen wurde eine weitere Methode entwickelt. Hierfür wurde SPE mit starkem Anionenaustauscher als Sorbenz zur Extraktion und Anreicherung der organischen Säuren verwendet. Durch eine Derivatisierung der Analyten (Veresterung) konnten die chromatographischen Eigenschaften sowie die Ionisierbarkeit der Analyten verbessert werden. Die Methodenentwicklung umfasste neben der Optimierung des Derivatisierungsprozesses, in deren Verlauf u.a. Derivatisierungsmittel, -zeit und -temperatur variiert wurden, auch die sorgfältige Optimierung der chromatographischen Trennung und massenspektrometrischen Detektion. Die Methode erlaubt die Quantifizierung aliphatischer Dicarbonsäuren (≥ C6), einschließlich Pinsäure, und zeigte sich auch für die Analyse aromatischer Carbonsäuren (wie Phthalsäure und Vanillinsäure) geeignet. Dies ermöglicht die Bestimmung wichtiger Markerverbindungen für biogene und anthropogene Quellen sowie für Waldbrände.

Die entwickelten Methoden wurden zur Analyse eines Eisbohrkerns aus dem oberen Grenzgletscher in den südlichen Schweizer Alpen angewendet. Die ermittelten Konzentrationsverläufe der α-Dicarbonylverbindungen sowie Mono- und Dicarbonsäuren umfassen die Zeitspanne von 1942 bis 1993. Zusätzlich wurden Messungen mit Hilfe von Ionenchromatographie am Paul Scherrer Institut (PSI) in Villigen (Kanton Aargau, Schweiz) durchgeführt. Eine umfassende Korrelations- und Hauptkomponentenanalyse der ermittelten Konzentrationen zeigte, dass die im Eisbohrkern vorhandenen organischen Verbindungen hauptsächlich durch Waldbrände und durch vom Menschen verursachte Schadstoffemissionen beeinflusst werden. So repräsentieren die Konzentrationsverläufe verschiedener, hoch korrelierter Verbindungen, z.B. der Pinsäure und des Waldbrandmarkers *p*-Hydroxybenzoesäure, die zeitlichen Abfolgen von Waldbränden in der Südschweiz. Die Konzentrationsverläufe anderer Verbindungen (z.B. Phthalsäure und Adipinsäure) zeigen Ähnlichkeiten zum Verlauf der Emissionen flüchtiger organischer Verbindungen (*volatile organic compounds*, VOC), die von Industrie und Verkehr verursacht werden. Im Gegensatz dazu zeigen die Konzentrationen an Oxalsäure und Ameisensäure Korrelationen zur Calciumionenkonzentration, was den Schluss zulässt, dass diese kleinen Säuren in ihrem Konzentrationsverlauf vom Mineralstaubtransport auf den Gletscher beeinflusst werden. Zusätzlich zur Analyse bekannter organischer Verbindungen wurde ein Screening der Eisbohrkernproben zur Untersuchung ihrer Zusammensetzung mittels ultrahochauflösender Massenspektrometrie durchgeführt. Von über 800 detektierten Verbindungen konnten zu 409 Verbindungen über die exakte Masse Summenformeln mit einer Abweichung kleiner als 2,5 ppm zugeordnet werden. Der Vergleich mit Literaturdaten anhand der Verhältnisse der Anzahl an Kohlenstoffatomen zu Wasserstoff- und Sauerstoffatomen (*van Krevelen*-Diagramm) deutete darauf hin, dass es sich bei den ermittelten Verbindungen größtenteils um aliphatische Spezies handelt. Eine Abschätzung des Oxidationsgrades zeigte im Vergleich mit Literaturdaten, dass die meisten Verbindungen Ähnlichkeiten zu Verbindungen aus Waldbrand-Aerosol aufweisen. Demzufolge deuten auch die Ergebnisse der Screening-Untersuchung auf einen Zusammenhang zwischen dem Auftreten von Waldbränden und den im Eisbohrkern gefundenen organischen Verbindungen hin. Zum ersten Mal

wurden im Rahmen der Analyse auch Organosulfate (OS) und Nitrooxyorganosulfate (NOS) in einem Eisbohrkern identifiziert. Ein Beispiel sind die NOS *m/z* 294, welche bereits mehrfach in atmosphärischen Aerosolproben und anderen Umweltproben wie Regen oder Nebel beschrieben wurde. OS und NOS sind Bestandteile des anthropogen verstärkten biogenen SOA (*anthropogenic enhanced biogenic* SOA, ABSOA), welches aus SO_2 (meist anthropogen emittiert) und ausschließlich biogenen Emissionen (z.B. Isopren, Monoterpene) gebildet wird. Das Vorkommen von OS und NOS im Gletschereis zeigt daher abermals, dass die chemische Zusammensetzung der Spurenkomponenten im Eis sowohl durch anthropogene als auch biogene Einflüsse bestimmt wird. Mit Hilfe des Screenings der Eisbohrkernproben konnte somit gezeigt werden, dass die hochauflösende Massenspektrometrie eine extrem leistungsstarke analytische Technik darstellt, um komplexe Mischungen organischer Spurenkomponenten in Eis zu entschlüsseln.

ABSTRACT

To study the environmental and climatic changes caused by anthropogenic activity as well as naturally occurring changes, it is necessary to know the atmospheric conditions of the past. Knowledge on past climate changes can also help to build and improve models for the prediction of future climate change. Ice cores are valuable environmental archives, as they preserve atmospheric aerosol deposited with snowfall. Hence, the analysis of aerosol-related chemical compounds in the ice samples can give information on past environmental and climatic conditions. Glaciers from mid latitude mountain areas, such as the Alps, serve as climate archives for regional climate change, covering a time span of several decades to some hundred years. So far, only limited studies describe the analysis of organic species in ice cores. These compounds however play an important role as constituents of secondary organic aerosol (SOA), which is a major part of atmospheric aerosol. In this context, α-dicarbonyls and dicarboxylic acids constitute important compound classes, for example, with the former playing an important role in the formation and growth of SOA, the latter being a major contributor to SOA mass.

In order to investigate the α-dicarbonyls glyoxal and methylglyoxal in environmental ice and snow samples, a new sensitive method was developed. Stir bar sorptive extraction with in-situ derivatization and liquid desorption (SBSE-LD) was used for sample extraction, enrichment and derivatization. Measurements were carried out using high performance liquid chromatography coupled to electrospray ionization tandem mass spectrometry (HPLC-ESI-MS/MS). As part of the method development, SBSE-LD parameters such as extraction time, derivatization reagent, desorption time and solvent, the effect of NaCl addition on the SBSE efficiency as well as measurement parameters of HPLC-ESI-MS/MS were evaluated. Calibration was performed using spiked ultrapure water samples, thus incorporating the complete SBSE and derivatization process. After the successful reduction of blank values through purification of the derivatization reagent with solid phase extraction (SPE) and additional heat treatment of all glassware, low limits of detection were achieved. The optimized method was applied for the analysis of snow samples from Mount Hohenpeissenberg (Germany) and samples from an ice core from Upper Grenzgletscher (Monte Rosa massif, Switzerland). Resulting concentrations of α-dicarbonyls in snow were 1-2 orders of magnitude higher than in ice core samples. The described method represents a simple, green and sensitive analytical approach to measure glyoxal and methylglyoxal in aqueous environmental samples.

A second method was developed, targeting dicarboxylic acids in environmental ice samples. SPE with strong anion exchange was used for extraction and enrichment of the acids from the aqueous sample matrix. A derivatization step was employed using esterification to enhance performance of the analytes during chromatography and electrospray ionization. The method development comprised the optimization of the derivatization procedure, evaluating the derivatization reagent, time, and temperature, as well as the optimization of chromatographic separation and mass spectrometric detection. Low limits of detection were achieved for all analytes. The optimized method was found to be capable of analyzing aliphatic dicarboxylic acids (≥ C6), including pinic acid, as well as aromatic mono-

and dicarboxylic acids (e.g. vanillic and phthalic acids), thus enabling the determination of important biogenic, anthropogenic and biomass burning marker compounds.

Concentration records of α-dicarbonyls and (di)carboxylic acids covering the time period of 1942 to 1993 were obtained by applying both methods to a glacier ice core from upper Grenzgletscher in the southern Swiss Alps. Additional measurements of major ions using ion chromatography were performed at Paul Scherrer Institute (PSI) in Villigen, Switzerland. A comprehensive correlation and principal component analysis of the resulting concentration data revealed biomass burning and anthropogenic emissions to be the main parameters influencing the concentration of organic compounds present in the ice. Ice core records of several, highly correlated compounds (e.g. pinic acid and the biomass burning marker *p*-hydroxybenzoic acid) represent the changes in forest fires in southern Switzerland; other compounds (e.g. adipic and phthalic acids) represent anthropogenic emissions of volatile organic compounds (VOCs). In contrast to this observation, the small organic acids oxalic acid and formic acid are both correlated to calcium-ions, thus suggesting their records to be affected by changing mineral dust transport to the drilling site. In addition to the analysis of known organic marker compounds, a non-target screening of the samples from Grenzgletscher was performed using ultrahigh resolution mass spectrometry. More than 800 compounds were detected, 409 of which were assigned a molecular formula. Through the comparison with other studies concerning carbon hydrogen and carbon oxygen ratios (visualized in a *van-Krevelen* diagram), the organic compounds present in the ice core were suggested to be mainly aliphatic species. The evaluation of the carbon oxidation state in comparison to literature data revealed that most of the compounds exhibit properties similar to biomass burning organic aerosol. Thus, the connection of biomass burning to the organic compounds detected in the ice core was also supported by the non-target screening approach. For the first time, organosulfates and nitrooxy organosulfates were detected in ice core samples, for example the nitrooxy organosulfates with *m/z* 294, which have often been described in aerosol related environmental samples in the literature. This again reveals the aerosol transported to the glacier to be influenced by anthropogenic as well as biogenic sources, as (nitrooxy) organosulfates contribute to anthropogenic enhanced biogenic SOA (ABSOA), which is formed from SO_2 emissions (mostly anthropogenic) and exclusively biogenic emissions (e.g., isoprene and monoterpenes). The non-target screening of the Grenzgletscher sample demonstrated that high resolution mass spectrometry is an extremely powerful tool for the exploration of the complex mixture of organic species present in ice.

CONTENTS

1 INTRODUCTION

1.1 Atmospheric chemistry

1.1.1 Primary and secondary aerosols

An aerosol is defined as a suspension of liquid or solid particles in a gas. When using the term in an atmospheric context, it is usually referred to the particulate phase only, although by definition an aerosol consists of both gas phase and particle phase [*Seinfeld and Pandis*, 2006].

Aerosols play an important role in atmospheric chemistry due to their impact on the radiative budget of the earth's atmosphere. Aerosol particles can scatter or absorb the solar radiation (*direct effect*) or act as cloud condensation nuclei (CCN), influencing the radiative properties, amount, and lifetime of clouds (*indirect effect*).

Concerning the direct effect, most secondary aerosols lead to a reduced radiative forcing ("cooling"). This is because the diameter of the particles is in the range of the radiation's wavelength, resulting in a very efficient scattering of solar radiation. This effect is called *Whitehouse Effect* and occurs for example after volcanic eruptions, which cause the formation of a large number of secondary sulfuric acid particles. In contrast, a positive influence on the radiative forcing ("warming") is caused by particles containing black carbon, as they can absorb solar radiation due to their large absorption cross-section for this type of radiation.

The indirect effect of atmospheric aerosol can be further divided into the first and second indirect effect. The first indirect effect (also called cloud albedo effect) states, that a raised number concentration of aerosol particles, serving as CCN, causes an increase in cloud formation and therefore enhances albedo. Furthermore, a higher number of CCN leads to a reduced droplet size within the cloud, resulting in a prolonged cloud lifetime (*second indirect effect* or *cloud lifetime effect*) [*Lohmann and Feichter*, 2005; *Seinfeld and Pandis*, 2006].

The estimations on radiative forcing of aerosols and other atmospheric compounds by the Intergovernmental Panel on Climate Change are illustrated in Fig. 1.1. While the direct effects of different classes of aerosol can be attributed to the radiative forcing with a high level of confidence, the level of scientific understanding concerning the influence of aerosol-cloud interaction on the net radiative forcing is still considered to be low (IPCC, 2013a).

Depending on their way of emission into the atmosphere, a distinction is made between two types of aerosols: Primary aerosols consist of particles emitted directly into the atmosphere, such as dust, (biomass) combustion particles (from anthropogenic sources, i.e. combustion engines as well as natural sources, i.e. forest fires, see also section 1.1.5), volcanic ashes, pollen and other plant debris, and sea salt. Secondary aerosols, e.g. sulfuric acid aerosol or secondary organic aerosol (SOA), are formed in the atmosphere after the conversion of volatile gaseous precursors into less volatile species, which either condense on existing particles or form new particles in a nucleation event [*Kroll and Seinfeld*, 2008]. The decrease in volatility is caused by the oxidation of the gaseous compounds by OH radicals, nitrate radicals, or ozone present in the atmosphere (see [*Griffin et al.*, 2002] for possible chemical mechanisms). Volatile organic compounds (VOC) acting as precursors for SOA formation can be of biogenic as well as anthropogenic origin (e.g., terpenes and alkenes, respectively).
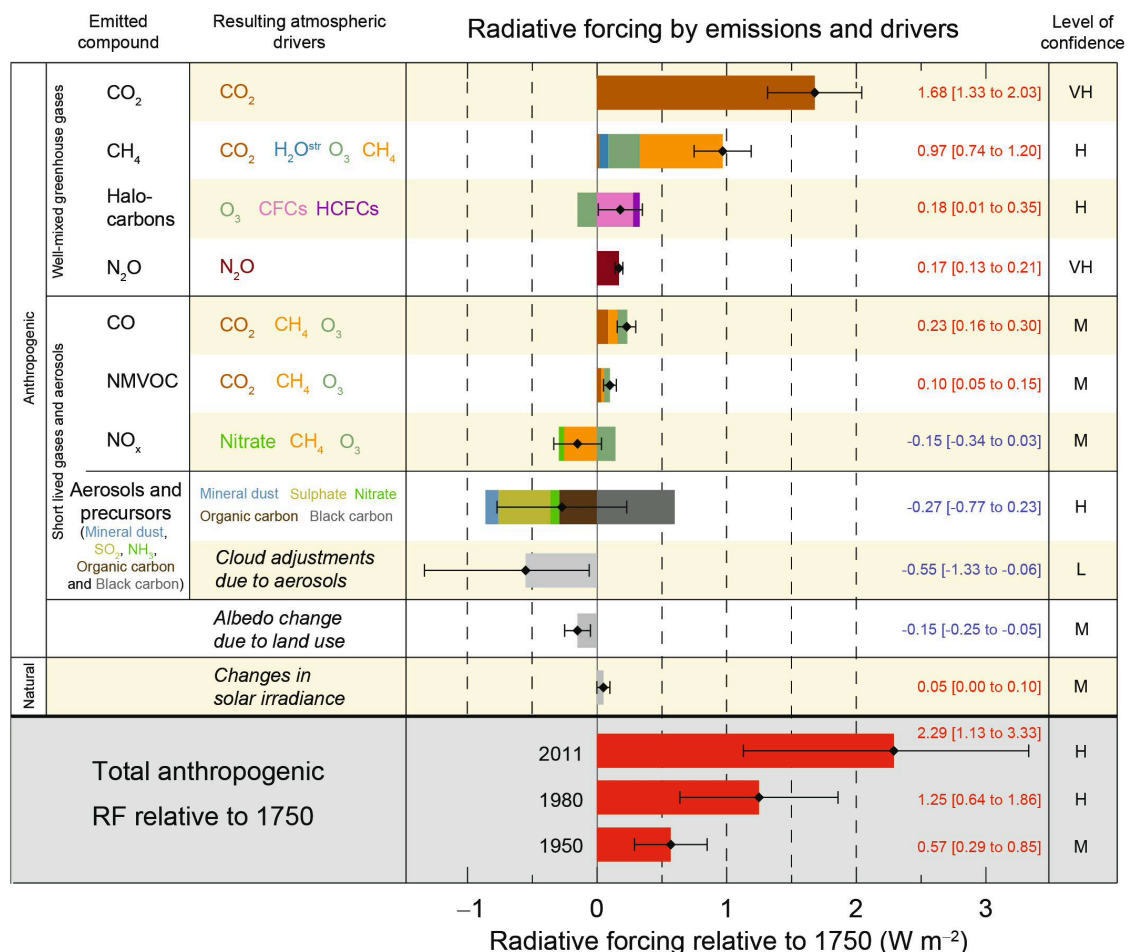

Fig. 1.1 Radiative forcing estimates in 2011 relative to 1750 and aggregated uncertainties for the main drivers of climate change (IPCC 2013a).

Recent studies suggest that SOA mass is not only increased by compounds formed by gas phase reactions but also by reactions in the aqueous phase (e.g. in cloud droplets or aqueous particles) [*Blando and Turpin*, 2000; *Ervens et al.*, 2011]. SOA can therefore be further divided into SOA consisting of compounds that partition into the (organic) particle phase after being formed in the gas phase (gasSOA) and SOA formed in cloud and aerosol water (aqSOA) [*Ervens et al.*, 2011]. The chemical processing of precursors in the aqueous phase is referred to as "cloud processing". Intensive research is conducted to enhance the understanding of aqueous phase organic reactions, as they often differ significantly from the already well-established gas phase chemistry. Model simulations suggest that the contribution of aqSOA to the total SOA mass could be almost as high as the one originating from gasSOA, especially when dealing with biogenic emissions of VOCs in the presence of anthropogenic pollutants (such as NO_x) at high relative humidity and cloudiness [*Ervens et al.*, 2011]. This makes cloud processing an important aspect of SOA formation.

1.1.2 Chemical composition of organic aerosols

Organic aerosols make up a large fraction of 20-90 % of the submicron aerosol mass [*Jimenez et al.*, 2009] and therefore may have a significant effect on radiative climate forcing and human health. However, there is still a high degree of uncertainty concerning sources, atmospheric transformation processes, and removal of organic aerosols. Despite of much recent progress in the understanding of chemical pathways leading to SOA, chemical models are still not able to comprehensively explain ambient SOA concentrations. A better understanding of the chemical nature of organic aerosol is mandatory [*Kanakidou et al.*, 2005].

Organic aerosol is immensely complex and may consist of hundreds of different organic compounds due to its various modes of formation (e.g., [*Schauer et al.*, 1996]). A major component of organic aerosols is the group of water soluble organic compounds (WSOCs), which accounts for a significant portion of the total organic carbon mass, ranging from 20 to 70 % ([*Pöschl*, 2005; *Wozniak et al.*, 2008; *Zhang et al.*, 2010] and references cited there). As only hygroscopic aerosol can act as CCN, WSOC play an important role concerning aerosol-climate interaction [*Saxena and Hildemann*, 1996].

Due to its highly complex composition, the chemical speciation of WSOC is still a challenge concerning extraction, separation and detection of known as well as unknown compounds, which are often present only in trace amounts. WSOC has been characterized at the molecular level mainly using gas chromatography-mass spectrometry (e.g. [*Mayol-Bracero*, 2002; *Samy et*

al., 2010; *Wang et al.*, 2006b]), thus being able to identify only a fraction of about 10 % of WSOC. Different techniques, such as high performance liquid chromatography (HPLC, [*Mayol-Bracero*, 2002]), ^{1}H-NMR [*Decesari et al.*, 2000], and FT-IR spectroscopy [*Duarte et al.*, 2005] were applied to characterize WSOC at a functional group level. Both molecular and functional group focusing approaches revealed mono- and dicarboxylic acids (including hydroxy carboxylic acids) and polyacidic compounds (i.e. macromolecular humic-like substances (HULIS)) as most abundant compound classes in WSOC, followed by neutral/basic compounds (such as alcohols, ethers, carbonyls and sugars). This high prevalence of acidic species in WSOC indicates SOA to be a major source of WSOC. Other sources of polar organic compounds include high-temperature processes leading to highly oxidized chemical species, such as food preparation (e.g. fatty acids [*Nolte et al.*, 1999; *Schauer et al.*, 1999]) and wood burning (e.g., vanillic acid and levoglucosan, [*Simoneit et al.*, 1993; *Zangrando et al.*, 2013]). Polar organic compounds emerging from biomass burning processes are presented in more detail in section 1.1.5.

1.1.3 Atmospheric implication of glyoxal and methylglyoxal

The two smallest α-dicarbonyls glyoxal (G) and methylglyoxal (MG) have received increasing scientific interest in recent years due to their important role in the formation and growth of SOA [*Fu et al.*, 2008]. As explained in chapter 1.1.1, SOA itself is of great interest because of its impact on the radiative budget of the earth's atmosphere (see also [*Mahowald et al.*, 2011]). G and MG are formed through gas phase oxidation of VOCs of both biogenic (i.e. isoprene) and anthropogenic (i.e. aromatics, alkenes) origin [*Carlton et al.*, 2009; *Fu et al.*, 2008; *Kawamura et al.*, 1996b]. According to model simulation results, the global sources for G and MG sum up to 45 Tg a^{-1} and 140 Tg a^{-1}, respectively, with 47 % of G and 79 % of MG originating from oxidation of biogenic isoprene [*Fu et al.*, 2008]. Besides secondary formation, G and MG can also be emitted directly into the atmosphere by biomass burning [*Fu et al.*, 2008].

The lifetime of the α-dicarbonyls in the gas phase is rather short (about 2 h) [*van Pinxteren and Herrmann*, 2013], as they are subject to photolysis. However, due to their high Henry's law coefficients, G and MG efficiently partition into the (aqueous) particle phase. Besides, the compounds are easily scavenged by precipitation (i.e. fog, cloud droplets, rain or snow), either directly from the gas phase or as component of aerosol particles [*Carlton et al.*, 2007; *Matsunaga et al.*, 2007]. In the aqueous phase, G and MG reversibly form hydrated monomers and oligomers. Through further aqueous phase chemistry (particularly in cloud water) α-

dicarbonyls can be oxidized by OH-radicals to form organic acids, especially oxalic and pyruvic acid, which are found in SOA [*Kawamura et al.*, 1996a]. Oligomerization of either G/MG or their oxidation products can also contribute to SOA formation [*Altieri et al.*, 2008; *Ervens and Volkamer*, 2010]. This makes G and MG important compounds when assessing SOA formation and composition. Only recently, Li et al suggested the irreversible uptake of α-dicarbonyls by aqueous particles to be a significant source of SOA in the Pearl river delta region in China [*Li et al.*, 2013]. Studying G and MG in environmental samples is crucial to extend the knowledge of local and global source and sink processes in order to improve model simulations for SOA formation [*Ervens and Volkamer*, 2010; *Fu et al.*, 2008].

Several studies from different geographical regions report G and MG concentrations in ambient aerosol from rural [*Kampf et al.*, 2012; *Mkoma and Kawamura*, 2013], marine [*Fu et al.*, 2013; *van Pinxteren and Herrmann*, 2013], and urban areas [*Kawamura and Yasui*, 2005; *Li and Yu*, 2005]. G and MG have also been reported in seawater [*Tedetti et al.*, 2006; *van Pinxteren and Herrmann*, 2013], cloud water [*Houdier et al.*, 2011], rain [*Kawamura et al.*, 2001a; *Matsunaga and Kawamura*, 2000], snow [*Gunz and Hoffmann*, 1990; *Houdier et al.*, 2011] and ice [*Kawamura et al.*, 2001b]).

1.1.4 Atmospheric implications of dicarboxylic acids

Organic acids play an important role in the chemical composition of the troposphere. They constitute a major fraction of the group of WSOCs, which in turn account for up to 70 % of the organic matter present in atmospheric aerosols. Especially low weight carboxylic acids like formic and acetic acid as well as dicarboxylic acids are found to be ubiquitous compounds in the gas and particle phase. Carboxylic acids are present in fog [*Decesari et al.*, 2000; *Fuzzi et al.*, 2002; *Munger et al.*, 1989], cloud water [*Keene et al.*, 1995; *Munger et al.*, 1989], rain [*Kawamura et al.*, 1996b; *Kawamura et al.*, 2001a], seawater [*Tedetti et al.*, 2006], snow [*Kippenberger et al.*, 2008; *Winterhalter et al.*, 2009] and ice [*Kawamura et al.*, 2001b; *Legrand et al.*, 2007b], as well as in the gas phase [*Khwaja*, 1995] and in aerosol particles [*Decesari et al.*, 2000; *Grosjean et al.*, 1978; *Ho et al.*, 2006; *Hsieh et al.*, 2007; *Hyder et al.*, 2012; *Kawamura and Ikushima*, 1993; *Kawamura et al.*, 1996a; *Kawamura and Sakaguchi F.*, 1999; *Kawamura and Yasui*, 2005; *Legrand et al.*, 2007b; *Mochida et al.*, 2003; *Pavuluri et al.*, 2010; *Plewka et al.*, 2006; *Zhang et al.*, 2010]. Organic acids have been investigated in marine, continental, urban and rural areas (see also [*Chebbi and Carlier*, 1996] for a comprehensive

review). The group of organic acids includes monocarboxylic acids, dicarboxylic acids, oxocarboxylic acids, and tricarboxylic acids.

Dicarboxylic acids constitute an important compound class, as they account for a main fraction of the known resolved organic compounds in aerosol particles [*Saxena and Hildemann*, 1996] and 0.3-11 % of WSOC [*Pavuluri et al.*, 2010; *Zhang et al.*, 2010]. Due to their high polarity and low molecular weight, dicarboxylic acids are water soluble and can therefore act as CCN, with oxalic acid showing the highest CCN ability [*Sun and Ariya*, 2006]. Dicarboxylic acids have been extensively studied in arctic [*Kawamura et al.*, 1996a], marine [*Kawamura and Sakaguchi F.*, 1999], rural [*Hyder et al.*, 2012; *Legrand et al.*, 2007a; *van Pinxteren et al.*, 2014], and suburban/urban [*Grosjean et al.*, 1978; *Hsieh et al.*, 2007; *van Pinxteren et al.*, 2014] aerosols, for example. In various studies, oxalic acid has been identified as the most abundant dicarboxylic acid present in SOA, followed by malonic and succinic acid (e.g., [*Kawamura and Ikushima*, 1993; *Kawamura et al.*, 1996a; *Neusüß et al.*, 2002]). This can be explained by oxalic acid being the end product of various organic oxidation chains starting from different gas phase precursors.

There are various sources for dicarboxylic acids present in the atmosphere. Primary sources include direct emission due to biomass burning [*Kundu et al.*, 2010; *Legrand and Angelis*, 1996; *Narukawa et al.*, 1999; *Pio et al.*, 2008], vehicle emission [*Kawamura and Kaplan*, 1987], and marine emission [*Mochida et al.*, 2003]. However, the main source of dicarboxylic acids is secondary production by atmospheric photooxidation of biogenic as well as anthropogenic VOCs [*Grosjean et al.*, 1978; *Yu et al.*, 1999; *Zhang et al.*, 2010]. Is has been suggested that small dicarboxylic acids (C2-C7) are formed mainly from anthropogenic precursors like alkenes, aldehydes, or other less oxygenated organic species [*Ervens et al.*, 2004; *Mochida et al.*, 2003]. Glutaric acid (C5) is produced by the oxidation of glutardialdehyde, cyclopentene, and cyclohexene [*Winterhalter et al.*, 2009]. The oxidative decay of cyclic alkenes is also a source for adipic acid (C6), as it originates mainly from the atmospheric oxidation of cyclohexene [*Hatakeyama et al.*, 1987; *Koch et al.*, 2000] and the ozonolysis of methylene-cyclohexane and 1-methyl-cyclohexene [*Koch et al.*, 2000]. In contrast to this, the C8-C10 dicarboxylic acids are mainly formed by the oxidation of biogenic compounds, such as unsaturated fatty acids [*Kawamura et al.*, 1996a; *Stephanou and Stratigakis*, 1993b].

The formation of dicarboxylic acids through chemical processes in clouds is still not completely understood, however model simulations suggest cloud processing to be a significant source of small dicarboxylic acids [*Ervens et al.*, 2004]. Possible reaction pathways in the gas and

aqueous phase are shown in Fig. 1.2. Altieri et al. reported the formation of oxalic acid through isoprene cloud processing [*Altieri et al.*, 2006].

Fig. 1.2 Schematic overview of aqueous-phase reactions resulting in the formation of dicarboxylic acids reported by Ervens et al. [*Ervens et al.*, 2004]. The shadowed area represents the gas phase.

Cis-Pinic acid (PIN) is an example of a dicarboxylic acid formed from exclusively biogenic precursors, as it is an oxidation product of the OH-oxidation or ozonolysis of α- and β-pinene, whose tropospheric lifetime is a few hours due to reaction with OH, ozone or NO_3 [*Atkinson and Arey*, 2003; *Seinfeld and Pandis*, 2006]. This was investigated in smog chamber studies, revealing PIN to be a major product of pinene oxidation and a precursor for SOA [*Christoffersen et al.*, 1998; *Hoffmann et al.*, 1998; *Johnson and Marston*, 2008; *Yu et al.*, 1999]. Recently, dimer esters of pinene oxidation products found in SOA gained scientific interest, possibly being involved in nucleation processes due to their low vapor pressure [*Kristensen et al.*, 2013]. PIN and other biogenic aerosol constituents have been investigated in a coniferous forest (Fichtelgebirge, Germany [*Plewka et al.*, 2006]), mixed forest (Denmark [*Kristensen and Glasius*, 2011]) and suburban area (Vavihill, Sweden [*Hyder et al.*, 2012]), for example.

1.1.5 Biomass burning markers

The combustion of biomass is an important source for primary aerosol particles. During biomass burning, particles with adsorbed organic compounds are injected into smoke plumes entering the global atmosphere. Biomass burning typically comprises wildfires, controlled burns, combustion of specific plant species fuels and fossil fuels (such as brown coal and peat), as well as other anthropogenic urban and industrial emission (e.g. heating, food cooking, tobacco smoking, etc.). The molecular alteration and transformation of organic species during combustion is not only determined by the nature of the burned material, but also by burning conditions such as heat intensity, aeration, and duration of smoldering. Thus, the distinct organic compounds attached to smoke particles provide a chemical fingerprint, which is specific for the biomass burning event and useful for identifying single or multiple vegetation species involved [*Simoneit*, 2002].

Ammonium and water-soluble potassium (K^+) have been used as tracers for wood smoke. Concerning those compounds, one must consider that they can also originate from emission sources other than biomass burning. Potassium can be transported with sea salt or mineral aerosols and can be emitted through biological activity, for example. Ammonium can be produced by lightning, soil processes, and agricultural activity (see [*Kehrwald et al.*, 2012] and references cited there). A specific, unequivocal biomass burning tracer for the decomposition of cellulose is levoglucosan (1,6-anhydro-β-D-glucopyranose), as it is only formed from cellulose at temperatures above 300 °C. Other, more vegetation specific biomass burning markers originate from lignin burning. Lignin is a major biopolymer in wooden tissue, derived mainly from the three aromatic alcohols *p*-coumaryl alcohol, coniferyl alcohol, and sinapyl alcohol, whose proportions vary significantly among different plant classes (see Fig. 1.3). *Gymnosperms* and *Angiosperms* are the two groups of seed producing plants (*Spermatophytes*). The lignin of *Gymnosperms* is dominated by coniferyl-type aromatic moieties. Conifers (such as pines, cypresses, and relative species) make up the largest group of *Gymnosperm* trees, which are referred to as softwood. *Angiosperms* (or *Magnoliophyta*) are flowering plants. The lignin of Angiosperm trees (also called hardwood) is characterized by aromatic moieties of sinapyl type. *Gramineae* is a plant family of *Angiosperms*, which is also called *Poaceae* or true grasses. The lignin of *Gramineae* is exceptional among *Angiosperms*, as it is dominated by aromatic moieties of the *p*-coumaryl-type. Since the products of lignin burning (phenols, aldehydes, ketones, acids, and alcohols) still carry the characteristic aromatic moieties, they can be attributed to the respective plant class. Vanillic acid is an example for a

coniferyl-type lignin burning product, indicating the burning of *Gymnosperm* species. *P*-hydroxybenzoic acid indicates the burning of grasses (*Gramineae*), as it is a marker compound for the coumaryl-type lignin degradation [*Simoneit*, 2002].
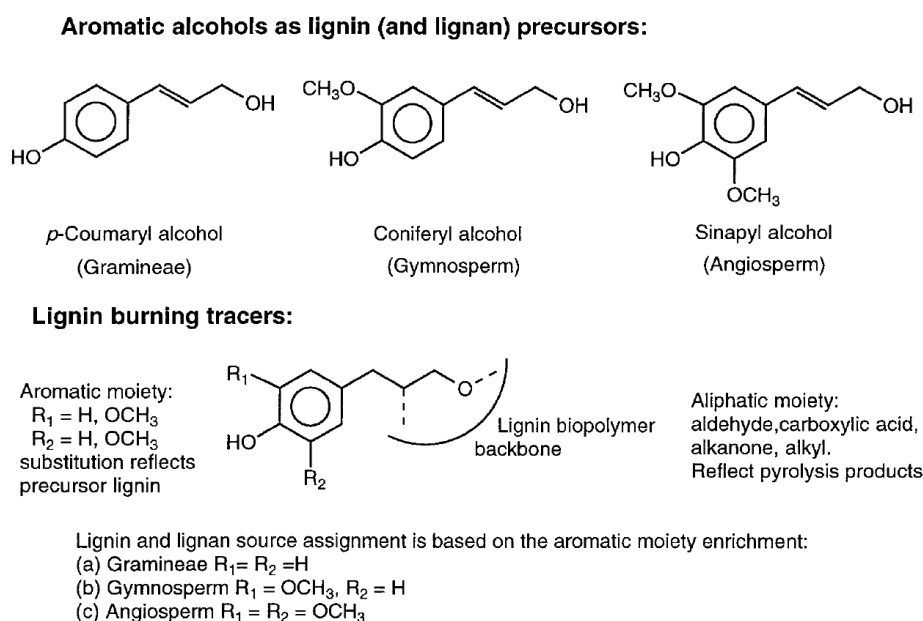
Fig. 1.3 Summary of the biochemical precursors for lignins and lignans, and of lignin burning products as tracers for biomass sources [*Simoneit*, 2002].

The analysis of biomass burning markers in ice cores can give valuable insights into the history of wildfires and changes in fire regimes through time [*Kehrwald et al.*, 2010]. Legrand and DeAngelis (1996) used ammonium, formate, and oxalate as tracers for forest fires in a Greenland ice core. There is only one study reporting the analysis of *p*-hydroxybenzoic acid (and other biomass burning markers like vanillic acid) in an ice core (Northeast Asia [*Kawamura et al.*, 2012]). Vanillic acid was also measured in an ice core from Greenland [*McConnell et al.*, 2007]. In general, low-altitude ice cores provide insight into the regional fire history, whereas polar ice cores reflect the effect of biomass burning on a global scale. In chapter 1.2, the use of ice cores for reconstructing historic climate parameters is explained in more detail.

1.1.6 Atmospheric implications of organosulfates and nitrooxy organosulfates

Organosulfates (OS) and nitrooxy organosulfates (NOS) are formed in the atmosphere from biogenic emissions interacting with anthropogenic pollution. Hence, they contribute to the so called anthropogenically enhanced biogenic SOA (ABSOA), which has received increasing attention by the scientific community over the last years. Enhanced formation of biogenic SOA was reported in the presence of acidic sulfate seed aerosol by Zang et.al. [*Zhang et al.*, 2012] as well as Jang et al. [*Jang*, 2002]. Surratt et al. [*Surratt et al.*, 2006] proposed acid-catalyzed particle phase reactions yielding OS, for example, to be a major source of SOA. Organosulfates have been identified as important SOA constituents in chamber as well as field studies [*Hatch et al.*, 2011; *Reemtsma et al.*, 2006; *Surratt et al.*, 2008; *Surratt et al.*, 2007], and are estimated to be responsible for a significant fraction of up to 30 % of ambient organic mass. Organosulfates have been found in aerosol particles [*Kundu et al.*, 2013; *Lin et al.*, 2012b; *Safi Shalamzari et al.*, 2013; *Stone et al.*, 2012; *Zhang et al.*, 2012], cloud water [*Pratt et al.*, 2013], and rainwater [*Altieri et al.*, 2006; *Altieri et al.*, 2009].

Proposed precursors for organosulfates and organonitrates in ambient SOA are isoprene [*Darer et al.*, 2011; *Froyd et al.*, 2010; *Schindelka et al.*, 2013] and monoterpenes like α-and β-pinene [*Iinuma et al.*, 2009]. The isoprene derived organosulfate MW 216 (measured as anion with *m/z* 215 [M-H]$^-$) is found to be the most abundant organosulfate in ambient aerosols according to many studies (see [*Schindelka et al.*, 2013] and references cited there). The nitrooxy organosulfates with MW 295 (NOS 295) are reported to be ubiquitous constituents of SOA particles (e.g., [*Kahnt et al.*, 2013]). In chamber studies NOS 295 have been identified as products of the oxidation of monoterpenes, such as α- and β-pinen, α-terpinen, and γ-terpinen. It has been found in organic aerosol samples from remote/arctic, urban, and rural environment (e.g., [*Gómez-González et al.*, 2012; *Hansen et al.*, 2014; *Lin et al.*, 2012a; *Vogel* 2014]), as well as in rain samples [*Altieri et al.*, 2009]. Organosulfates and nitrooxy organosulfates have not been reported in ice core samples, so far.

1.2   Ice cores as climate archives

The earth is and has always been object to a constant change concerning biological, chemical and physical aspects. Changes concerning the earth's climate can have immediate or future effects. To study the global climatic and environmental changes caused by anthropogenic activity as well as naturally occurring changes, it is necessary to know the environmental and especially atmospheric conditions of the past. This can be achieved by analyzing climate archives like for example ice cores, sediments or speleothemes, which preserve information on past environmental and climatic conditions. Knowledge on past climate changes can not only help to understand ongoing climate change caused by human activity but also lead to improved models for climate change prediction [*Cecil et al.*, 2004]. Ice cores are either obtained from polar ice sheets in Antarctica or Greenland or from glaciers located in high or mid latitude mountain areas.

1.2.1   Polar ice cores

Today's state of knowledge about climate change and naturally or anthropogenically influenced variability largely results from the analyses of polar ice cores. The drilling of ice cores at the Vostok site in Antarctica started in the early 1970s, the GRIP (Greenland Ice Core Project) was put up in Greenland in the early 1990s and about 10 years later, ice cores were drilled at the sites Dome C and Dronning Maud Land in Antarctica within the scope of the EPICA campaign (European Project for Ice Coring in Antarctica) [*Maggi et al.*, 2006]. The obtained ice core from Dome C is 3.3 km long and dates back about 800,000 years, making it the oldest continuous core ever retrieved. A recent project in Greenland is the NEEM (North Greenland Eemian Ice Drilling) project, which was realized from 2007 to 2012. The polar ice cores are drilled in areas of low and continuous snow accumulation, usually far from pollution sources due to their remote location. As a consequence, the resulting records from polar ice cores allow retracing global climate conditions and atmospheric parameters over several hundred thousand years.

1.2.2   Ice cores from mid-latitude glaciers

In contrast to ice cores from polar regions, those originating from mid-latitude glaciers provide regionally influenced climate records due to their immediate vicinity to natural and anthropogenic emission sources. Glaciers can only be found at mountain sites in distinct

regions on earth, which have been defined by the Randolph Glacier Inventory (RGI) as shown in Fig. 1.4. In Europe, glaciers can be found in the northern part of Scandinavia and in the Alps.
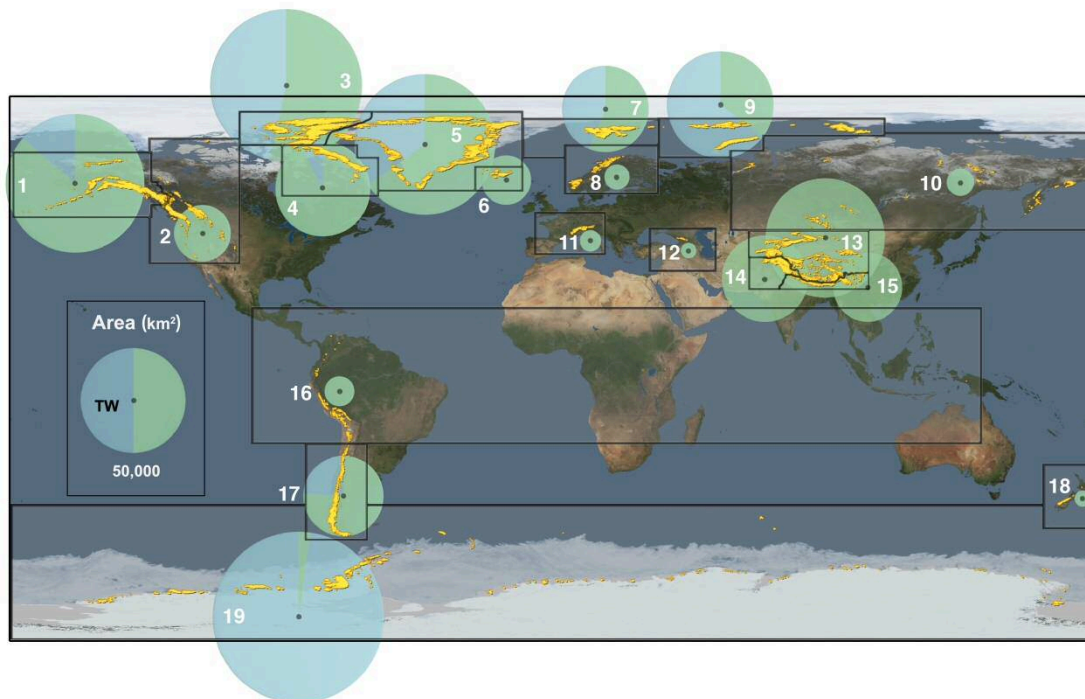
Fig. 1.4 Global distribution of glaciers (yellow, area increased for visibility) and area covered (diameter of the circle), sub-divided into the 19 Randolph Glacier Inventory (RGI) regions (white number). The area percentage covered by tidewater (TW) glaciers in each region is shown in blue (IPCC 2013b).

In this section, the alpine region as a source area for glacier ice cores is presented in more detail. The three main glacier sites where ice cores were drilled are the *Col du Dome* (*CDD*) glacier (near the Mont Blanc summit, 4250 m a.s.l.) in the French Alps and the *Colle Gnifetti (CG)* glacier (Monte Rosa Massif, 4454 m a.s.l.) and *Colle del Lys* (*CDL*) saddle (at the upper part of *Lys* glacier, Monte Rosa Group, 4250 m a.s.l.), both located near the Swiss-Italian border (Fig. 1.5). At alpine sites above 4000 m a.s.l., the mean annual temperature is usually below -10 °C. Those glaciers are called "cold glaciers", since melting of snow in the summer is mostly prevented and percolation rarely takes place, thus enabling the accumulation of annual snow layers. Low accumulation sites (e.g., *CG*) provide long sequences, whereas high-accumulation sites (e.g., *CDD*) can provide information about the seasonal variation the compounds in the ice [*Maggi et al.*, 2006].
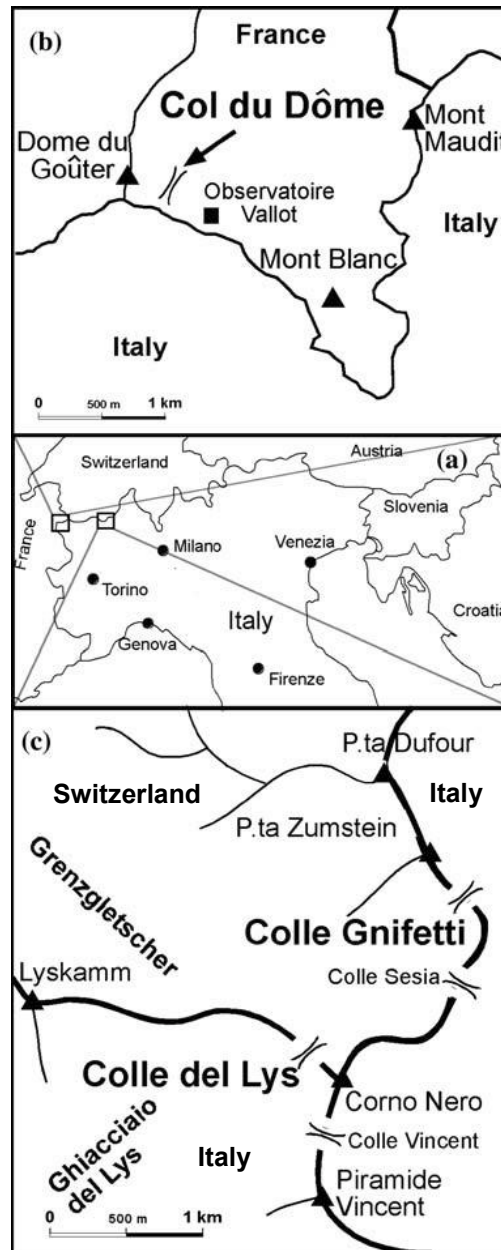
Fig. 1.5 Maps of the main glacier sites described in the text. (a) Map of northern Italy (b) *CDD* in the French Alps (C) *CDL*, *CG*, and *Grenzgletscher* in the Italian and the southern Swiss Alps [*Maggi et al.,* 2006].

Drawbacks of the use of alpine ice cores as climate archives are the high impact of local meteorological conditions on the accumulation of snow and the rather short time period covered by the ice cores (ranging from several decades to several centuries). Nevertheless, alpine ice cores constitute indispensable archives of regional climate history. As the Alps are located in a densely populated and highly industrialized area, ice cores from alpine glaciers provide historic records of atmospheric pollution in Europe. Anthropogenic emissions have

altered the composition of the atmosphere in a strong way, which became immediately obvious in case of the acid rain in the 1970s, for example. Thus, most of the studies based on alpine ice cores focus on the human impact on the composition of the atmosphere. Major aerosol constituents, such as sulfate, nitrate, ammonium, black and elemental carbon, as well as trace constituents, such as heavy metals, gaseous compounds (e.g. methane) and radionuclides (tritium, ^{137}Cs, ^{36}Cl, and ^{129}I) were analyzed in ice cores, revealing an increase in concentration after the beginning of industrialization. However, due to the introduction of restrictive environmental laws and voluntary controls, many of the pollutants show a decrease in concentration since the beginning of the 1970s. This is caused by the use of filter systems for exhaust gases in power plants and industry, for example, as well as the use of lead-free gasoline, catalytic converters, and oils with lower sulfur content [*Schwikowski*, 2004].

1.2.3 Inorganic and organic matter in ice cores

In the following, an overview is given about chemical species reported in different studies analyzing ice cores from alpine and polar regions:

Sulfate and **nitrate** levels in the mid-troposphere were investigated by analyzing alpine ice cores from *CDD* [*Preunkert et al.*, 2001, 2003] and *Fiescherhorn* glacier (Swiss Alps, north of *Monte Rosa*, [*Schwikowski et al.*, 1999]).The sulfate levels found in alpine ice cores are believed to be largely caused by anthropogenic activity, as they exhibit good correlations to the emission of SO_2 from the major industrialized countries in Western Europe, especially from the countries in proximity to the alpine region (France, Italy, Germany, Switzerland, and Spain). Similar results are obtained for summer nitrate records, which show the emission trend of NO. Sulfate and nitrate were also analyzed in an ice core from southern Greenland, also revealing an increasing trend due to anthropogenic emissions [*Fischer et al.*, 1998a; *Mayewski et al.*, 1986]. Greenland ice cores also allow the determination of pre-industrial, and therefore mainly naturally influenced sulfate levels, originating from volcanic or biogenic emissions [*Fischer et al.*, 1998b].

Ammonium records were measured in the *Fiescherhorn* glacier by Schwikowski et al. [*Schwikowski et al.*, 1999] and in an ice core from *CG* [*Doscher et al.*, 1996], revealing an increase of ammonium in precipitation over the last century. High ammonium, sulfate, and nitrate concentrations are often found at the same time, indicating anthropogenic origin. The production of ammonium aerosol can be explained by the increase in ammonium formation

from ammonia, due to the rising amount of acidic anthropogenic aerosol since the beginning of the 20th century.

Other ions, such as Ca^{2+}, Mg^{2+}, K^+, Na^+, Cl^-, and F^- have also been studies in ice cores. These ions do not show a clear seasonal variation, but can be attributed to atmospheric dust (Ca^{2+}, Mg^{2+}, and K^+) and to marine aerosol (Na^+, Cl^-), giving hints concerning the trajectory of air masses [*Schwikowski et al.*, 1999]. Ice core records of Cl^- from *CDD* and *Fiescherhorn* revealed the variation of atmospheric HCl during the last century, caused by industrialization, coal combustion, and waste incineration [*Legrand et al.*, 2002; *Schwikowski et al.*, 1999]. F^- and Cl^- were analyzed in an ice core from *Upper Grenzgletscher* (Swiss Alps, *Monte Rosa Massif*) by Eichler et al. [*Eichler et al.*, 2000a], attributing the non-sea-salt Cl^- to HCl emissions from waste incineration, whereas F^- records were assigned to HF emissions from the aluminium industry in the Swiss Rhone valley.

Heavy metals (e.g., **Cu**, **Cd**, **Zn**, and **Pb**) emitted by human activities were also analyzed in ice cores from *Dome du Gouter* at the *Mont Blanc Massif* [*van de Velde et al.*, 2000] and *Cole Gnifetti* at the *Monte Rosa Massif* [*Barbante et al.*, 2004; *Schwikowski et al.*, 2004]. In the latter study, high concentrations of lead were determined in the 1970s, which was explained by use of leaded gasoline. Gabrielli et al. reported records of a large number of atmospheric trace elements (Li, Mg, Cr, Mn, Co, Cu, As, Rh, Cd, Ba, and Bi) in an EPICA ice core from Dome C, Antarctica [*Gabrielli et al.*, 2005].

Mineral dust is another atmospheric compound detected in ice cores. It is deposited at the glacier sites during so called *Saharan dust events* (where the term "*Saharan*" refers not only to the desert *Sahara*, but to the whole region of North Africa). Long distance atmospheric transport processes carry the mineral particles from their emission sources to the Alps, which function as a barrier for air masses, leading to frequent precipitation. The calcareous dust particles can influence the acidity of the precipitation due to their buffering properties. As the dust is colored red, yellow, or brown, the precipitated dust layers are clearly visible in the ice and can be used as stratigraphic markers for dating, as explained in section 1.2.4 in more detail [*Maggi et al.*, 2006]. Mineral dust was analyzed in an ice core from *Fiescherhorn* glacier [*Schwikowski et al.*, 1999], for example.

In contrast to the well-established analysis of inorganic species in ice cores, **organic compounds** have been analyzed in (alpine) ice cores to a much smaller extent (see [*Legrand et al.*, 2013a] for review).

Concentrations of monocarboxylic acids, mainly **formic acid** and **acetic acid**, which also play a role in the acidity of the precipitation, have been determined in ice cores from the Alps (*CDD*, [*Legrand et al.*, 2003]), Greenland [*Legrand and Angelis*, 1996; *Legrand et al.*, 1992] and Antarctica [*Angelis et al.*, 2012]. These compounds can be attributed to vegetation emission, boreal forest fires or anthropogenic (vehicle) emissions. Short **dicarboxylates (C_2-C_5)** were analyzed in distinct sections of alpine firn and ice cores from *CDD* and *CG* [*Legrand et al.*, 2007b]. Historic records of **dicarboxylic acids (C_2-C_{10})**, **oxocarboxylic acids (C_2-C_9)**, and **α-dicarbonlys (C_2-C_3)** in an ice core from Greenland were reported by Kawamura et al. [*Kawamura et al.*, 2001b]. Long-chain **carboxylic acids (*fatty acids*, C_{14}-C_{22})** were also detected in an ice core from Greenland [*Kawamura et al.*, 1996c].

Formaldehyde was analyzed in a firn core from Lys glacier [*Largiuni*, 2003] and ice cores from Greenland [*Staffelbach et al.*, 1991]. It is a marker compound for the oxidative capacity of the atmosphere, formed by the oxidation of methane, for example.

Few studies report the concentrations of **persistent organic pollutants** (POPs) in ice cores (e.g., [*Lacorte et al.*, 2009; *Villa et al.*, 2003; *Wang et al.*, 2008]). Seasonal variations of **organochlorine pesticides** and **polychlorinated biphenyls** were determined by Villa et al. in a firn core from *Lys Glacier* at the *Monte Rosa Massif* in Italy to obtain information about local and global transport patterns of POPs, as well as possible air-snow-interactions [*Villa et al.*, 2006].

Polycyclic aromatic hydrocarbons (PAHs), such as phenanthrene, fluoranthrene (Fla) and pyrene (Pyr), were analyzed in ice cores from *CG* [*Gabrieli et al.*, 2010]. The ratio of Fla/(Fla+Pyr) is used for source assignment of the emitted PAHs, distinguishing between coal and wood combustion, which was the common fuel of the 19th century, and the combustion of crude oil, diesel, and gasoline. A value higher than 0.5 indicates a dominance of coal and wood combustion, whereas a decrease in the ratio (observed during the 20th century) shows an increase in the combustion of crude oil, diesel and gasoline, reaching a maximum in the 1980s. In the last decades, the trend is inversed again due to an increase in domestic wood (pellets) combustion and the significant reduction of mobile emissions.

In addition to these studies reporting target analyses of specific organic compounds, there are several studies dealing with sum parameters, characterizing certain fractions of organic matter in ice cores. The sum parameter dissolved organic carbon (DOC) refers to the water soluble fraction of organic carbon. The sum of DOC and the water-insoluble organic carbon (WinOC),

which is also called particulate organic carbon (POC), is the total organic carbon (TOC) present in an environmental sample. The total carbon content (TCC) is the sum of WinOC, DOC and the inorganic parameter elemental carbon (EC), which is also referred to as black carbon (BC).

DOC was determined using several ice cores from *CDD* to evaluate the fossil contribution to the DOC using radiocarbon analysis [*May et al.*, 2013].

Humic-like-substances (HULIS) are a class or organic compounds of oligomeric or polymeric character, which show physical and chemical similarity to humic and fulvic acids. They consist mainly of aromatic compounds with aliphatic chains, carrying carboxyl, hydroxyl, or carbonyl functional groups. Therefore, HULIS exhibit polar, poly-acidic, and chromophoric properties. HULIS were analyzed in an ice core from *CDD* [*Guilhermet et al.*, 2013] and in discrete ice cores sections extracted from *Mount Rosa* and *Mount Blanc* glaciers [*Legrand et al.*, 2007b].

Only recently, a study comprising the analysis of both **inorganic** compounds (ions Na^+, Ca^{2+}, NH_4^+, Cl^-, NO_3^-, SO_4^{2-}, and the sum parameter **BC**) and **organic** compounds in alpine ice cores from *CDD* was published by Preunkert and Legrand [*Preunkert and Legrand*, 2013]. The organic compounds analyzed on a molecular level were **formaldehyde** and short chain (C_1-C_5) **mono- and dicarboxylates**. Furthermore, the organic (sum) parameters **HULIS**, **DOC**, and **WinOC** were investigated. The light mono- and dicarboxylates, formaldehyde and HULIS accounted for more than half of the DOC found in the ice [*Legrand et al.*, 2013b]. An increase in sub-micron atmospheric aerosol by a factor of 3 from the 1950s to the late 1980s was reported. This is partly explained by the well-investigated increase in anthropogenic emissions of sulfur dioxide and ammonia, leading to raised concentrations of atmospheric sulfate and ammonium by a factor of 5 and 3, respectively. Besides, a rather unexpected increase in water-soluble organic aerosol by a factor of 3 since the 1950s was observed, attributed mainly to an increase in biogenic emissions [*Legrand et al.*, 2013b]. Therefore, besides the evaluation of anthropogenic influences on atmospheric composition, biogenic sources for the highly abundant organic matter in aerosols have to be brought into focus and investigated in more detail using ice cores [*Legrand et al.*, 2002].

1.2.4 Dating of ice cores

Glacier ice cores can cover time periods of several decades up to thousands of years. For dating the ice core, different strategies can be applied, which depend on accuracy and time-scale requirements. To improve dating accuracy, they are often used in combination [*Eichler et al.*, 2000b]:

A frequently applied dating technique is the use of the decay of **radioactive isotopes**. For time-scales of about 100 years, the nuclide ^{210}Pb is suitable, as it has a half-life of 22.3 years. ^{210}Pb is a product of ^{222}Rn in the natural ^{238}U decay series. It is continuously formed in the troposphere from ^{222}Rn, attached to aerosol particles, and deposited on the Earth's surface by wet and dry deposition. In addition to the dating of ice cores, ^{210}Pb is also commonly used for the dating of (lake) sediments [*Tinner et al.*, 1998].

A second technique is the assignment of dates to so called **reference horizons**. Those are formed by stratigraphic marker compounds, which originate from known historical events, for example Saharan dust events (1947, 1977 and 1990). The dust deposited is even visible as a yellow band in the ice core. Other markers result from radioactive fallouts, for example large Tritium peaks from thermonuclear weapon tests in 1959 and 1963 and a peak of ^{137}Cs, emitted after the Chernobyl accident in 1986.

A third dating strategy is **annual-layer counting**. Requirements for this approach are high snow accumulation and minimal post-depositional snow erosion at the alpine site together with a regular distribution of precipitation during the year. Besides, a pronounced seasonal variation of the species present in the ice core is mandatory, which is the case for δ^{18}O, for example: Since the fractionation of the stable isotopes of oxygen is temperature dependent, the different temperatures of air masses during snow deposition in summer and winter are represented by the variation of the δ^{18}O values. In addition to this, many aerosol components, such as ammonium, sulfate, nitrate, sodium, and chloride show a strong seasonal variation. This can be explained by the different conditions of the planetary boundary layer (PBL) during the year. The PBL is the part of the troposphere closest to the Earth's surface and directly affected by it. In winter, the PBL is stably stratified and vertical exchange between the PBL and the free troposphere is hindered by stable thermal inversions at low-altitude. Thus, the transport of emissions from the ground to the high altitude glacier site is limited. The concentrations of chemical species found in the winter snow can therefore be assigned to advection-dominated, free troposphere conditions and possibly result from long-range

transport processes. However, in spring and summer, convection-dominated processes take place and the vertical exchange between the PBL and the free troposphere is possible. Emissions from regional sources are transported very efficiently to the glacier and are deposited with the precipitating snow. Therefore, concentrations in summer snow layers are much higher compared to the rest of the year, revealing a seasonal pattern. Like counting the rings of a tree, the resulting maxima and minima in the record are counted to determine the age of the ice [*Eichler et al.*, 2000b; *Maggi et al.*, 2006].

1.3   The study site

1.3.1   The Grenzgletscher in the southern Swiss Alps

The samples analyzed in this work originate from an ice core from the *Grenzgletscher* glacier on the *Monte Rosa massif* in the southern Swiss Alps near the Italian border (4200 m a.s.l., 45°55′ N, 7°52′ E). The drilling site is characterized by a high annual net accumulation with an annual accumulation rate of 2 m w.e. as it is located in the flowline of Colle Gnifetti. At this site, wind erosion of accumulated precipitation is much lower than on the Colle Gnifetti saddle, where especially in winter much of the precipitation is removed by wind erosion, leading to a low net accumulation of only 30 cm per year. Using radar sounding experiments the glacier thickness at the drilling site was estimated to be approximately 190 m with a relatively flat glacier geometry (slope of about 10°) revealing the suitability of the upper Grenzgletscher to serve as a climate archive (see Fig. 1.6).
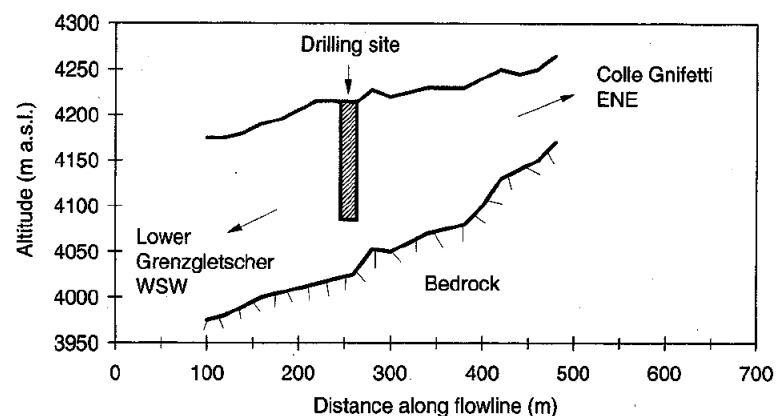
Fig. 1.6 Schematic cross-section of upper Grenzgletscher at the drilling site [*Eichler et al.*, 2000b].

An ice core 125 m in length was recovered in October 1994 by a team from PSI in Villigen, Switzerland. The drilling was performed using an electromagnetic drill with an inner diameter of 7.8 cm. Two hundred forty ice core sections were recovered, each 50-80 cm long. The ice core sections were packed in polyethylene bags and kept at -25 °C during transport and storage. Dating of the ice core was performed by Anja Eichler using the dating strategies presented in section 1.2.4 [*Eichler et al.*, 2000b]. By combining the different dating techniques, an excellent dating accuracy of ±2 years for the time before 1970 and <±1 year for the period of 1970 to 1993 was achieved.

1.3.2 Forest fires in southern Switzerland

In southern Switzerland, forest fires occur on a regularly basis. The mean annual burned area is about 500 ha, which is 3-5 % of the woodland area. The mean extent of a single woodland fire ranges from 5 to 500 ha. Ninety percent of the fires are caused by human activity, the less frequent natural forest fires are mainly caused by lightning. Information about forest fires has been documented in different historical archives in Switzerland since the nineteenth century. The data was collected and organized in the Swissfire database by the Research Institute WSL (Swiss Federal Institute for Forest, Snow and Landscape Research) and the FOEN (Swiss Federal Office for the Environment) [*Conedera et al.*, 1996; *Pezzatti et al.*, 2005; *Tinner et al.*, 1998].

1.4   Thesis motivation

Atmospheric aerosols play an important role in the investigation of anthropogenically forced climate change and atmospheric chemistry in general, as discussed in chapter 1.1. The characterization of aerosol compounds at a molecular level allows for novel insights on potential sources of organic aerosol. Through the analysis of aerosol constituents used as marker compounds for certain environmental conditions, information about the source of the aerosol (biogenic or anthropogenic, urban, rural or marine) is accessible. However, investigating the chemical composition of aerosols is still a major challenge, as they may comprise thousands of different chemical compounds.

In high altitude and high latitude regions, organic aerosols are deposited with snow. As the snow is compressed to firn and ice over the years, the chemical composition of the atmosphere is preserved in a natural archive in the ice. By analyzing ice core samples, information about the atmospheric composition in the past – interrelated with the climate – is accessible. Marker compounds, such as biomass burning markers or anthropogenic pollutants can give hints to certain historical events like forest fires or reveal general anthropogenic influences, respectively. Even though no direct source assignment is possible for many major organic aerosol compounds, as they emerge from anthropogenic as well as biogenic precursors (e.g. G and MG), historical records in combination with other marker compounds can give valuable hints about the oxidative capacity of the atmosphere in the past. Additionally, chemical analysis of snow and ice on a molecular level can increase the understanding of processes happening in the seasonal snow layer after deposition, as organic compounds may undergo transformation processes such as physical exchange ("wind pumping"), photochemical production from other precursors or degradation [*Ariya et al.*, 2011; *Dominé and Shepson*, 2002]. Until now, very little is known about these complex processes.

Alpha-dicarbonyls and dicarboxylic acids play an important role concerning SOA formation and growth, thus constituting significant atmospheric chemical species. However, the investigation of ice core chemical composition has been focused mainly on inorganic parameters or sum parameters like TOC with limited analysis of organic and especially polar species. For example in addition to studies reporting VOCs and carboxylic acids and persistent organic pollutants (POPs) in snow [*Sieg et al.*, 2008; *Winterhalter et al.*, 2009] and ice [*Lacorte et al.*, 2009], respectively, there is only one study targeting G and MG in ice cores [*Kawamura et al.*, 2001b], and a few in snow and frost flowers [*Douglas et al.*, 2012; *Houdier et al.*, 2011; *Matsunaga and*

Kawamura, 2000]. Concerning (di)carboxylic acids, including the biomass burning markers vanillic acid and *p*-hydroxybenzoic acid, studies are also still limited (e.g., [*Kawamura et al.*, 2012; *McConnell et al.*, 2007]). There is only one study describing the analysis of dicarboxylic acids including the biogenic compound pinic acid in Alpine snow [*Kippenberger et al.*, 2008]. Also, pinic acid has not been reported in ice cores, yet.

Therefore, the main aims of this doctoral work were as follows:

- Development of analytical methods for the qualification and quantification of polar compounds (α-dicarbonyls, mono- and dicarboxylic acids) in ice cores using HPLC-ESI-MS.
- Application of the developed methods for the analysis of a glacier ice core from Upper Grenzgletscher in the southern Swiss Alps, as well as the determination and interpretation of the resulting historic records.

In addition to the quantitative analysis of defined compounds of interest, an additional aim was the qualitative characterization of the complex mixture of WSOC in the ice using high-resolution mass spectrometry, allowing for novel insights concerning the composition and possible sources of aerosol derived WSOC deposited at the glacier site.

The detailed description of the conducted research and the discussion of the results are given in chapters 3 to 5. Chapter 3 is based on a first author publication describing the method development for the quantification of glyoxal and methylglyoxal in snow and ice using SBSE-HPLC-MS. The cited literature is included in the references section (section 7.5) of the thesis.

2 ANALYTICAL METHODS AND INSTRUMENTS

The analytical procedures developed and carried out during the doctoral work regarding the analyses of α-dicarbonyls as well as dicarboxylic acids in aqueous samples comprise sample extraction and enrichment, derivatization, chromatographic separation using reversed phase (RP) high-performance liquid chromatography (HPLC) and mass spectrometric detection. In this chapter, a short overview about the principles of the analytical methods and the used mass spectrometers is given.

2.1 Sample extraction and enrichment

2.1.1 Solid Phase Extraction

Solid phase extraction (SPE) is a commonly used sample preparation technique for the extraction and enrichment of analytes from an aqueous matrix [*Cammann*, 2001]. The sample is applied to a polypropylene or glass cartridge containing a sorbent material by means of a low pressure. Through interaction with functional groups of the solid phase, the target analyte is retained on the sorbent material, while other compounds are eluted with the sample solution. After an optional washing step, the target analyte is eluted from the solid phase, using a different solvent with higher elution strength than the original sample (see Fig. 2.1).
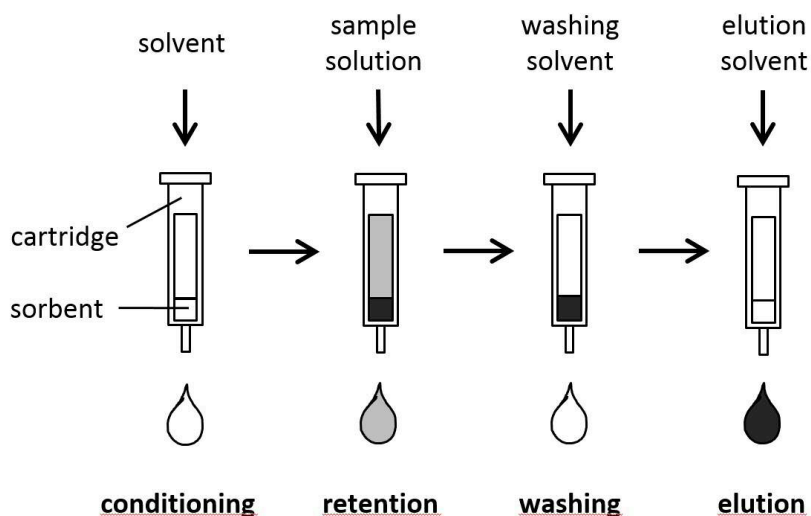

Fig. 2.1 SPE procedure

23

SPE is not only useful for the enrichment of analytes but also for the elimination of certain contaminations, that are retained on the solid phase, whilst the compounds of interest are eluted due to weaker interactions with the sorbent.

Common sorbent materials are silica based materials, modified with different chemical moieties, such as C8, C18, and CN, strong or weak anion or cation exchange materials, or solid phases based on polymer structures with different functional groups. An overview about different solid phase materials and their applicability to certain matrices and analytes is given in Table 2.1. Several comprehensive reviews present the theoretical principles as well as the wide field of applications for SPE in analytical chemistry in more detail [*Hennion*, 1999; *Liška*, 2000; *Poole*, 2003; *Poole et al.*, 2000].

Table 2.1 Common materials used in SPE with corresponding sample matrices and examples for possible analytes (adapted from [*Cammann*, 2001])

SPE modes		Sample Matrix	Analyte polarity	Possible analytes
Reversed Phase	e.g. C18*, C8, CN modified silica	polar, e.g. aqueous solution	nonpolar to moderately polar	hydrocarbons, esters, pesticides
Normal Phase	e.g. silica, diol	nonpolar, e.g. hexane,	polar	alcohols, aldehydes
Ion Exchange e.g. strong anion exchange*	quaternary amine bonded silica with Cl⁻ counterion	polar e.g. aqueous solution	ionic	anions, organic acids

*SPE phase types used in the method presented in this work (see chapters 3 and 4)

2.1.2 Stir bar sorptive extraction

Stir bar sorptive extraction (SBSE) is an equilibrium technique which uses stir bars with polydimethylsiloxane (PDMS) coating (Fig. 2.2). The extraction is based on the partitioning of the solutes between the siloxane phase (stir bar coating) and the aqueous sample. In a second step, the analytes are recovered from the stir bar. This is achieved either by thermal desorption (TD) using a thermal desorption device attached to a GC system or by liquid desorption (LD). In the latter case, the analytes are desorbed by a solvent with higher elution strength than the original sample. LD is compatible with LC-MS analysis and does not require additional hardware.

PDMS coating (film thickness 1 mm)

magnetic rod

glass core

10 mm
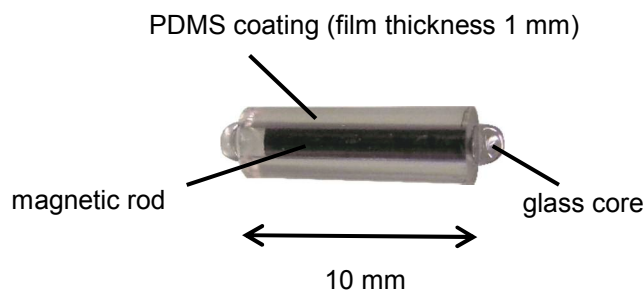
Fig. 2.2 Stir bar for the stir bar sorptive extraction technique

Compared to solid phase micro extraction (SPME), which is based on the same sorptive extraction principle, SBSE requires less technical equipment and can achieve higher extraction efficiency due to a larger volume of the siloxane phase. No time consuming evaporation of the aqueous sample is needed, as the stir bar can be added directly to the sample. SBSE-LD is a "green" extraction technique, because it is less solvent intensive than liquid-liquid extraction (LLE). In contrast to the frequently used solid phase extraction (SPE), SBSE-LD is less labor- and cost-intensive because the stir bars are easy to handle and can be reused multiple times [*Baltussen et al.*, 1999; *David and Sandra*, 2007; *Prieto et al.*, 2010; *Sánchez-Rojas et al.*, 2009].

2.2   High performance liquid chromatography

Due to its high versatility regarding the use of column materials, eluent compositions and detection modes for the analysis of a wide range of compounds, high performance liquid chromatography (HPLC) is one of the most common techniques in analytical chemistry. There are several textbooks dealing with HPLC (e.g., [*Meyer*, 2009]). In this chapter, a short overview on the basic principles of HPLC is given.

The HPLC separation is based on the partitioning of the analytes between a stationary phase in the column and a mobile phase flushed trough the column by means of a high pressure. In reversed-phase (RP)-HPLC, the stationary phase consists of silica gel particles modified with *n*-alkyl chains (C18, C8, C4) or other moieties (hexylphenyl, pentafluorophenyl, CN). Polar eluents, such as H_2O, acetonitrile (ACN), or methanol (MeOH), are used as mobile phase. Therefore, the intensity of the interactions with the stationary phase decreases with increasing polarity of the analytes, so does the retention time. In normal-phase (NP) HPLC, the retention time increases with the polarity of the analytes, as in this case a polar stationary phase (silica gel) and a non-polar mobile phase (hexane) are applied. The use of gradient elution can

enhance the chromatographic separation and help to prevent carry over by starting the chromatographic run at a polar eluent composition and ending it at an eluent composition of the lowest polarity possible as a cleaning step before the next run.

Standard analytical HPLC columns contain particles of 3-5 μm in diameter, and build up a pressure of up to 250 bar, depending on eluent composition, flow rate, and column dimension. A chromatographic run takes 30 min in average. In the last decade, ultra high performance liquid chromatography (UHPLC) has significantly improved LC performance compared to standard HPLC. In UHPLC, sub 2 μm particles are used, which are packed in the column with higher density. This allows the application of short columns (e.g. 50 mm in length), resulting in shorter analysis time (factor 5-10) and increased resolution power. Although the applied flow rates are usually higher than in HPLC, the total solvent consumption is significantly reduced due to the shortening of analysis time. Because of the small particle size and higher packing density, the pressure built up in an UHPLC system is much higher compared to an HPLC system and can reach up to 1000 bar. Therefore, UHPLC systems have to consist of special pumps, tubing, and fittings to resist high pressure conditions.

2.3   Mass spectrometry

2.3.1   Electrospray ionization

Atmospheric pressure ionization methods have become indispensable tools in analytical chemistry as they enable the combination of liquid chromatography and mass spectrometry. Using different types of ionization such as electrospray ionization (ESI), atmospheric pressure chemical ionization (APCI) or atmospheric pressure photo ionization (APPI), API sources have greatly extended the range of compounds accessible for mass spectrometric analyses. High molecular weight, polar, or thermally labile compounds are readily ionized using the relatively "soft" API, whereas conventional techniques such as electron ionization (EI), chemical ionization (CI) or fast atom bombardment are not expedient for this purpose. An overview of the range of analytes accessible is given in Fig. 2.3.

Among all API techniques, ESI is the most extensively used, targeting biomolecules as well as small molecules [*Gross*, 2013]. ESI is based on the formation of gaseous ions from a mist of electrically charged droplets in an electric field. The ESI process can be divided into three main steps: The first step is the formation of droplets at the needle tip connected to the HPLC

outlet. The second step is the decrease in droplet size due to evaporation of the solvent, and the final step is the formation of gaseous ions (Fig. 2.4).
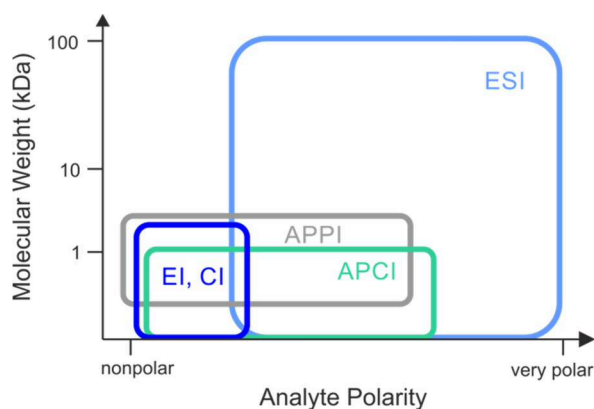
Fig. 2.3 Relative applicability of ionization techniques as function of analyte polarity and molecular weight (adapted from [*Rosenberg*, 2003]). API techniques cover a wide range of analytes concerning analyte polarity and molecular weight.
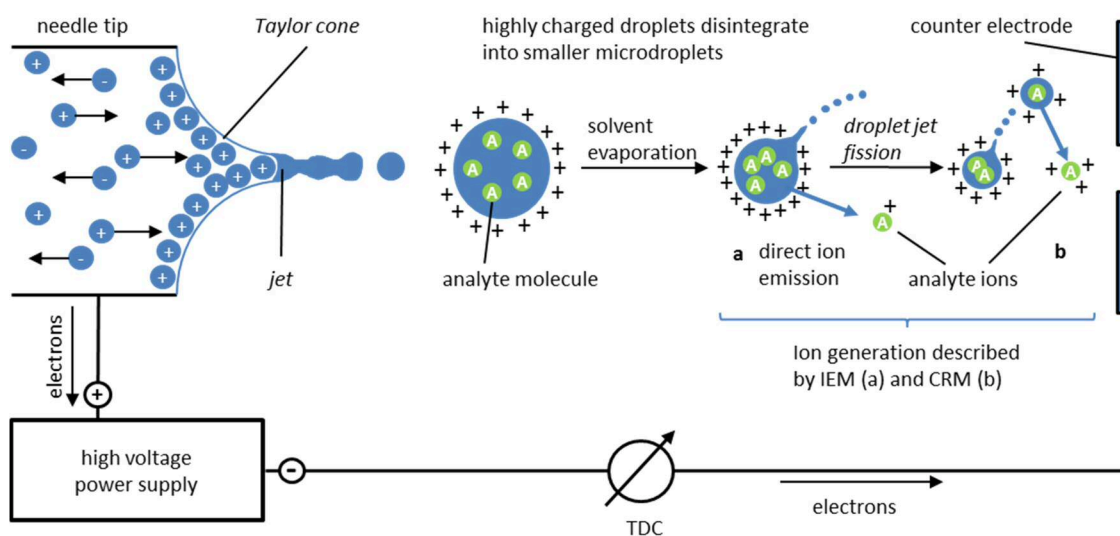
Fig. 2.4 Schematic illustration of the electrospray ionization process. The formation of ions is explained using two models: IEM (**a**) and CRM (**b**) (adapted from [*Gross*, 2013]).

The sample solution coming from the HPLC outlet is led through a metal spray capillary (about 10 µm in diameter), to whose tip a high voltage of about 4 kV is applied. Through the electric field between the tip of the capillary and a counter electrode at the entrance to the mass spectrometer, the ions present in the solution are accelerated towards or away from the counter electrode, depending on their charge. This leads to an excess of ions of the same polarity at the liquid's surface in the tip of the capillary. The meniscus of the liquid forms a

Taylor cone. Once the surface tension is overcome by the electric field, the tip of the *Taylor cone* converts into a *jet* (also called *liquid filament*), that carries a large excess of similarly charged ions. The actual spray emerges through the disintegration of the jet into small droplets, that repel each other because of the like charge. The droplet size is decreased by means of a heated counter gas stream (*Dry-gas*, usually N_2) that causes evaporation of the solvent. When the electrostatic repulsion exceeds the surface tension of the droplet, its size reaches the so called *Rayleigh limit* and a cascading disintegration into smaller units occurs. Like the jet ejected from the *Taylor cone*, several microdroplets are ejected from the parent droplet. This process is called *droplet jet fission.*

The formation of gaseous ions can be explained by two different models: The ion emission model (IEM) assumes the emission of ions from the surface of highly charged microdroplets. It is well suited for describing the formation of small ions (see Fig. 2.4a). The charge residue model (CRM) describes the complete desolvation of ions after successive decrease of the droplet size due to evaporation and droplet jet fission, until a single ionized molecule is left. This model is suited for the describing the ionization of large molecules (Fig. 2.4b).

As with all API techniques, ESI is a very soft ionization technique. This is partly caused by the relatively low temperatures the analyte molecules are exposed to (the desolvation even has a cooling effect), but mainly due to the absence of collision partners like electrons or atoms. Therefore, almost no fragmentation occurs during ESI. Typical ions generated in ESI are protonated ions in the positive mode ($[M+H]^+$ with M = molecule) and deprotonated ions $[M-H]^-$ in the negative mode. Adduct formation mainly occurs in the positive mode ($[M+Na]^+$, $[M+K]^+$, $[M+NH_4]^+$).

A great advantage of ESI towards other ionization techniques is the possibility of forming multiply charged ions. This enables the analysis of large biomolecules, as with a high charge even the high mass of a large biomolecule yields a small *m/z* ratio, accessible for standard mass analyzers. A further advantage of ESI is its ability to work with polar, volatile solvents, such as ACN, MeOH, and water, which are standard solvents in HPLC.

The heated electrospray ionization (HESI) source applied in this work is a new type of ESI source, developed by Thermo Scientific. Prior to spray generation, the solvent flow coming from the HPLC is led through a heated capillary to enhance vaporization. This is very effective especially for eluent compositions with high water content, which are often applied at the beginning of the chromatographic run using gradient elution.

2.3.2 HCT(+) ion trap mass spectrometer

The *HCT(+)* ion trap mass spectrometer used in parts of this work comprises a quadrupole ion trap (QIT). In this chapter, the working principles of this type of mass analyzer are presented [*Gross*, 2013; *Yoshinari*, 2000].

A QIT consists of a ring electrode and two hyperbolic end cap electrodes of which the latter are electrically connected (see Fig. 2.5). Ions can enter the trap through an opening in one of the end cap electrodes and exit it through a second opening in the opposite end cap electrode, to reach the detector (usually a secondary electron multiplier). In order to trap ions in the QIT, a three-dimensional quadrupole field is generated by applying direct current (DC) and radio frequency (RF) potentials to the ring electrode, while keeping the end cap electrodes at ground potential. Equation 2.1 gives the quadrupole field U_{QIT}, where U and V are the amplitudes of the DC and RF alternating current (AC) applied to the ring electrode and ω is the angular frequency.

$$U_{QIT} = U - V cos(\omega t)$$
(2.1)

Depending on the *m/z* ratio of the ions and the applied potential, stable trajectories for the ions are formed inside the trap volume. To enhance sensitivity and resolution, helium is inserted into the QIT as a buffer gas. The ions are focused in the center of the trap, as they lose kinetic energy due to collisional cooling.
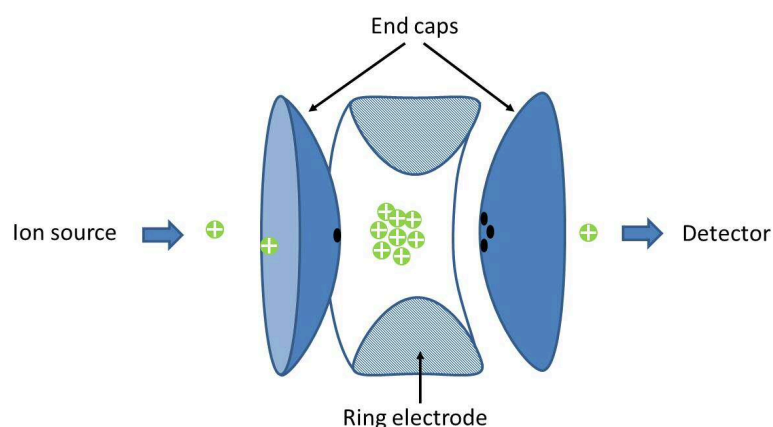
Fig. 2.5 Cross section of an ion trap mass analyzer

The ion trajectories in a three-dimensional quadrupole field can be described by differential equations of the *Mathieu type*, resulting in the *Mathieu parameters* a and q given in Equ. 2.2 and 2.3, where m and e are the ion mass and charge, respectively.

$$a_z = -\frac{8eU}{\omega^2 m r_0^2} \qquad\qquad q_z = \frac{4eV_{RF}}{\omega^2 m r_0^2} \qquad\qquad \textbf{(2.2) + (2.3)}$$

To yield stable ion trajectories in the QIT, i.e. for successful ion storage, radial and axial trajectories have to be stable at the same time. The solutions to the Mathieu equations can be determined using a function of the type $e^{(\alpha+i\beta)}$, with the requirements of α to be zero and the two additional stability parameters for both the radial and axial component, β_r und β_z, to be in the range of 0 to 1. The delimited stability region for ions trapped in the QIT is visualized in Fig. 2.6.
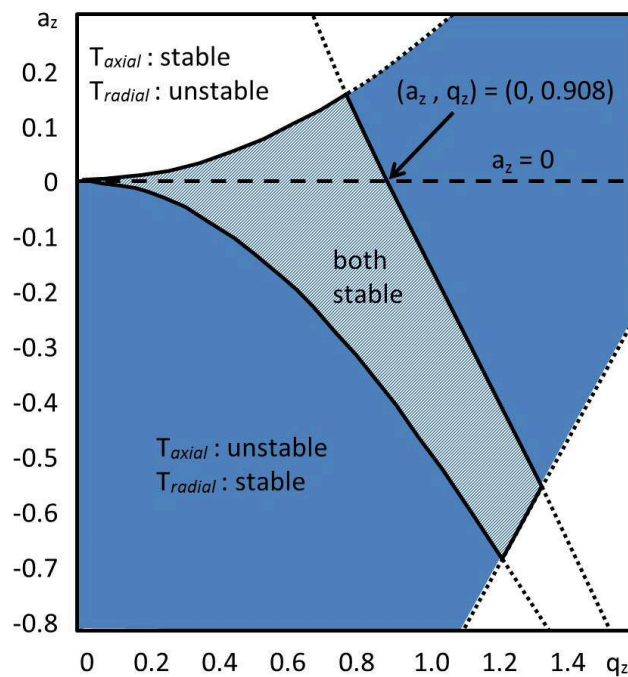
Fig. 2.6 Stability diagram of ion trajectories (T$_{axial}$, T$_{radial}$)

Most QITs are operated in the *mass-selective instability mode,* which means that an RF AC is applied to the ring electrode, while both end cap electrodes are at ground potential. Thus, as no DC current is applied (U=0), the parameter a_z turns zero, and the stability region is reduced to a stability line along the q_z-axis. By raising the AC potential (V), q_z is raised and ions exceed the stability limit at q_z=0.908 in order of increasing *m/z*, meaning they are ejected from the trap as their trajectories become unstable. A second possibility for ejecting ions from the trap (i.e. to perform a scan) is *resonant ejection*. The oscillation of a certain ion can be divided into a radial and an axial secular frequency, both described by the *Mathieu parameters* a and q. By applying an additional RF voltage with matching axial frequency to the end cap electrodes, the

ion is ejected from the trap. Scans based on *resonant ejection* can be carried out from low to high mass and vice versa, therefore this mode can be applied to isolate ions with a certain *m/z* ration in the trap by ejection all ions below and above the targeted mass to charge ratio. Quadrupole ion traps are capable of performing all steps of tandem MS analysis subsequently in the volume of the ion trap, which is why they are also called tandem-in-time mass analyzers. The ions of interest are isolated in the ion trap and dissociated by collision-induced dissociation (CID) with helium atoms present in the trap. The resulting product ions can either be analyzed as a complete fragment spectrum or distinct ions can be isolated to perform further MS/MS experiments. Depending on the initial intensity of the parent ion, several MS/MS cycles (MS^n) are possible. Tandem MS experiments are a very helpful tool for structure elucidation.

2.3.3 Q-Exactive hybrid quadrupole-orbitrap mass spectrometer

The Q-Exactive hybrid quadrupole-orbitrap mass spectrometer allows qualification and quantification of compounds using high resolution, accurate mass (HRAM) detection. Fig. 2.7 shows a schematic view of the instrument. The ions generated in the ion source (**1**, HESI or APCI) are focused by a lens stack (**2**) and are further transmitted by a bent flatapole (**3**) before they enter the quadrupole (**4**) for optional precursor ion selection. The (selected) ions are focused in the C-trap (**5**), from where they are either directly transmitted to the orbitrap (**6**) for HRAM detection or led into the higher-energy collisional dissociation (HCD) cell (**7**) for fragmentation. The resulting product ions are focused in the C-trap before being transmitted to the orbitrap for detection.

The orbitrap consists of a central, spindle-shaped electrode and an outer, barrel-shaped electrode, which is composed of two parts, separated by an isolating ceramic ring (Fig. 2.8). The ions are trapped in the orbitrap by means of an electrostatic field, which forces the ions to oscillate around the central electrode on complex orbits. This movement is a combination of a rotational movement around the central electrode and an axial oscillation along the axis of the electrode. The axial oscillation is induced by the electrostatic field gradient, as the ions are injected tangentially into the trap from a peripheral point.
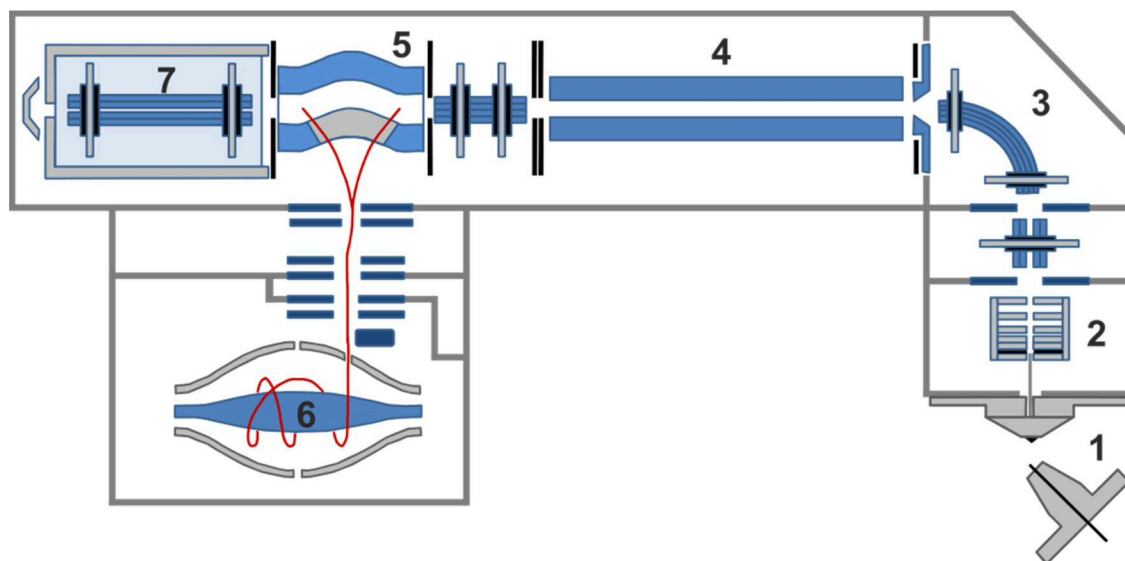
Fig. 2.7 Schematic view of the Q Exactive hybrid quadrupole-orbitrap mass spectrometer used in this work. The marked components are the ion source region (1), lens stack (2), bent flatapole (3), quadrupole (4), C-trap (5), orbitrap (6) and HCD cell (7) (adapted from [*Thermo Fisher Scientific*]).
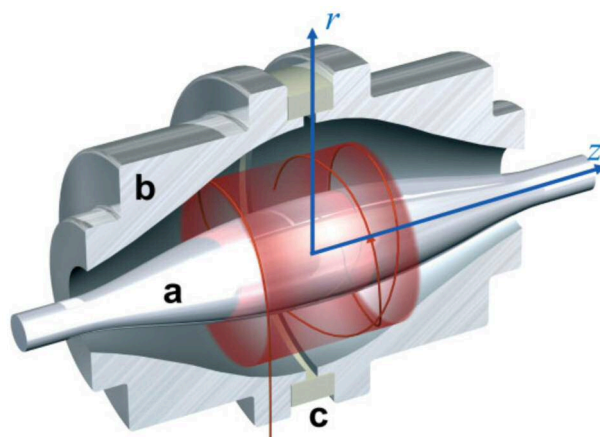
Fig. 2.8 Cross section of the Thermo Fisher Orbitrap™. The Orbitrap consists of a spindle-shaped central electrode (**a**) and a barrel-shaped outer electrode, which is composed of two parts (**b**), separated by a ceramic ring (**c**). The movement of the ions along the z-axis is highlighted [*Scigelova and Makarov*, 2006].

The frequency (ω_{axial}) of the axial oscillation does not depend on the tangential velocity or the special distribution of the circulating ions, but on their *m/z* ratios (see Equ. 2.4).

$$\omega_{axial} = \sqrt{k\left(\frac{z}{m_i}\right)} \tag{2.4}$$

Therefore, all ions move with the same amplitude, but with different frequencies depending on their *m/z* ratios. As the ions are orbiting in the trap, they induce an image current in the

two parts of the outer electrode, which is detected and multiplied. The image current is converted by *fast Fourier transform* to yield a mass spectrum [*Gross*, 2013].

The instrument has a maximum resolution power of 140,000 at *m/z* 200 and a mass accuracy of <3ppm with external and <1ppm with internal calibration, in the latter case using a certain lock mass for internal mass calibration during the measurement. To reach a performance like this, the transient time of the ions in the trap has to be long enough to enable the successful recording of the image current signal. By applying an ultrahigh vacuum (UHV), the mean free path of the ions is sufficiently extended to allow them orbiting around the central electrode ten to hundred thousand times. The injection into the trap is another crucial step, as the ions gain their velocity only from being injected peripherally into the orbitrap. To guarantee a reproducible injection, concerning geometrical, temporal, and energetical requirements, the ions are trapped, accumulated, and thermalized in a bent quadrupole called C-Trap (see Fig. 2.7), from where they are injected into the orbitrap as a distinct ion package using electrostatic lenses [*Gross*, 2013].

3   METHOD DEVELOPMENT: GLYOXAL AND METHYLGLYOXAL

Method development for the quantification of glyoxal and methylglyoxal in aqueous samples by Stir Bar Sorptive Extraction and Liquid Desorption-HPLC-ESI-MS

3.1   Introduction

The analysis of carbonyl compounds usually comprises a derivatization step. This is crucial regarding GC analyses as it improves volatility and stability of the analytes, for example. A commonly used derivatization approach is pentafluorobenzyl hydroxylamine (PFBHA) derivatization with GC-ECD detection [*Bao et al.*, 1998]. A study using PFBHA derivatization in combination with GC-MS was recently presented for the analysis of glyoxal (G) and methylglyoxal (MG) in seawater and marine aerosol [*van Pinxteren and Herrmann*, 2013]. Derivatization with BF_3/*n*-butanol, which yields the corresponding dibutyl acetals, was applied for the measurement of G and MG in rain and snow, also using GC and GC-MS [*Kawamura*, 1993].

However, with the continuous development of atmospheric pressure ionization (API) techniques such as electrospray ionization (ESI), the number of applications using LC and LC-MS has increased enormously over the last decades. The possibility of using various column materials, eluent compositions, and detection modes makes LC(-MS) a promising tool to meet the increasing needs of analytical measurements. Although not obligatory, derivatization is a powerful strategy to enhance the capabilities of LC(-MS) in various ways, i.e., concerning chromatographic, ionization, and detection properties [*Xu et al.*, 2011]. The most frequently used derivatization reagent for the analysis of carbonyl compounds with LC is 2,4-dinitrophenylhydrazine (DNPH) [*Kampf et al.*, 2011; *Wang et al.*, 2009]. A selective derivatization of α-dicarbonyls was also achieved using aromatic diamino compounds such as 2,3-diaminonaphthalene (DAN). The resulting highly fluorescent derivatization products were quantified using fluorescence detection [*Neng et al.*, 2007]. Dansylacetamidooxyamine derivatization with LC-fluorescence detection was used for the highly sensitive analysis of α-dicarbonyls and hydroxyacetaldehyde as well as monoaldehydes [*Houdier et al.*, 2011].

The aim of this study was the development of a new simple LC-MS method for the sensitive quantification of G and MG in snow and ice. Stir bar sorptive extraction (SBSE, see chapter 2.2) with in situ derivatization is applied for extraction and enrichment of the analytes.

3.2 Experimental section

3.2.1 Chemicals and materials

G and MG (40 % (*w*) aqueous solutions) were purchased from Acros Organics (Thermo Fisher Scientific, Geel, Belgium). *O*-benzyl hydroxylamine hydrochloride (BHA·HCl, 99 %), *O*-(2,3,4,5,6-pentafluorobenzyl)hydroxylamine hydrochloride (PFBHA·HCl, GC derivatization grade), 4-fluorobenzaldehyde (98 %), sulfuric acid (95-98 %), dichloromethane (HPLC grade), acetonitrile (HPLC gradient grade), and formic acid (LC-MS grade) were purchased from Sigma-Aldrich (Steinheim, Germany). Hydrochloric acid (30 %) was obtained from Merck (Darmstadt, Germany). Sodium hydroxide was purchased from Carl Roth (Karlsruhe, Germany). Sodium chloride (HPLC grade) was purchased from Fisher Chemical (Geel, Belgium). Ultrapure water (18.3 MΩ cm) was obtained using a Milli-Q water system from Millipore (Bedford, USA). PDMS coated stir bars (Twister®, film thickness 1 mm, length 10 mm) were purchased from Gerstel (Mülheim, Germany). SPE cartridges (Discovery DSC-18, 1 mL, 100 mg bed weight) were purchased from Supelco (Sigma-Aldrich, Steinheim, Germany).

3.2.2 Reduction of blank values

The small α-dicarbonyls G and MG are ubiquitous compounds because they originate from various sources, either by direct emission or by formation from biogenic as well as anthropogenic precursors. Therefore the focus of the method development was on the reduction of contamination levels. G and MG are likely to be incorporated into the sample preparation procedure through contaminated materials such as glass vessels and pipette tips as well as reagents. Irregularly appearing blank values were attributed to insufficiently cleaned glass vessels, whereas the initially observed high background levels of Glyoxal and Methylglyoxal were attributed to insufficient chemical purity of the commercially obtained derivatization reagent.
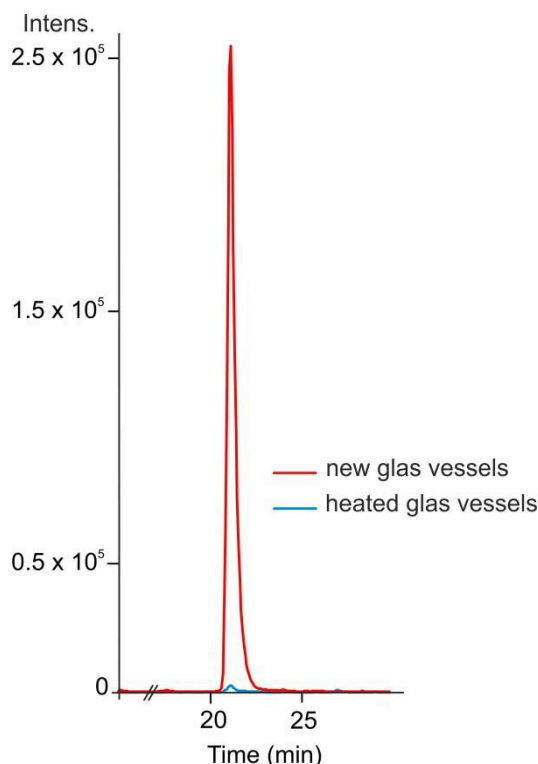
Fig. 3.1 Extracted ion chromatograms (EIC) of G-bis-BHA (MRM transition m/z 269 →91, ESI(+) mode) in a solution of 100 µL BHA (8.5 mM) in 15 mL of ultrapure water using new glass vessels (red) or heated vessels (blue). The background signal of G-bis-BHA can be reduced significantly by heat treatment.

3.2.2.1 Glass vessels

Contamination levels of new glass vessels were compared to those from pre-cleaned, heated glass vessels (Fig. 3.1), revealing a significant reduction in blank value for the latter. The blank value could also be reduced by rinsing the vessels with different solvents multiple times. Yet, as this unnecessarily raised the method's workload and the solvent consumption per sample, the heating approach was applied. All glass vials (sample flasks, extraction vials, liquid desorption vials and storage vials) were flushed with ultrapure water and cleaned by heating at 450 °C for 8 h prior to use.

3.2.2.2 Preparation and clean-up of derivatization solution

As the derivatization reagent benzylhydroxylamine hydrochloride (BHA·HCl) was not commercially available in high purity and was contaminated with MG in particular, purification was essential. BHA·HCl was purified adapting a method described by Matsunaga and Kawamura [*Matsunaga and Kawamura*, 2000]. Briefly, BHA·HCl was dissolved in ultrapure water. Sodium hydroxide pellets were flushed with MeOH and added to the solution. Free

benzylhydroxylamine was extracted with dichloromethane and precipitated as BHA·HCl by adding 8 M HCl solution. The precipitate was filtered and dried under reduced pressure.

A stock solution was prepared by diluting 125 mg purified BHA·HCl in 20 mL ultrapure water. The stock solution was stored at 4 °C. It was stable over several months, for neither visible changes of the solution nor changes in derivatization efficiency were observed. To further reduce the contamination level of the derivatization solution, an aliquot of the stock solution was purified SPE with a C18 stationary phase prior to sample preparation: The SPE cartridge was conditioned with 2x800 µL ACN and washed with 2x800 µL ultrapure water. Four milliliters of the BHA solution were applied to the cartridge by means of a low pressure to retain possible contaminants. The eluted solution was collected and applied for derivatization on the same day.

3.2.3 SBSE procedure

Prior to use, the stir bars were put in glass vials filled with 2-3 mL ACN and cleaned in an ultrasonic bath for 30 min before stirring in 3 mL fresh ACN at 1,000 rpm overnight. These cleaning steps were repeated after every analysis to avoid carry over.

For extraction, spiked water samples (for calibration) or environmental samples were filled into 20 mL screw-cap vials with PTFE-septa. One hundred fifty microliters of internal standard solution (4-fluorobenzaldehyde) and 100 µL of derivatization solution (BHA) were added. The pH was adjusted to 3.5 with 0.1 M sulfuric acid. The stir bars were removed from the storage vials using magnetic rods, dried carefully with a lint-free tissue and added to the sample solution. The vials were closed tightly and put on a 15-point magnetic stirring plate for 20 h at 1,000 rpm. After extraction, stir bars were removed from the extraction solution and transferred into 5 mL vials containing 1.5 mL ACN as stripping solvent for liquid desorption. After stirring for 3 h at 500 rpm, the stir bars were removed from the vials. The desorption solution was transferred to an autosampler vial and provided for analysis. Stir bars were cleaned as described above and stored in ACN until further use. An overview of the SBSE-LD procedure is shown in Fig. 3.2. During method development, several important SBSE parameters such as extraction time (2-20 h), liquid desorption time (0.5-20 h) and solvent (MeOH, ACN) were optimized.
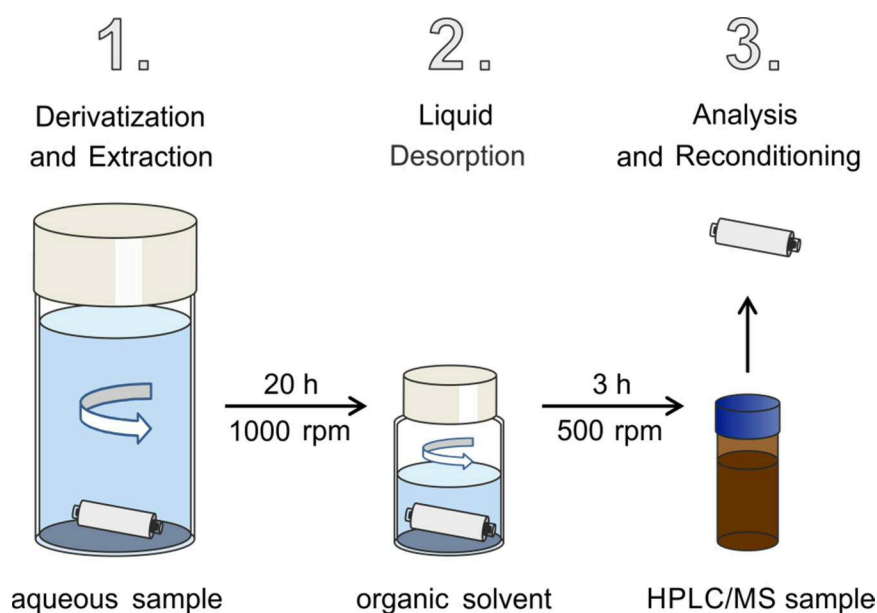
Fig. 3.2 Sample preparation using SBSE

3.2.4 Liquid chromatography – mass spectrometry

The HPLC-ESI-MS/MS measurements were carried out using a HPLC system (Agilent 1100 series, composed of degasser, binary gradient pump, auto sampler, column oven, and diode array detector, Agilent Technologies, Germany) coupled to a HCT-Plus ion trap mass spectrometer (Bruker-Daltonics, Bremen, Germany). The analytical column (Pursuit XRs 3 C8 150x2.0 mm, 3 µm particle size, Varian, Germany) was heated to 30 °C during analysis. Eluent A (ultrapure water with 2 % ACN and 0.04 % formic acid) and B (ACN with 2 % ultrapure water) were used in gradient mode with a constant flow rate of 200 µL/min. The gradient started with an eluent composition of 50 % B. The fraction of B was raised to 99 % within 30 min and held at 99 % for 10 min. An equilibration time of 20 min was needed to reestablish the starting conditions for the next run. The injection volume was 20 µL.

The ESI source was operated in positive ion mode with 35 psi nebulizer pressure, 9 L/min dry gas flow (both N_2), 350 °C dry gas temperature, and 4.5 kV capillary voltage. All other electronic parameters were set using the smart tune option for the respective *m/z* values of the analyte molecular ions. Analysis was performed using the multi reaction monitoring (MRM) mode which significantly reduces background noise: The protonated molecular ions $[M+H]^+$ of the derivatization products (*m/z* 269 and *m/z* 283 for glyoxal-bis-oxime and methylglyoxal-bis-oxime) were isolated and fragmented in the ion trap using CID. Helium was used as collision gas with an optimized fragmentation amplitude of 0.7 (specific parameter of the instrument).

The most abundant fragment ions (*m/z* 91 for both glyoxal-bis-oxime and methylglyoxal-bis-oxime) were monitored and used for quantification.

3.2.5 Preparation of standards for quantification

Stock solutions of G and MG with concentrations of 506 and 471 ng/mL, respectively, were prepared daily by diluting the commercially available solutions with ultrapure water. To obtain method development and calibration solutions, volumes of 15 mL ultrapure water were spiked with distinct volumes of G (or MG) stock solution and 5.7 µg/L of the internal standard. The spiked solutions were treated as described in the "SBSE procedure" section above. That way, the calibration standards run through the whole extraction procedure just like the real samples and analyte loss during extraction or liquid desorption is corrected for. Besides, there was no need for synthesizing the bis-oximes (which are not commercially available) as they were formed during the extraction/derivatization process.

For each analyte, five calibration standards were prepared with spiked amounts of G (or MG) ranging from 1 to 60 ng. Blank measurements (n=5) were conducted using 15 mL of ultrapure water to obtain values for the evaluation of the analytical limits and determine contamination levels of glassware, reagents, and stir bars.

3.2.6 Sampling

Snow samples were collected on a field next to the Meteorological Observatory at Hohenpeissenberg on Mount Hohenpeissenberg (977 m a.s.l., 47°48'N, 11°00'E) in Bavaria, Germany. Preheated 500 mL glass sample flasks were filled with snow and sealed firmly using screw caps with PTFE-coated septa. Samples were collected in triplicate from the surface and from 30 cm depth.

Ice core samples were obtained from a 125 m long ice core from the upper Grenzgletscher, Monte Rosa massif (4,200 m a.s.l., 45°55' N, 7°52' E) in the southern Swiss Alps. Drilling and storing conditions as well as glaciochemical dating of the ice core are described elsewhere (see [*Eichler et al.*, 2000a; *Eichler et al.*, 2000b]). Samples from two different years (1959 and 1991) were analyzed as a proof of principle.

After collection, all samples were kept frozen and stored at -20 °C. On the day of analysis, the samples were thawed at room temperature and analyzed immediately to prevent any kind of decay.

3.3 Results and discussion

3.3.1 Method development

3.3.1.1 Derivatization

The SBSE efficiency of a particular analyte can be estimated using the octanol/water partitioning coefficient ($K_{O/W}$) which is a reliable approximation for the partitioning coefficient between the PDMS phase and water ($K_{PDMS/W}$). Together with the phase ratio (V_{Water}/V_{PDMS}) the value of $logK_{O/W}$ is used to determine the recovery of a certain analyte. Using commercially available stir bars with PDMS volume of 124 μL, only analytes with $logK_{O/W}$ of>3 can be extracted with a recovery higher than 80 % [*David and Sandra*, 2007]. Because G and MG exhibit very low $logK_{O/W}$ values (-0.69 and -0.58 for G and MG, respectively), extraction of G and MG with PDMS coating does not prove satisfactory. Therefore, derivatization was applied to convert the analytes into less polar bis-oximes ($logK_{O/W}$ 3.40 and 3.69 for G-bis-BHA and MG-bis-BHA, respectively). The $logK_{O/W}$ values were calculated using ALOGPS 2.1 [2005; *Tetko et al.*, 2005].

Previous experiments also revealed that the analytes in their underivatized form showed poor chromatographic separation on a reversed phase HPLC column and low ionization efficiencies during ESI [*Kampf et al.*, 2011]. Conversion into larger and less polar compounds improved chromatographic properties and ionization efficiencies.
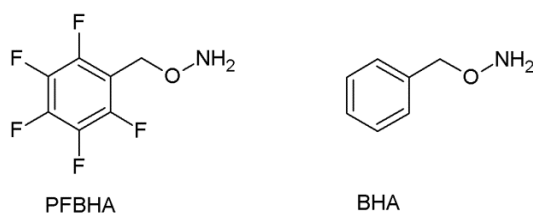
Fig. 3.3 Derivatization reagents tested during method development

The most frequently used derivatization reagent for carbonyl compounds in combination with LC is DNPH. DNPH is soluble only in diluted strong mineral acids, but strong acidic conditions may damage the stir bar's PDMS coating. Hence, the water soluble derivatization reagents PFBHA (*O*-(2,3,4,5,6-pentafluorobenzyl)hydroxylamine) and BHA (*O*-benzylhydroxylamine) were tested (Fig. 3.3). PFBHA is a common derivatization reagent for GC analyses and therefore available in high purity, which eliminates the need for purification. Nevertheless, both G and MG PFBHA-derivatives showed strong variations in ionization efficiency with

unacceptably high relative standard deviation (RSD) values up to 60 % in triplicate measurements. Better results were obtained using BHA as derivatization reagent (RSD<12 %), although purification is necessary because it is not commercially available in GC derivatization grade like PFBHA.

In the aqueous sample, the free form of G and MG is in equilibrium with hydrated monomeric and oligomeric forms. During derivatization, the derivatization reagent is used in excess (10,000 fold excess compared to a glyoxal concentration of 1 ng/mL) and under acidic conditions (pH 3.5) to ensure that the equilibrium is shifted towards the free monomeric form, which is accessible for the derivatization. That way, the measurements comprise the sum of free monomeric, hydrated, and reversibly formed higher oligomeric compounds [*Houdier et al.*, 2011; *Kampf et al.*, 2012].
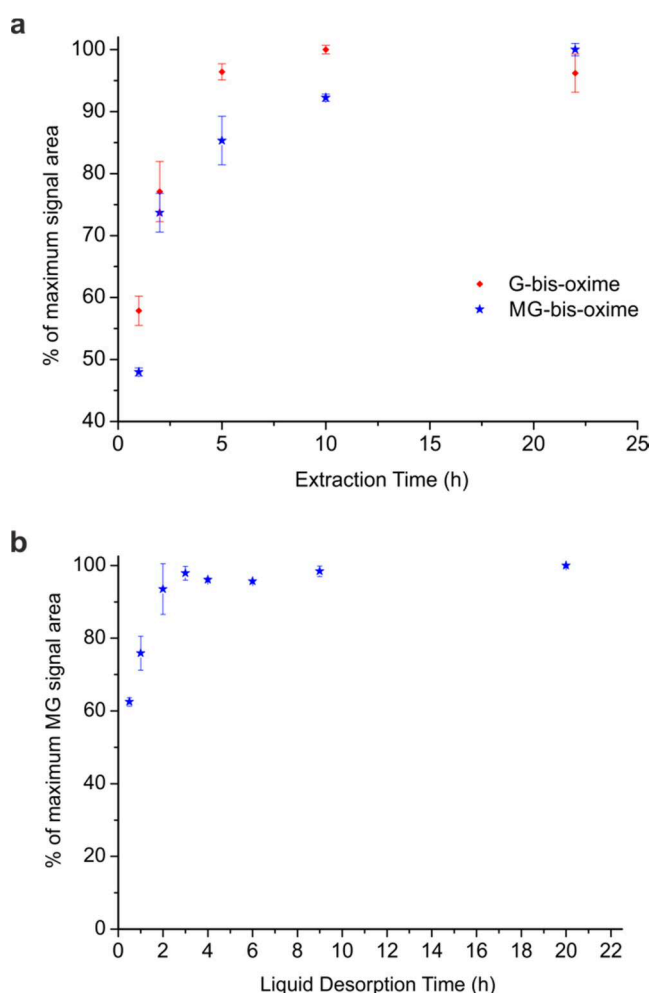
Fig. 3.4 Optimization of extraction time (a) and liquid desorption time (b)

3.3.1.2 Time course of extraction and liquid desorption

Because SBSE is an equilibrium technique based on the partitioning of the analyte between the aqueous phase and the PDMS phase, the stirring times to reach equilibrium during extraction and liquid desorption were determined. Different extraction times (1, 2, 5, 10, and 22 h) were tested for both G- and MG-bis-oximes. A stirring speed of 1,000 rpm was used and liquid desorption parameters were set as follows: stirring time 3 h, stripping solvent 1.5 mL ACN, stirring speed 500 rpm.

As shown in Fig. 3.4a, in case of G, the equilibrium is reached after about 10 h, whereas for MG, a longer extraction time up to 22 h is needed. Therefore, an optimal extraction time of 20 h is used, which furthermore allows extraction overnight. As the curve for the extraction of both analytes is similar, liquid desorption time was optimized using only MG. An extraction time of 20 h, stripping solvent of 1.5 mL ACN and stirring speed of 500 rpm was applied. Liquid desorption times of 0.5, 1, 2, 3, 4, 6, 8, and 20 h were tested. The equilibrium is reached after about 3 h with no significant change at longer stirring times, so 3 h is determined as optimal liquid desorption time (Fig. 3.4b).

3.3.1.3 Liquid desorption solvent

MeOH and ACN were tested as stripping solvents for liquid desorption. Using ACN, higher signal areas of the bis-oximes were obtained, therefore ACN was chosen as the stripping solvent in further optimization steps. A volume of 1.5 mL is needed to completely immerse the stir bar in the stripping solvent and to ensure that it is covered while stirring. For the same reason, the stirring speed was adjusted to 500 rpm during liquid desorption (instead of 1,000 rpm during extraction).

3.3.1.4 Additional optimization

Ionic strength and pH of the sample solution play an important role in the efficiency of the SBSE process. Derivatization is also influenced by pH which makes the process more complex. To ensure equal conditions for all samples and standards, they were acidified to a pH of about 3.5 with sulfuric acid prior to SBSE.

The influence of ionic strength on the extraction process was evaluated by adding 5-30 wt% NaCl to the aqueous sample solutions. No significant change in SBSE efficiency was observed. Therefore, no NaCl addition was applied in the method.

3.3.1.5 Sample volume

The effect of different sample volumes on extraction efficiency was determined by spiking a distinct volume of a standard solution containing G and MG to different volumes (5–70 mL) of ultrapure water. No significant differences in signal area were observed; hence, in the chosen volume range, the efficiency of the SBSE-LD process is independent of the sample volume, which can be adjusted depending on the expected concentration of the analytes in the environmental sample.

3.3.1.6 Chromatographic separation and MS

The HPLC parameters were optimized for baseline separation and short retention times of G- and MG-bis-oximes. Separation was tested using C18, C8, and phenylhexyl columns. The best results based on peak shape and short retention time were obtained using a C8 column with gradient elution, heated to 30 °C. Electrospray and MS parameters were optimized for maximum signal intensity in the positive mode. Selectivity of the detection was enhanced using MRM. During an MRM cycle, a targeted parent ion is isolated in the ion trap mass analyzer, followed by CID (helium as collision gas) and isolation of a particular daughter ion from the resulting fragmentation spectrum.
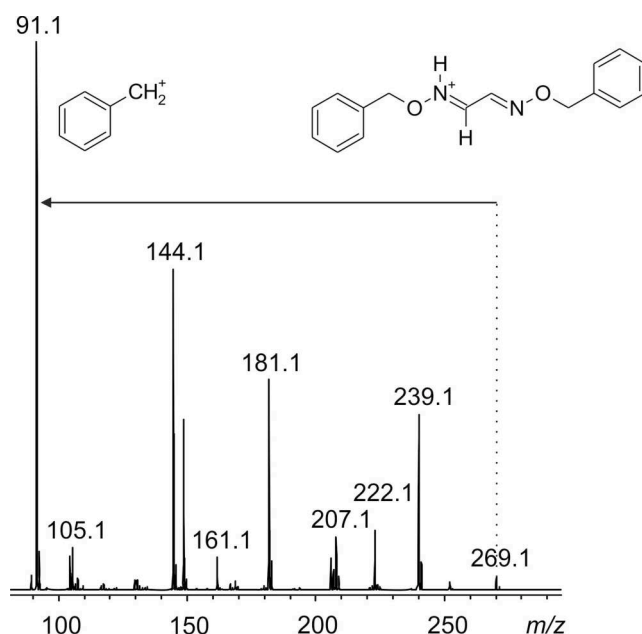
Fig. 3.5 MS² spectrum of G-bis-BHA. The most abundant fragmentation to the fragment used for quantification (m/z 91) is highlighted.

This daughter ion is used for quantification. The same cycle is successively repeated for the three parent ions *m/z* 269 (G), *m/z* 283 (MG), and *m/z* 230 (internal standard) multiple times during the chromatographic run. In initial MS/MS experiments, the fragment *m/z* 91 was identified as the most abundant product ion of both G- and MG-bis-oxime (see Fig. 3.5 for a fragment spectrum of G-bis-oxime). Therefore *m/z* 269→*m/z* 91, *m/z* 283→*m/z* 91 and *m/z* 230→*m/z* 91 (for G, MG, and internal standard) were used as product ion transitions in MRM mode (see Fig. 3.6).
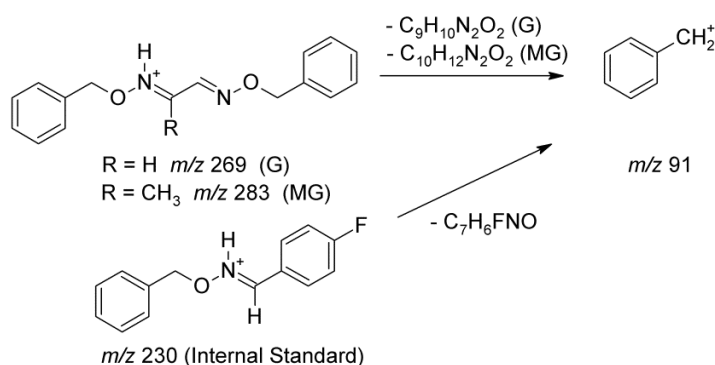
Fig. 3.6 Fragmentation of the precursor ions [M+H]$^+$ of the analytes G-bis-oxime and MG-bis-oxime and the internal standard oxime to yield the product ion used for quantification

3.3.2 Validation

Calibration functions for G and MG were obtained by linear regression analysis. Calibration parameters are summarized in Table 3.1. To determine the instrumental limits of detection and quantification, the standard deviation of the blank samples (n=5) was multiplied by 3 and 10, respectively, and divided by the slope of the linear regression function. Instrumental limits of detection (ILOD) based on the amount of analyte in the liquid desorption extract were 242 and 213 pg/mL for G and MG. Method limits of detection and quantification based on a sample volume of 15 mL were 16 and 54 pg/mL for G and 14 and 47 pg/mL for MG, respectively.

Table 3.1 Calibration data for the quantification of G and MG

	Slope[a]	Intercept[a]	R^2	Recovery (%)	ILOD (ng/mL)	ILOQ (ng/mL)
G	0.037	-0.018	0.9988	78.9±5.6	0.242	0.807
MG	0.025	-0.034	0.9941	82.7±7.5	0.213	0.711

[a] Determined using the measured signal area quotient (analyte/internal standard)

To determine the recovery of the analytes, snow samples were spiked with G and MG at three different concentration levels (5–15 ng/mL) and analyzed in triplicate. The masses of the spiked samples were corrected by subtracting the masses of the unspiked snow sample and then compared to the nominal spiked masses. The results of the different spike levels were averaged to determine the recovery of the respective target compound. Recoveries were 78.9±5.6 % for G and 82.7±7.5 % for MG, respectively. Method inter-batch precision was evaluated by calculation the RSD in percent from different triplicate analyses of snow and ice samples measured on different days. A precision of 7.2±4.9 % for G and 11.4±5.9 % for MG was determined. Intra-batch precision was determined by analyzing an ice core sample in triplicate on the same day and gave 2.5 % for G and 5.5 % for MG, respectively.

3.4 Application

The performance of the described method was tested by analyzing fresh snow samples from Hohenpeissenberg, southern Germany, and ice core samples from Upper Grenzgletscher in the southern Alps, Switzerland. G was detected in both snow samples and ice core samples and MG was detected in the snow samples and one of the ice core samples. Snow samples were collected from the surface and from a layer in 30 cm depth in triplicate with a meltwater sample volume of 5 mL used for analysis. Concentrations (corrected for recovery) were 16.3±1.2 ng/g (280.8±20.7 nM) for G and 3.5±0.4 ng/g (48.6±5.6 nM) for MG in the surface snow samples. Similar concentrations were found in the layer 30 cm below the surface (15.4±1.4 ng/g for G and 3.6±0.3 ng/g for MG, respectively), indicating no age difference between the two layers. The obtained concentrations are in the same order of magnitude as concentrations reported in other field studies from urban and rural areas: 200–7100 nM for G and 30–60 nM for MG ([*Gunz and Hoffmann*, 1990], sampled in southern California), 44.8 and 25.0 nM for G and MG in Tokyo snow ([*Kawamura*, 1993], converted from micrograms per liter values). Concentrations reported in this study are one order of magnitude higher than those found in remote, polar areas, i.e., 13.9 and 6.9 nM for G and MG in Greenland snow [*Kawamura*, 1993] and 13.9–37.1 nM and 1.9–6.5 nM for G and MG in surface snow from Barrow, Alaska [*Houdier et al.*, 2011]. This can be explained by the much longer distance between polar regions and possible emission regions of G and MG or their precursors.

Ice core samples from two different years (sample 1: 1959, sample 2: 1991) were analyzed. Resulting concentrations were 0.178 ng/g (3.06 nM) for G and 0.126 ng/g (1.75 nM) for MG in

sample 1 and 0.085 ng/g (1.46 nM) for G in sample 2 with MG below detection limit. The meltwater sample volume used for analysis was 15 mL. The concentration values are in the same order of magnitude as reported in a field study focusing on the chemical composition of a Greenland ice core (0.023–1.14 ng/g for G and 0.031–1.36 ng/g for MG, [*Kawamura et al.*, 2001b]).

The concentrations measured in the ice core are much lower (almost two orders of magnitude for G) than the concentrations in the fresh snow samples. Obviously, as this is only a limited dataset, it is not possible to draw reliable conclusions regarding the fate of G and MG in the snow or ice samples; however, the described analyses show the good applicability of the method to the given issue of detecting small and even trace amounts of G and MG in snow and ice core samples.

3.5   Conclusion

We have described the development and optimization of a new, sensitive, and selective method using stir bar sorptive extraction with liquid desorption and HPLC-MS/MS to quantify the α-dicarbonyls glyoxal and methylglyoxal in molten ice and snow. Key SBSE parameters such as extraction and liquid desorption time, derivatization, salt addition, and desorption solvent were optimized. Method detection limits were in the low pg/mL-range. The method was successfully applied to snow and ice core samples from the Alpine region. For snow samples, a sample volume of only 5 mL is sufficient; for less concentrated samples like ice cores, the sample volume can be adjusted to larger volumes (e.g., 15 mL) without loss of extraction efficiency.

Analyses of snow samples from different depth and location may give hints for the interaction of G and MG between snow and atmosphere. A larger dataset is needed improve the understanding of the complex processes occurring in the snowpack. Historic records of G (and MG) in ice cores can give hints concerning the oxidative capacity of the atmosphere, as the analytes are tracers of VOC oxidation chemistry and SOA. Besides, ice core data may be of great benefit especially in connection with other marker compounds of biogenic and anthropogenic origin to get information on qualitative and quantitative changes of emission sources over time.

4 METHOD DEVELOPMENT: DICARBOXYLIC ACIDS

Development of a new method for the quantification of (di)carboxylic acids in ice core samples using SPE-(U)HPLC-ESI-HRMS

4.1 Introduction

Monocarboxylic acids and dicarboxylic acids were found to be important constituents of SOA [*Chebbi and Carlier*, 1996; *Decesari et al.*, 2000; *Grosjean et al.*, 1978; *Saxena and Hildemann*, 1996; *Seinfeld and Pankow*, 2003]. Especially dicarboxylic acids exhibit potential CCN activity due to their hygroscopic properties and may affect the chemical and physical properties of organic aerosols [*Sun and Ariya*, 2006]. Hence, their determination is of great interest to examine both present-day and historic SOA composition, investigating wet precipitation samples and ice core samples, respectively.

The most common analytical technique for the analysis of dicarboxylic acids in aqueous environmental samples is GC with flame ionization detection or MS detection. To enable GC(-MS) analysis, the conversion of (di)carboxylic acids into less polar derivatives with higher volatility and stability is necessary. GC with boron trifluoride (BF$_3$)/*n*-butanol derivatization was employed for the analysis of C$_2$-C$_{10}$ dicarboxylic acids in rain [*Kawamura et al.*, 1985; *Sempéré and Kawamura*, 1996], snow [*Sempére and Kawamura*, 1994], and ice samples [*Kawamura et al.*, 2001b]. BF$_3$/methanol derivatization was applied for the investigation of *o*-phthalic acid in snow samples [*Zuo et al.*, 2011].

In recent years, HPLC (-MS) has proved an attractive alternative to GC(-MS), especially due to the possibility of using soft ionization techniques, such as ESI for the detection of high molecular weight and polar compounds. Another benefit of HPLC is its high versatility concerning column materials and eluent compositions, also comprising UHPLC for fast separation. Although not obligatory, the use of a derivatization combined with HPLC may further enhance the capabilities of LC(-MS), e.g. concerning chromatographic, ionization, and detection properties [*Xu et al.*, 2011]. HPLC-MS was employed for the analysis of dicarboxylic acids (≥C$_5$) in Alpine snow [*Kippenberger et al.*, 2008; *Winterhalter et al.*, 2009]. Nevertheless, this method is not suited for low molecular weight dicarboxylic acids, as they show poor

chromatographic separation in RP-HPLC due to their small size and high water solubility. Besides, their ionization efficiency during ESI is very low, as these compounds easily decompose through decarboxylation. This especially applies to oxalic acid, which is a molecule basically consisting of two carboxyl groups attached to each other. Small dicarboxylic acids can be analyzed using ion chromatography [*Legrand and Angelis*, 1995], which is again not suitable for larger dicarboxylic acids.

However, by using a derivatization technique, it is possible to extend the range of dicarboxylic acids accessible by HPLC-MS, as the resulting derivates are more stable and can be efficiently ionized by ESI. Besides, the decrease in polarity leads to enhanced chromatographic properties in RP-chromatography compared to the original compounds. Studies reporting an HPLC derivatization approach use *o*-phenylenediamine derivatization [*Steinberg et al.*, 1985] and esterification with *n*-butanol/acetyl chloride [*Elgstoen*, 2008], both for investigating oxalic acid. The former approach is limited to oxalic acid due to structural requirements, because two vicinal carbonyl moieties are needed to obtain the bicyclic quinoxilinol derivative.

As the analytes are only present in trace amounts in ice core samples, enrichment has to be performed prior to analysis. Additionally, extraction from the aqueous phase is necessary, as the derivatization is not possible in an aqueous matrix, in most cases. The studies based on the BF_3/alcohol protocol from Kawamura et al. [*Kawamura et al.*, 2001b; *Kawamura et al.*, 1985; *Sempére and Kawamura*, 1994; *Sempéré and Kawamura*, 1996; *Zuo et al.*, 2011] employ an initial evaporation step of the aqueous sample at 50 °C using a rotary evaporator prior to derivatization and extraction. As large sample volumes are applied (100 mL to 2 L) and only one sample can be handled at a time (assuming a standard rotary evaporator), this is a time consuming and labor intensive process. Therefore, SPE was chosen as the enrichment method during the doctoral work, enabling the simultaneous preparation of six meltwater samples. SPE with strong anion exchange is a very selective technique for the extraction of carboxylic acids from an aqueous matrix (see section 2.1.1) and has been used for the analysis of oxalic acid in human plasma [*Elgstoen*, 2008], for example. Other interesting atmospheric marker compounds, like biomass burning markers, often also feature a carboxylic acid group, which makes them accessible for this technique as well.

The aim of this study was the development of a new method for the sensitive quantification of (small) dicarboxylic acids, including oxalic acid, in snow and ice samples. SPE with strong anion exchange for extraction and enrichment was applied, followed by derivatization (esterification)

to enhance chromatographic and mass spectrometric properties, and analysis using UHPLC-HRAM-MS.

4.2 Experimental section

4.2.1 Chemicals and materials

Oxalic acid (99.9 %), malonic acid (99 %), succinic acid (>99.0 %), glutaric acid (99 %), adipic acid (>99.5 %), pimelic acid (98 %), sebacic acid (99 %), phthalic acid (>99.5 %), 4-methylphthalic acid (99 %), vanillic acid (>97 %), succinic acid-2,2,3,3-d4 (98 atom % D), ammonium hydroxide (puriss. p.a.), acetyl chloride (>99.0 %), butanol (99.7 %), pentanol (99 %), and methanol (HPLC grade) were purchased from Sigma-Aldrich (Steinheim, Germany). Suberic acid (99 %), 4-hydroxybenzoic acid (99 %), and dodecanedioic acid (99 %) were obtained from Acros Organics (Geel, Belgium). *Cis*-Pinic acid ((1'R,3'R)-2-[3'-Carboxy-2'2'-dimethylcyclobutyl]acetic acid) was synthesized following a protocol by Moglioni et al. [*Moglioni et al.*, 2000]. Acetonitrile (LC-MS grade) and water (LC-MS grade) were purchased from Fisher Scientific (Geel, Belgium). Formic acid (LC-MS grade) was purchased from LGC Standards (Wesel, Germany). Hydrochloric acid (30 %) was obtained from Merck (Darmstadt, Germany). Ethanol (HPLC gradient grade) and isopropanol (LC-MS grade) were purchased from Carl Roth (Karlsruhe, Germany). Ultrapure water (18.3 MΩ cm) was obtained using a Milli-Q water system from Millipore (Bedford, USA). SPE cartridges (SB, 3 mL, 500 mg bed weight) were purchased from Macherey-Nagel (Düren, Germany).

4.2.2 SPE procedure

The SPE cartridges were equilibrated with 2x2.5 mL MeOH and 2x2.5 mL ultrapure water by means of reduced pressure in a vacuum manifold. Throughout the whole procedure, a flow rate of less than 1 mL/min was applied to ensure complete retention. To remove contaminations, the cartridges were eluted with three portions (each 1.5 mL) of 0.16 M hydrochloric acid (HCl) in ACN followed by 10 mL of ultrapure water. To change the counter ion of the strong anion exchange sorbent material from chloride to formate, 5x2.5 mL of 0.5 M formic acid were applied to the cartridges, followed by 2x2.5 mL of ultrapure water and 4.0 mL of ammonium hydroxide solution (pH 7-8). To about 80 mL of each melted ice sample, 0.1 mL of ammonium hydroxide solution were added for pH adjustment (pH 7-8). A volume of about 1.5 mL was left in the cartridges before starting the sample retention to prevent the sorbent

from running dry before the sample flow reached the cartridge. The samples were applied to the cartridges using reservoirs. After the retention step, a washing step was performed by applying 2.5 mL ammonium hydroxide solution to the cartridges, followed by 2.5 mL of ultrapure water and 1 mL of ACN. The cartridges were sucked dry for about 1 min before elution. Elution was performed manually with 1 mL of HCl in ACN using a flow rate of less than 1 mL/min and the eluate was reduced to a volume of about 200 μL by means of a gentle nitrogen stream and heating to 35 °C. The elution step was repeated three times (4 mL HCl in ACN in total). After the last extraction step, 25 μL of the internal standard solution were added to the residual eluate before evaporation to complete dryness. The vacuum manifold used for conducting the SPE extraction process is shown in Fig. 4.1. During method development, the main focus lay on the reduction of high blank values present on the sorbent material.
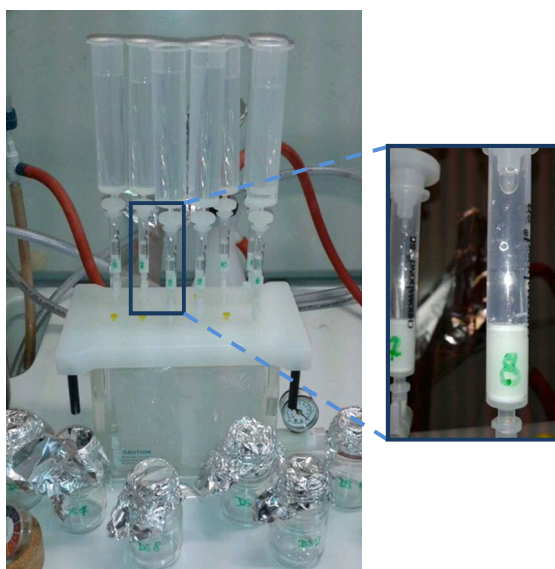
Fig. 4.1 Vacuum manifold for SPE. Up to seven samples were prepared at the same time. The picture shows the cartridges placed onto the vacuum manifold with filled sample reservoirs connected to the SPE tubes. The enlarged section shows a single SPE cartridge containing the sorbent material between two frits, while the sample is applied dropwise to the cartridge by means of low pressure.

4.2.3 Derivatization

Pentanol with 10 % acetyl chloride was used as derivatization solution for the esterification of the analytes' carboxylic acid groups. The solution was stored at 4 °C and was stable over several months.

For derivatization, 100 μL of the derivatization solution were added to the extraction residue. The solution was heated to 70 °C for 30 min in a closed vial, cooled to room temperature and evaporated to dryness under a gentle stream of nitrogen at a temperature of 30 °C. Care was

taken to remove the vial from the evaporation unit immediately upon complete solvent evaporation in order to prevent analyte loss. The residue was dissolved in 500 µL of eluent solution (ACN/H$_2$O 80/20 v/v) and provided for LC-MS analysis. Method development comprised optimization of the derivatization reagent, time, temperature, and evaporation parameters.

4.2.4 Liquid chromatography – mass spectrometry
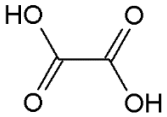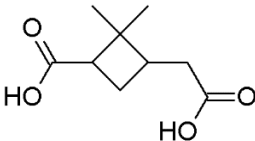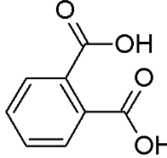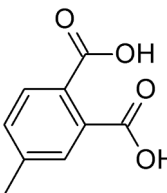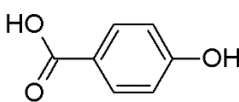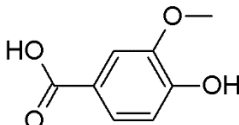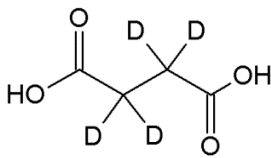
For the chromatographic separation, an *UltiMate 3000* UHPLC system (Dionex, Thermo scientific, Germany) was used. The UHPLC system was composed of degasser, binary gradient pump, temperate auto sampler, and temperate column compartment. The autosampler temperature was set to 20 °C and the analytical column (Hypersil Gold, C18, 50x2.0 mm, 1.9 µm particle size, Thermo Scientific) was tempered to 25 °C during analysis. Eluent A (ultrapure water with 2 % ACN and 0.04 % formic acid) and B (MeOH) were used in gradient mode with a flow rate of 500 µL/min. The optimized gradient was 60 % B at 0 min, 60 % B at 0.5 min, 70 % B at 1.0 min, 99 % B at 2.0 min, 99 % B at 5.0 min, and 60 % B at 5.1 min. The injection volume was 10 µL per run. High resolution mass spectra were obtained using a *Q-Exactive™* hybrid quadrupole orbitrap mass spectrometer (Thermo Scientific, Germany) equipped with a HESI source. The optional heating of the solvent flow was not applied in this method, as the high fraction of organic solvent (60 %) at the beginning of the chromatographic run allowed stable spray conditions without additional heating. The HESI source was operated in positive ion mode with 40 psi sheath gas, 20 psi aux gas (both N$_2$), 350 °C capillary temperature, and 3.5 kV spray voltage. The Full-MS mode was performed within a scan range of *m/z* 100-500, with a resolution setting of 70,000. The common contaminant ion *m/z* 391.28423 (diisooctyl phthalate, plasticizer) was used as a lock mass for internal mass calibration during mass analysis. Data analysis was performed using the software XCalibur® (Thermo Scientific) for both signal identification and integration.

4.2.5 Preparation of standards for quantification and method development

Stock solutions of the target analytes oxalic acid (OXA), malonic acid (MAL), succinic acid (SUC), glutaric acid (GLU), adipic acid (ADI), pimelic acid (PIM), suberic acid (SUB), sebacic acid (SEB), dodecanedioic acid (DOD), phthalic acid (PHT), 4-methylphthalic acid (MPH), pinic acid (PIN),

Table 4.1 Analytes contained in the standard mixture for quantification

Analyte			Derivate ions	
			$[M+H]^+$	$[M+Na]^+$
Name	M (g/mol)	Structure		
			m/z	*m/z*
Oxalic acid	90.04		231.15909	253.14103
Malonic acid	104.06	n=1	245.17474	267.15668
Succinic acid	118.09	n=2	259.19039	281.17233
Glutaric acid	132.12	n=3	273.20604	295.18798
Adipic acid	146.14	n=4	287.22169	309.20363
Pimelic acid	160.17	n=5	301.23733	323.21928
Suberic acid	174.20	n=6	315.25299	337.23493
Sebacic acid	202.25	n=8	343.28429	365.26623
Dodecanedioic acid	230.30	n=10	371.31559	393.29753
Pinic acid	186.21		327.25299	349.23493
Phthalic acid	166.13		307.19039	329.17233
4-Methyl phthalic acid	180.16		321.20604	343.18798
p-Hydroxybenzoic acid	138.12		209.11722	231.09917
Vanillic acid	168.15		295.19039	317.17233
Succinic acid-d4	122.11		263.21549	285.19744

vanillic acid (VAN), *p*-hydroxybenzoic acid (PHB), and the internal standard succinic acid-2,2,3,3-d4 (see Table 4.1) with concentrations between 10 and 40 mM in MeOH were prepared and stored at -20 °C until needed. A solution containing 100 µM of each standard (*standard solution 1* (*S1*)), was prepared by diluting the stock solutions with MeOH.

S1 was prepared monthly and stored at 4 °C. To obtain standards for quantification and method development, *S1* was diluted with MeOH to obtain solutions *S2* and *S3* with analyte concentrations of 10 µM and 0.5 µM, respectively. The *internal standard solutions 1* and *2* (*IS1* and *IS2*) were prepared accordingly. Five calibration standards were prepared by transferring distinct volumes of the standard solutions to autosampler vials and adjusting the total volume to 500 µL with MeOH before evaporation and derivatization (see Table 4.2). For the optimization of the derivatization procedure, standards containing 0.5 or 1.0 nmol of each analyte were used.

Table 4.2 Calibration standards for (di)carboxylic acids

Calibration level	Amount of analyte (nmol)	Volume of S3 (µL)	Volume of S2 (µL)	Volume of IS2 (µL)	Volume of MeOH (µL)
1	0.025	50	0	25	425
2	0.05	100	0	25	375
3	0.1	200	0	25	275
4	0.3	0	30	25	445
5	0.5	0	50	25	425

4.3   Results and discussion

4.3.1   Method development

4.3.1.1   Derivatization

Starting with parameters adopted from a method for the analysis of oxalic acid (using butanol as derivatization reagent, 65 °C derivatization temperature, and 15 min derivatization time) [*Elgstoen*, 2008], several derivatization parameters were optimized to extend the method's applicability to other (di)carboxylic acids besides oxalic acid.

Evaporation temperature

The evaporation temperature of the heating block during the last evaporation step was varied (30 °C, 40 °C, 50 °C), revealing a significant analyte loss using temperatures above 30 °C, especially for the derivatization products of small dicarboxylic acids.

Derivatization time

Different derivatization times (10, 20, 30, 40, 50, and 60 min) were tested using butanol derivatization for oxalic, pinic and suberic acid at 70 °C and the resulting signal areas were compared. No significant trend in signal area depending on derivatization time was observed for oxalic and suberic acid. In case of pinic acid, only the signal of 10 min derivatization time was significantly lower than all the rest. Therefore, a derivatization time of 30 min was chosen to ensure complete derivatization.

Derivatization reagent

Different aliphatic alcohols (methanol, ethanol, isopropanol, butanol, and pentanol) were tested as derivatization reagent for the esterification of acids. The assays were performed in triplicate with a derivatization time of 30 min at a temperature of 70 °C. 100 µL of the respective alcohol with 10 % acetyl chloride were applied for derivatization. As the method comprises an evaporation step, a compromise between evaporation time and analyte loss due to volatility of the derivatization product has to be found. The evaporation time after the derivatization increases with the molecular weight of the alcohol (and the resulting derivatization product), whereas the volatility decreases, reducing the risk of analyte loss during evaporation (see Fig. 4.2). The resulting signal areas of the different analytes depending on the derivatization reagent are given in Fig. 4.3. The sum of all peak areas is highest using butanol and pentanol as derivatization reagent and about three times lower in case of methanol, ethanol and isopropanol (Fig. 4.3a). Here, the signal areas of oxalic, malonic, succinic, and glutaric acid are very low or even not assignable. This might either be caused by low derivatization efficiency or by product loss during evaporation. Fig. 4.3b shows the proportional distribution of the different analytes based on the total observed signal area. Using butanol and pentanol derivatization, almost equal signal areas for all tested analytes are obtained, with a larger area for oxalic acid using pentanol. Average RSD values of triplicate analyses for all analytes are highest for ethanol derivatization (18 %) and lowest for butanol and pentanol derivatization (8 and 9 %, respectively). To avoid analyte loss during evaporation,

which seems to be the most critical point concerning the derivatization procedure, pentanol was chosen as the derivatization reagent.
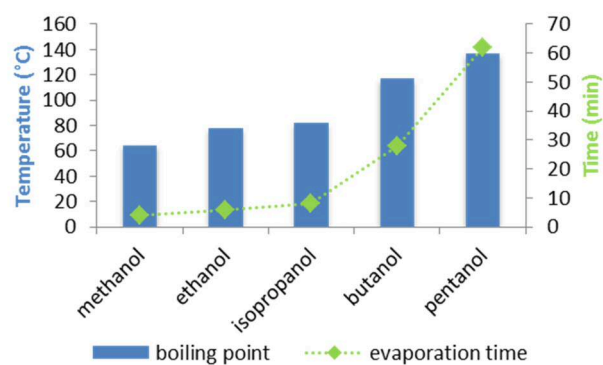
Fig. 4.2 Boiling points and evaporation time (100 µL, 30 °C, gentle stream of N_2) of different alcohols tested for derivatization
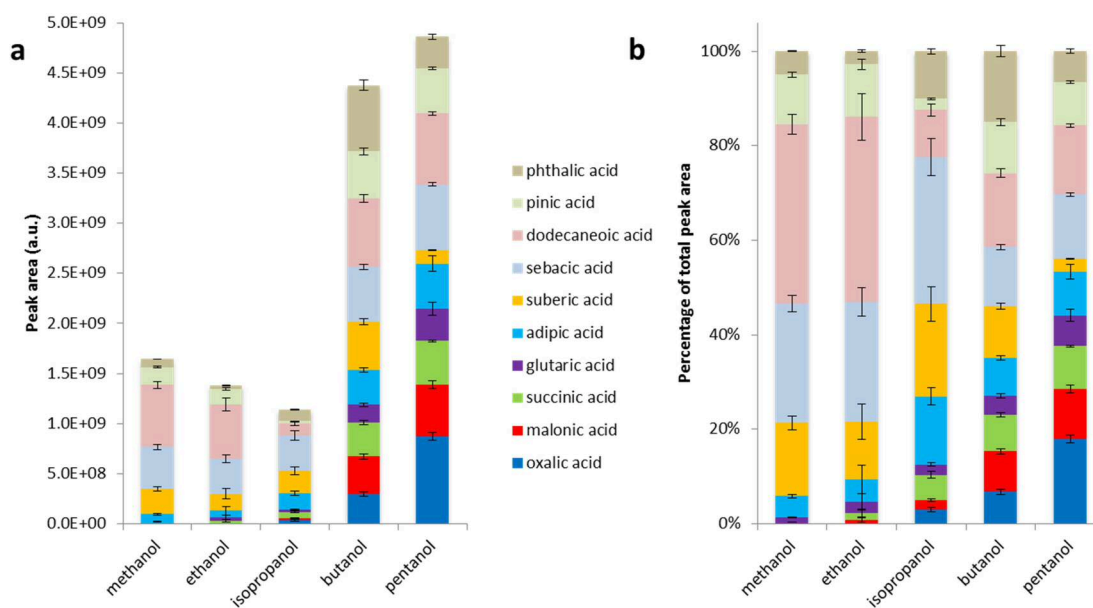
Fig. 4.3 Peak areas obtained after the derivatization of 10 dicarboxylic acids with different derivatization reagents (**a**) and percentage of the different acids on the total peak area (**b**). The error bars result from triplicate assays.

4.3.1.2 SPE procedure

The sample preparation was optimized based on an SPE protocol for the enrichment of oxalic acid from human plasma samples [*Elgstoen*, 2008]. Briefly, the parameters of the method targeting oxalic acid in human plasma samples were as follows: sample volume of 0.5 mL, SPE cartridges (size 1 mL) with strong anion exchange (SAX) sorbent (quaternary amines with chloride counter-ion, 100 mg bed weight), equilibration with ACN and 5 % ACN in H_2O, elution with 0.4 mol/L HCl in ACN. Initial SPE optimization was conducted using 1 mL-cartridges with 100 mg sorbent mass. For the analysis of ice samples, larger SPE cartridges containing 500 mg sorbent mass were used to enable the processing of larger ice sample volumes of 50-100 mL.

Reduction of blank values

The extraction of ultrapure water (without spiking) revealed large background concentrations of especially OXA present on new, unused cartridges. As this was also the case for SPE cartridges from several different suppliers with background levels being unreproducible, a cleaning step was added to the SPE protocol. To remove possible contamination levels before sample retention, the cartridges were pre-eluted with HCl in ACN, followed by washing with water. The effect of the improved protocol on the reduction of blank levels present on the SPE cartridges is shown in Fig. 4.4.
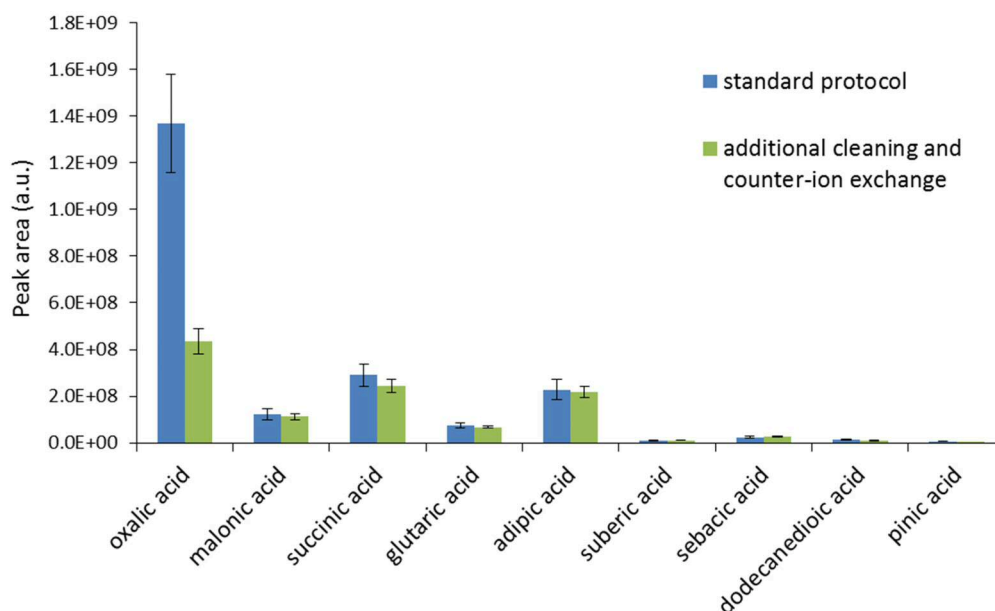
Fig. 4.4 Blank levels present on unused SPE cartridges using different SPE protocols. The given peak areas correspond to the respective diesters.

The blank level of oxalic acid could be reduced significantly, whereas blank levels for other analytes remained unchanged. In general, larger dicarboxylic acids (<C6), including PIN, showed very low contamination levels compared to the smaller analytes. As the contamination present on the SPE cartridges could not be eliminated completely, all sample results are being corrected by results of method blanks including SPE.

Optimization of retention behavior

For small dicarboxylic acids, especially oxalic acid, low and unreproducible extraction efficiencies were observed (often <20 %). This can either be caused by insufficient retention of the analyte by the SAX sorbent, or by incomplete elution of the adsorbed molecules. To test the elution for completeness, a spiked sample (10 mL of ultrapure water spiked with 0.5 nmol of each analyte) was applied to a pre-cleaned SPE cartridge. Successive elution was performed using five aliquots of 1 mL HCl in ACN (0.1 M), which were analyzed separately. The resulting signal areas for the individual analytes are shown in Fig. 4.5. For all analytes, elution was completed after the third fraction. The signal areas resulting from the fourth and fifth fraction lay in the range of blank measurements. The major amount of larger dicarboxylic acids (≥C5) is eluted in fraction 2, whereas smaller dicarboxylic acids (C2-C4) mainly elute with fraction 3, which indicates stronger retention for the latter. This is consistent with the small dicarboxylic acid exhibiting lower pK_a values, thus forming stronger interactions with the quaternary amine moieties of the SAX sorbent. However, as elution was shown to be complete, the critical step during SPE was assumed to be insufficient retention, possibly causing the observed analyte loss.

In order to enhance retention characteristics of small dicarboxylic acids, especially oxalic acid, the counter ion of the SAX sorbent was changed from chloride to formate. Formate has lower selectivity for the sorbent, thus enhancing the anion exchange process for small analytes. Based on an SPE application note from International Sorbent Technology Ltd. [*K. Rasmussen*, 1989], the sorbent was rinsed with 0.5 M formic acid followed by ultrapure water before sample retention. Additionally, the pH of the sample was adjusted to 7-8 with NH_4OH to ensure the analytes being present in their ionic (deprotonized) form. However, no improvement in extraction efficiency was achieved for C2-C5 dicarboxylic acids. Small dicarboxylic acids show significantly lower pK_a values compared to their higher homologues (e.g., oxalic acid: pK_{a1} 1.23, pK_{a2} 4.19 and adipic acid: pK_{a1} 4.43, pK_{a2} 5.42). Concerning pH adjustment, a pH of 7-8 of the sample solution during retention should suffice for effective retention, as both acid groups of the analytes are deprotonized, enabling ionic interactions

with the SAX phase. During elution with a strong acid (0.1 M HCl in ACN), however, small dicarboxylic acids are possibly not protonated completely, impeding elution from the column. Possible further optimization of SPE is discussed in section 4.4.
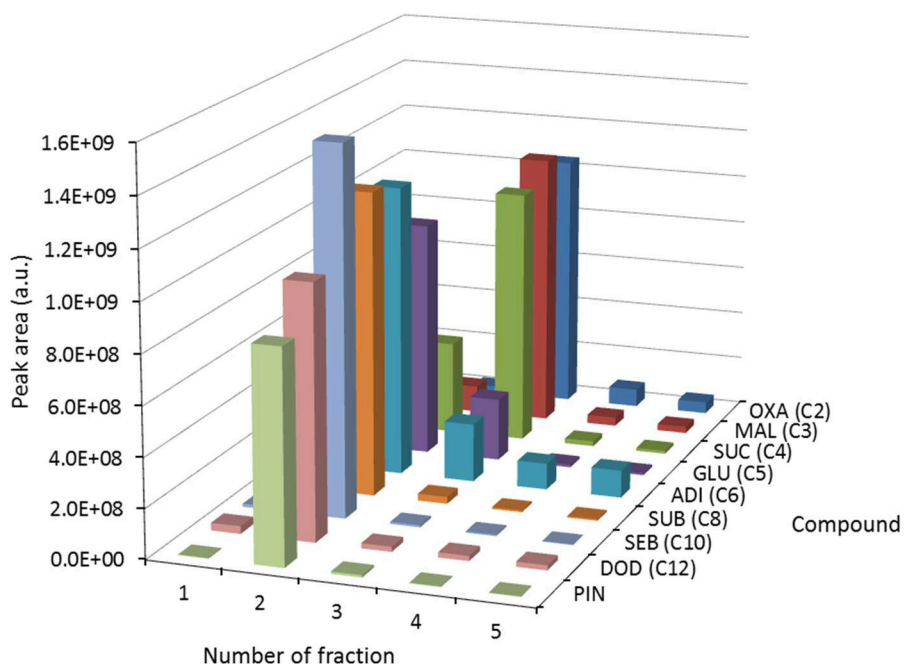
Fig. 4.5 Test for completeness of SPE elution. Peak areas of individual compounds were measured in five consecutive fractions eluted during SPE.

4.3.1.3 Chromatographic separation and MS

An UHPLC method was developed using a derivatized standard sample. The LC parameters were optimized for baseline separation of the analytes' derivatives using a C18 column (50 mm x 2.1 mm, 1.9 µm particle size). To ensure equal conditions for each chromatographic run, the column was tempered to 25 °C during analysis. Binary mixtures of ACN/H_2O and MeOH/H_2O were tested in gradient elution mode. Best results concerning peak shape and homogenic peak area for short and larger dicarboxylic acids were obtained using MeOH/H_2O. The optimized gradient is given in section 4.2.4. Electrospray and MS parameters were optimized for maximum signal intensity in the positive ion mode. Mass spectra were acquired in the *Full MS* mode, i.e. the total ion current was recorded. Analyte peaks were identified by retention time compared to derivatized standards and their accurate mass.

Adduct formation

Electrospray ionization in the positive ion mode often leads to the formation of other adduct ions besides the protonated molecular ion. The main adducts formed are alkali metal or ammonium adducts ($[M+Na]^+$, $[M+K]^+$ or $[M+NH_4]^+$). In case of the carboxylic acid esters, dipentyl oxalate formed only the sodiated molecular ion, whereas the protonated molecular ion was not observed. All other esters formed both the protonated and sodiated species. For quantification, the sum of the areas resulting for both ions was determined.

4.3.2 Validation

Linear regression analysis was applied to obtain calibration functions for all analytes present in the standard mixture (see Table 4.1). The resulting calibration parameters are presented in Table 4.3.

Table 4.3 Calibration data for the quantification of (di)carboxylic acids

Compound	Slope[a]	Intercept[a]	R^2	ILOD (pmol/ mL)	ILOQ (pmol/ mL)	LOD (**pmol**/kg water)	LOD (**pg**/g water)
OX	1.72	0.04	0.9993	1.94	6.48	24.30	2.19
MAL	3.60	0.01	0.9989	0.04	0.12	0.45	0.05
SUC	3.96	0.01	0.9999	0.23	0.78	2.93	0.35
GLU	4.07	0.02	0.9999	1.09	3.62	13.58	1.79
ADI	4.00	0.02	0.9963	0.76	2.52	9.46	1.38
PIM	4.00	0.04	0.9992	0.37	1.22	4.58	0.73
SUB	4.22	0.01	0.9977	0.09	0.30	1.13	0.20
SEB	4.51	0.02	0.9991	0.10	0.32	1.20	0.24
DOD	4.32	0.02	0.9984	1.79	5.97	22.39	5.16
PIN	2.68	0.01	0.9985	0.14	0.47	1.75	0.33
PHT	1.72	0.02	0.9964	1.86	6.20	23.25	3.86
MPH	1.91	0.01	0.9968	0.14	0.46	1.72	0.31
VAN	0.017	-0.0002	0.9985	10[b]	30[b]	125	21.02
PHB	0.029	-0.0002	0.9981	5.05	16.84	63.14	8.72

[a] Determined using the measured signal area quotient (analyte/internal standard), [b] estimated values due to non-existing blank signals

The instrumental limits of detection (ILOD) and quantification (ILOQ) were determined by multiplying the standard deviation of the blank samples (n=5) by 3 and 10, respectively, and

dividing by the slope of the linear regression function. Method limits of detection (LOD) (also given in Table 4.3) are based on a sample volume of 80 mL and were in the range of 0.05 pg/g for MAL to 21.02 pg/g for VAN.

Recovery and method precision results are given in Table 4.4. The recovery of the analytes was determined by spiking melted ice core samples with the target analytes mixture in triplicate. A detailed description of the ice core sampling is given in chapter 5.1. After correcting the determined results of the spiked samples by subtracting the results of the unspiked ice samples, they were compared to the amount of substance spiked to the samples. This was performed twice and the results were averaged to determine the recovery of the respective target compound.

Table 4.4 Recovery and precision data of (di)carboxylic acids

Compound	Recovery (%)	Precision (%, n=3)
OX	ND	66.5
MAL	ND	70.5
SUC	ND	52.5
GLU	ND	27.1
ADI	87.6 ± 42.9	7.3
PIM	109.1 ± 26.1	4.6
SUB	115.7 ± 8.3	9.0
SEB	109.2 ± 7.4	12.3
DOD	111.0 ± 4.3	7.3
PIN	111.6 ± 4.1	4.6
PHT	75.9 ± 20.4	22.0
MPH	61.4 ± 7.0	15.4
VAN	56.5 ± 10.1	8.9
PHB	53.2 ± 11.7	13.8

ND: Non-determinable, see text for further details.

The measurement precision – as a measure for the variance caused by the analytical system (UHPLC-ESI-MS system) – was determined by fourfold measurement of each sample. Using an internal standard, the resulting measurement precision was 3 (±2) % for all analytes. Method intra-batch precision was evaluated by calculating the RSD in percent from the triplicate analysis of an ice sample measured on the same day. VAN and PHB were not detected in the ice core sample used for evaluating the precision of the method. Therefore, the spiked

triplicate samples used for recovery analysis were applied to calculate the precision of VAN and PHB. Due to the limited sample volume, no additional precision evaluation was possible. The precision values of OX, MAL, and SUC are very high (66.5, 70.5, and 52.5 %, respectively), revealing that the SPE protocol in its actual modification is still in need of improvement concerning the quantitative extraction of small dicarboxylic acids. However, all other targeted analytes exhibit good to excellent precision values below 20 % with an average precision of 10.5 % (except for PHT and GLU with 22.0 and 27.1 %, respectively, which is still acceptable). Recovery values are not given for the four smallest dicarboxylic acids analyzed, as the results were inconsistently varying or recovery could not be calculated at all. This can also be attributed to the insufficient precision caused by the SPE.

4.4   Conclusion and outlook

A new method for the quantification of dicarboxylic acids in snow and ice employing SPE, followed by derivatization and UHPLC-ESI-MS analysis, was developed and validated using glacier ice core samples. Method parameters concerning derivatization (time, temperature, reagent), liquid chromatography and SPE were optimized. Method detection limits were in the low pg/g range. Inter-batch precision was below 20 % for most analytes (10.5 % in average). The method was successfully applied for the quantification of larger dicarboxylic acids (≥ C6) in an ice core from upper Grenzgletscher in the southern Swiss Alps (see chapter 5). However, further optimization has to be conducted concerning the still limited applicability of the method to small dicarboxylic acids (≤C5). While the derivatization and LC-MS part of the method showed excellent performance for both small and larger dicarboxylic acids, SPE with strong anion exchange worked well only for larger dicarboxylic acids. High and unreproducible background concentrations of especially oxalic acid were found on new SPE cartridges. By applying an additional cleaning step, these blank values could be lowered significantly. However, the extraction efficiency of small dicarboxylic acids was not improved by the cleaning step. Also, the exchange of the counter-ion of the SAX sorbent did not enhance retention capacities, neither did the adjustment of the sample pH.

Further optimization is needed concerning retention and elution during SPE. If elution is detected to be the critical step, a higher concentrated acidic solution might be necessary for the complete elution of the analytes. Nevertheless, this has been avoided yet due to possible damage to the analytical column. Investigations should also include effects possibly caused by

the sample matrix. New polymer-based anion exchange materials for SPE should be tested as well. It may be likely, that a second protocol for small dicarboxylic acids has to be developed, focusing only on small dicarboxylic acids and their specific chemical characteristics. Additionally, the use of a reference method (such as ion chromatography for oxalic acid) might be beneficial during method development.

5 FIELD MEASUREMENT

An ice core from upper Grenzgletscher in the southern Swiss Alps (see chapter 1.3.1 for information about the drilling site) was analyzed for α-dicarbonyls and (di)carboxylic acids applying the methods developed during the doctoral work (described in chapters 3 and 4). Analysis of major ions (ammonium (AMM), nitrate (NIT), sulfate (SUL), Ca^{2+} (CAL), formate (FOR), and oxalate (OXA)), as well as pH measurements, were conducted at PSI. Additionally, a non-target screening of the glacier ice core samples was performed, using UHPLC-HRAM-MS.

5.1 Sampling

Samples were cut out from the ice core sections at -20 °C in a cold room at the PSI in Villigen, Switzerland, using a modified band saw (stainless steel blades, tabletops and saw guides covered with PTFE). All surfaces the ice came into contact with were cleaned with ethanol before and after cutting each ice core section to prevent cross contamination. To reduce potential contaminations from drilling, transport, or storage, the outer layer (about 0.5 cm) of each ice core section was removed with the band saw. To obtain annual averages, equal aliquots of the ice sections belonging to a certain year (2 to 9 sections per year) were combined in a pre-cleaned glass jar. The jars were closed tightly using screw caps with PTFE-coated septa and kept frozen until analysis. Forty-nine samples were prepared, covering the years 1942 to 1991 (with the exception of 1969, as no ice core sections from the year 1969 were available). In order to investigate the seasonal variation of the targeted compounds in the ice during the years 1992 and 1993, aliquots of two ice core sections each were combined, yielding 10 samples in total. Ultrapure water was frozen to obtain procedural blank samples, which were treated like real ice core samples to correct for possible contamination from sample preparation and analysis.

To evaluate if the applied sampling strategy was representative for the assigned years and thus the dating information from A. Eichler et al. [2000a] could be adapted for the ice core samples, the resulting ice core record of FOR was compared to the ice core record of FOR that had been obtained by A. Eichler [2000c], comprising 2148 distinct ice samples (Fig. 5.5). The records obtained by 1-year sampling (black dots) and 1-year averaging (blue diamonds) shows excellent agreement, revealing that the sampling was representative for the distinct years.

Fig. 5.1 Ice core cutting in the cold room at PSI.

5.2 Method application

5.2.1 UHPLC method adaption

All measurements of the glacier ice core samples were conducted using the UHPLC-HRMS system described in sections 2.3.3 and 4.2.4. The HPLC-MS method for the analysis of glyoxal and methylglyoxal (chapter 3) had to be transferred to an UHPLC method: The eluent composition (A: ultrapure water with 2 % ACN and 0.04 % formic acid, B: ACN with 2 % ultrapure water) remained unchanged, except that water and ACN of higher purity (LC-MS grade) were used. The flow rate was raised from 200 to 500 µL/min. The injection volume was reduced to 10 µL per run. The optimized gradient was 50 % B at 0 min, 50 % B at 0.25 min, 75 % B at 1.0 min, 75 % B at 1.2 min, 99 % B at 1.25 min, 99 % B at 4.0 min, and 50 % B at 4.1 min. Including a re-equilibration time of 3 min, this led to a shortening of analysis time per run by a factor of eight as well as a reduced solvent consumption by a factor of three compared to the conventional HPLC method.

5.2.2   Results and discussion

5.2.2.1   Ice core records from 1942 to 1993

Ice core records covering the period from 1942 to 1993 were obtained for nine dicarboxylic acids (C6-C10, C12, MPH, PIN, and PHT), two monocarboxylic acids (VAN and PHB), and two α-dicarbonyls (G and MG). The concentration range and average concentrations of the compounds detected in the ice core are presented in Table 5.1.

Table 5.1 Concentrations of dicarboxylic acids, monocarboxylic acids, and α-dicarbonyls analyzed in the glacier ice core (time period 1942-1993)

		Concentration (ng/g ice)		
	Abbreviation (Cn)	Average	Minimum	Maximum
Dicarboxylic acids				
Adipic acid	ADI (C6)	0.52	BDL	2.4
Pimelic acid	PIM (C7)	0.15	BDL	0.86
Suberic acid	SUB (C8)	0.099	BDL	0.44
Azelaic acid	AZE (C9)	0.12	BDL	0.45
Sebacic acid	SEB (C10)	0.029	0.002	0.11
Dodecanedioic acid	DOD (C12)	0.022	BDL	0.11
Pinic acid	PIN	0.22	BDL	0.92
Phthalic acid	PHT	0.099	BDL	0.47
4-Methylphthalic acid	MPH	0.029	BDL	0.22
Monocarboxylic acids				
Vanillic acid	VAN	0.067	BDL	0.36
p-Hydroxybenzoic acid	PHB	0.021	BDL	0.15
α-Dicabonyl compounds				
Glyoxal	G	0.38	BDL	1.8
Methylglyoxal	MG	0.046	BDL	0.27

The concentrations of major ions determined with ion chromatography (including OXA and FOR) as well as the results of pH measurements of the ice samples conducted at PSI [*Eichler et al.*, 2000b] are shown in Table 5.2. The most abundant organic compound detected in the ice

core was FOR with an average concentration of 64 ng/g, followed by OXA, ADI, G, and PIN with 15.9, 0.52, 0.38, and 0.22 ng/g, respectively.

Table 5.2 Ice core ion concentrations determined with ion chromatography and pH values

Ions	Abbreviation	Concentration (ng/g)		
		Average	Minimum	Maximum
Ammonium	AMM	99	39	253
Nitrate	NIT	214	81	550
Sulfate	SUL	534	20	2062
Ca^{2+}	CAL	186	10	740
Formate	FOR	64	5	165
Oxalate	OXA	15.9	1.5	49

Other parameters	Average	Minimum	Maximum
pH	6.05	5.04	6.58

The concentration of OXA in the ice core ranges from 1.5 to 49 ng/g, with an average concentration of 15.9 ng/g. These values are about seven times higher than those reported in a study by Kawamura et al. [*Kawamura et al.*, 2001b], comprising the analysis of dicarboxylic acids and α-dicarbonyls in a Greenland ice core, covering the time period from 1540 to 1989. The concentration ranges of C6-C10 dicarboxylic acids are comparable to those reported by Kawamura et al., with the exception of AZE, for which concentrations determined in this work (BDL–0.45 ng/g, average 0.12 ng/g) were about five times lower compared to the values reported by Kawamura et al. (<0.06–2.38 ng/g, average 0.64 ng/g). PHT concentrations ranged between BDL and 0.47 ng/g with an average value of 0.099 ng/g, which is also about five times lower than reported in the Greenland ice core. DOD and MPH have not been reported in ice cores, yet. Their concentrations in the Grenzgletscher ice core were found to be comparable to that of SEB, with an average value of 0.022 ng/g and 0.029 ng/g, for DOD and MPH, respectively. PIN has also not yet been reported in ice cores. Its concentration in the Grenzgletscher core is 0.22 ng/g in average, ranging from BDL to 0.92 ng/g. These values are comparable to those detected for PIM.

Average concentrations of G and MG were 0.38 ng/g (ranging from BDL to 1.76 ng/g) and 0.046 ng/g (BDL–0.27 ng/g), respectively. Interestingly, the mean concentration of MG is about eight times lower than the average concentration of G. Concentration records of G and MG

concentrations in ice core have only been reported by Kawamura et al. [*Kawamura et al.*, 2001b], although they are ubiquitous compounds in atmospheric aerosols and precipitation (see section 1.1.3). The results obtained for G are comparable to the concentrations found by Kawamura et al. (0.023–1.14 ng/g, average 0.26 ng/g), however, MG concentrations determined in this work are much lower than reported in the Greenland ice core (0.031–1.36 ng/g, average 0.21 ng/g).

Concentrations of VAN ranged from below detection limit (BDL), which is 0.021 ng/g ice, to 0.36 ng/g with an average value of 0.067 ng/g. These concentrations lay in the same range as reported in an ice core from Greenland (0.01-0.125 ng/g, [*McConnell et al.*, 2007]) and Ushkovsky ice cap in Northeast Asia (BDL-0.13 ng/g, [*Kawamura et al.*, 2012]). The concentration of PHB ranged from BDL (0.0087 ng/g) to 0.151 ng/g with an average concentration of 0.021 ng/g. Compared to the study by Kawamura et al. from the Ushkovsky ice cap, which is the only study reporting PHB in ice cores, our results are about ten times lower. Furthermore, the average concentration of PHB is about three times lower than that of VAN, whereas Kawamura et al. reported PHB concentrations in the Ushkovsky ice core to be 16 times higher than that of VAN. Such differences are likely to result from distinctions in sources and atmospheric transport of biomass burning aerosol to the respective glacier site.

The historic records obtained for the (di)carboxylic acids and α-dicarbonyls are shown in Fig. 5.2, Fig. 5.3, and Fig. 5.4. Three year averages were calculated to compensate for fluctuations in concentration due to possible changes in the efficiency of the aerosol transport to the glacier site. All the obtained records, based on three year averages, exhibit fluctuations of about one order of magnitude in concentration during the examined time period. Concentration minima are found to occur from the middle of the 1940s to the beginning of the 1950s for all compounds, followed by an increase in concentration starting in about 1950-1955. Depending on the individual compound, the maximum concentrations are reached around 1955 (e.g., AZE), 1960 (e.g., VAN), between 1965 and 1970 (e.g., PIN), or only in the late 1970s to early 1980s (e.g., ADI), before a second minimum is observed during the 1980s for all compounds except for MG. During this period from 1984 to 1989 the concentrations dropped to zero or levels near the detection limit, before they increased again in the early 1990s. This sudden drop in concentration was also observed by Eichler et al. [*Eichler et al.*, 2001] for certain ionic species detected in the same ice core and was attributed to the relocation of ions with meltwater in the firn section of the glacier. While the normal seasonal pattern of ions like Cl^-, F^-, NO_3^-, and NH_4^+ was preserved, the concentrations of K^+, Mg^{2+}, or
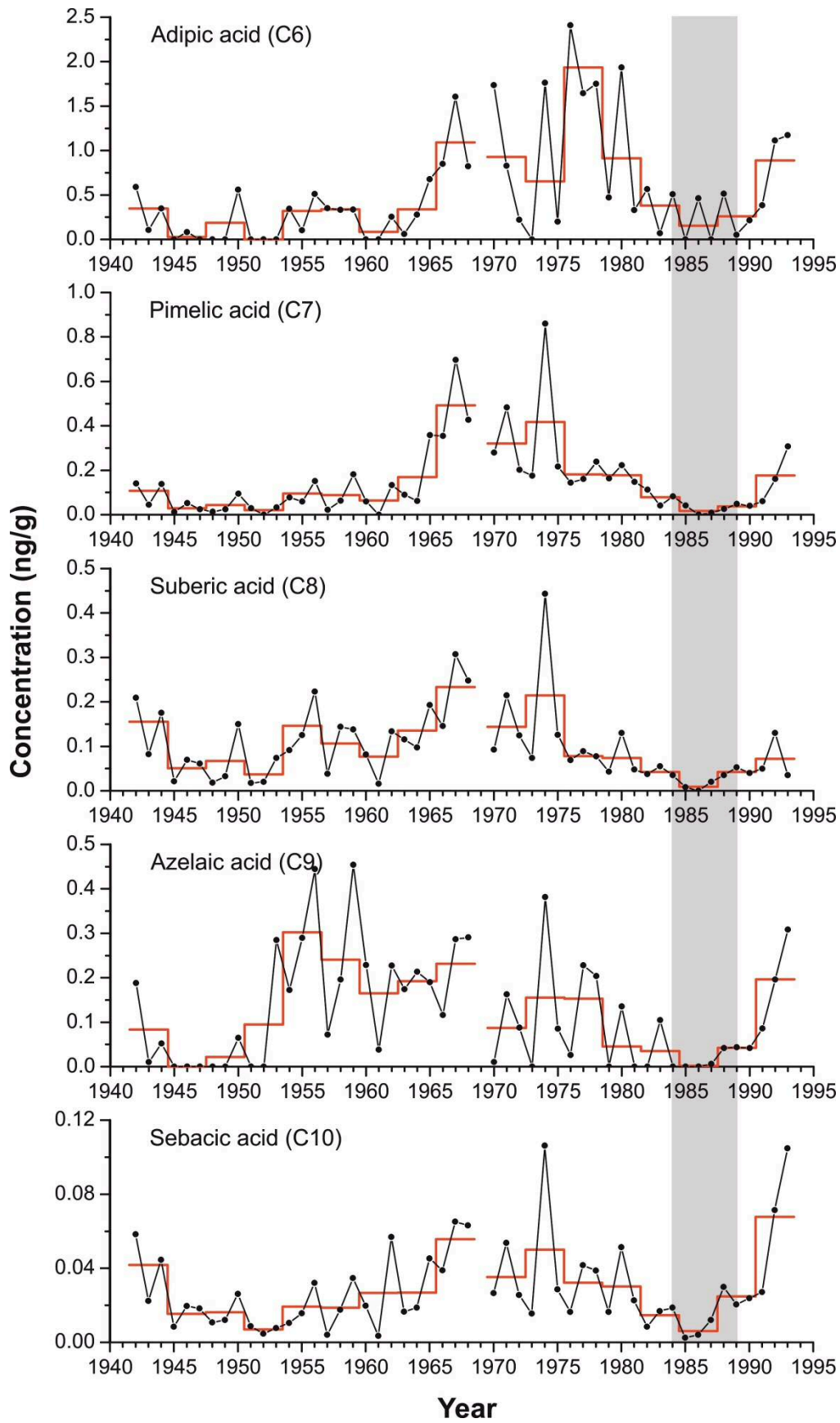
Fig. 5.2 Ice core records of dicarboxylic acids C6-C10 in the alpine ice core from upper Grenzgletscher (with three year average as bold line (red) and period influenced by meltwater marked gray).
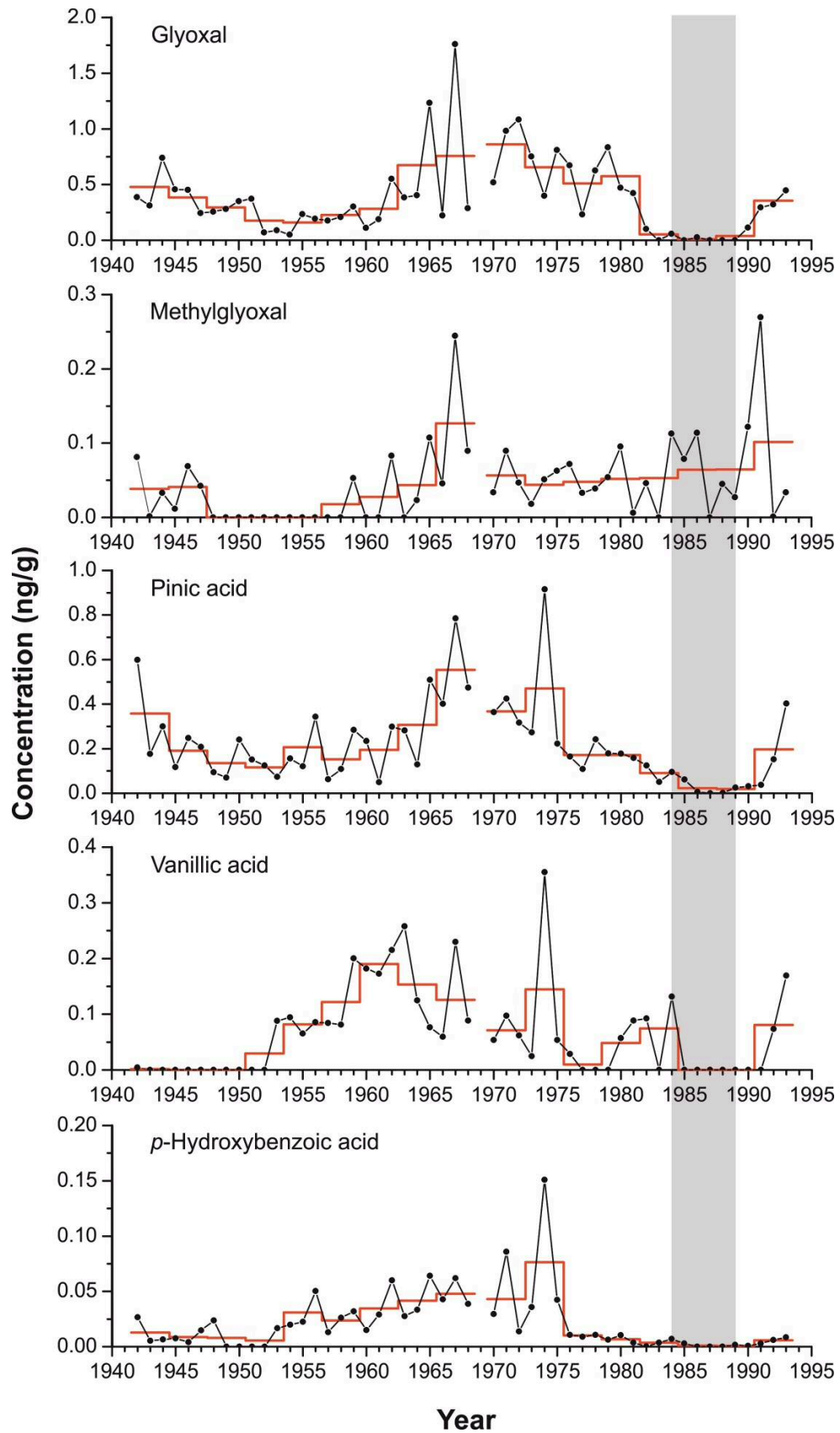
Fig. 5.3 Ice core records of α-dicarbonyls (glyoxal and methylglyoxal), pinic acid, and monocarboxylic acids (vanillic and *p*-hydroxybenzoic acid) in the alpine ice core from upper Grenzgletscher (with three year average as bold line (red) and period influenced by meltwater marked gray).

Ca^{2+}, for example, were significantly decreased. Eichler et al., 2001 suggested rearrangement processes during snow metamorphism in the ice to be the main reason for the fractionation of the ions. Depending on the solubility of an ionic compound in ice, it is located either inside the grain or at its surface. In the latter case, the ion is prone to be relocated by percolating water. As the possibility of being incorporated into the ice lattice is rather unlikely for the organic compounds detected in the ice core because of the molecule size, they are assumed to be located at the grain surfaces. The observed decrease in concentration during the period 1984-89 can thus not be interpreted as an atmospheric signal, but is due to a post-depositional leaching of the organic species.
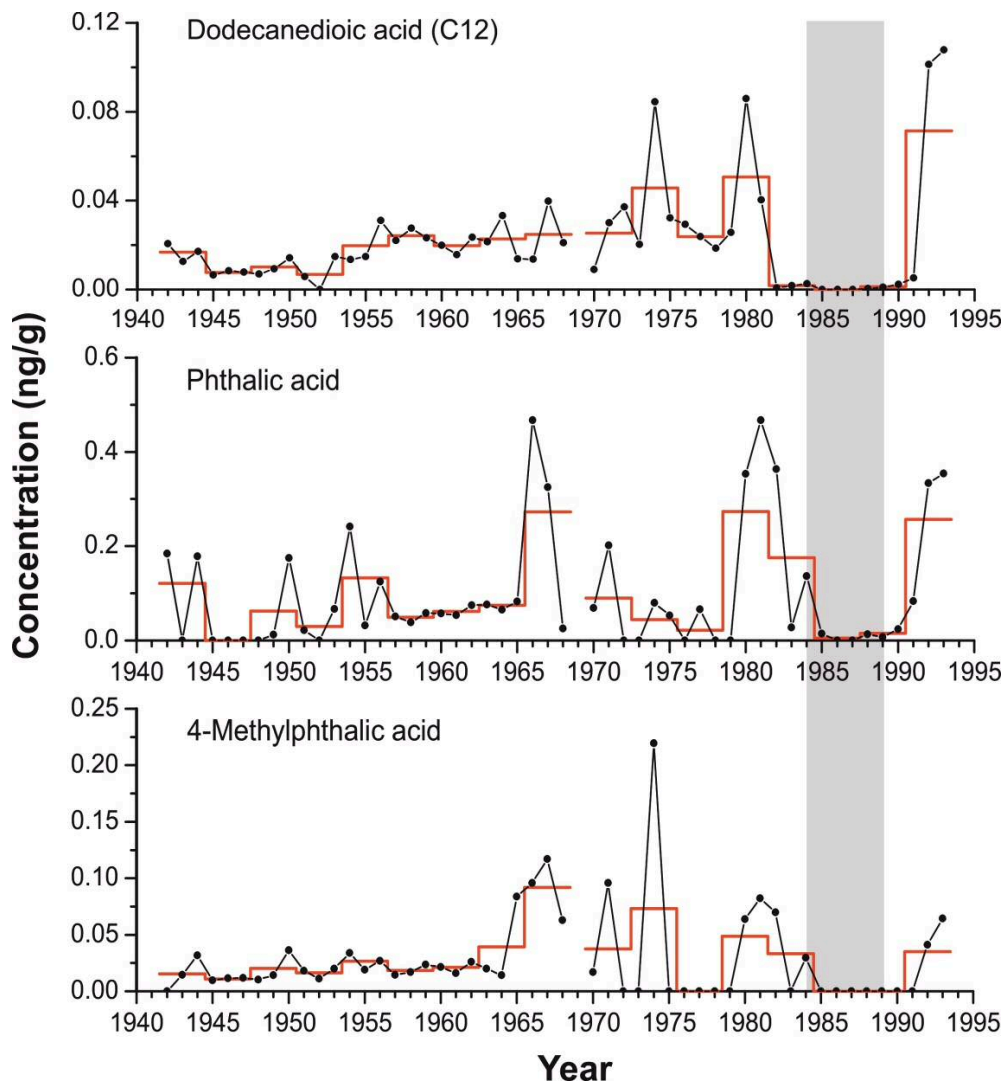
Fig. 5.4 Ice core records of dicarboxylic acids (C12, phthalic acid, and methylphthalic acid) in the alpine ice core from upper Grenzgletscher (with three year average as bold line (red) and period influenced by meltwater marked gray).

Interestingly, no significant decrease in concentration was detected for MG. The ratio MG/G is about 0.13 in average during the time not influenced by meltwater influx, yet raises up to 7 during the percolation period. This indicates a fractionation of G and MG possibly caused by the leaching process. Further investigation of the post-depositional behavior of organic compound in the ice is necessary, as for example solubility data of organic species in ice are lacking so far.
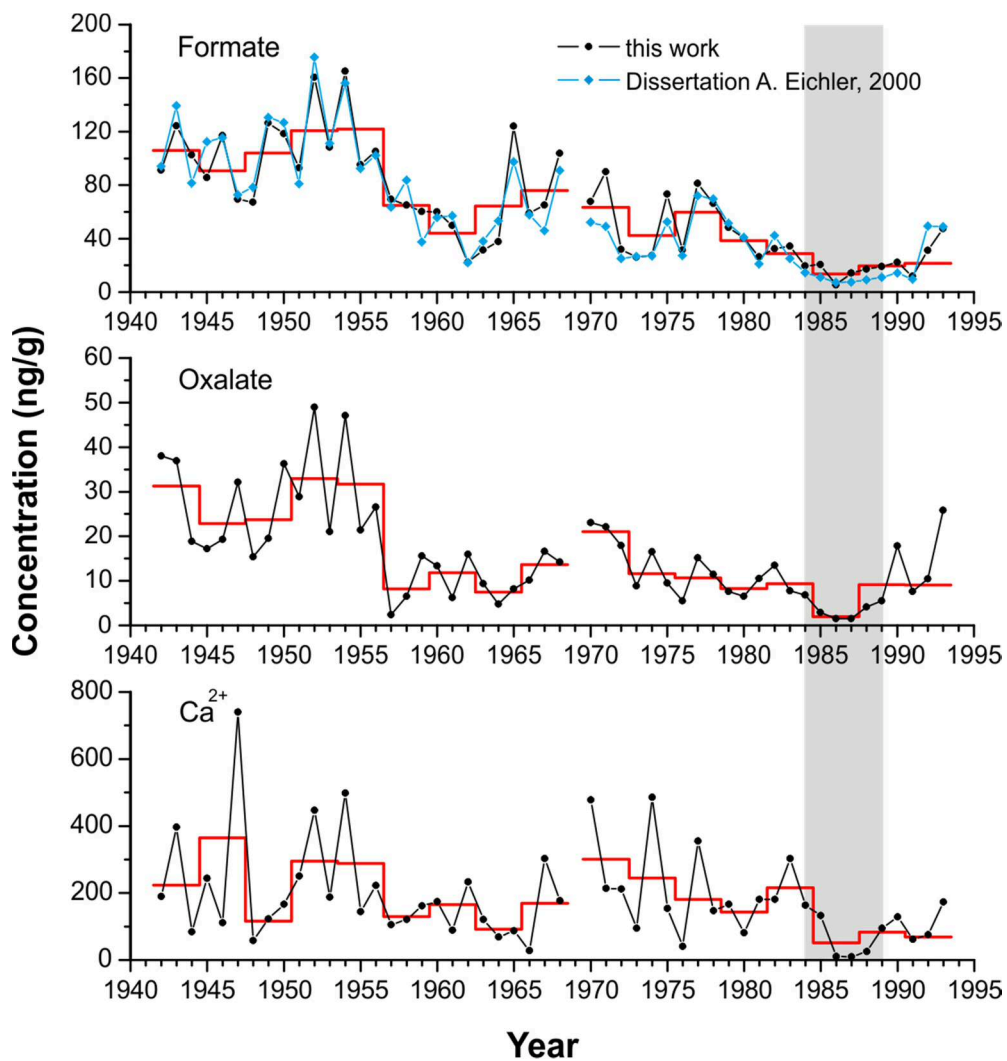
Fig. 5.5 Ice core records of ions calcium, oxalate, and formate in the alpine ice core from upper Grenzgletscher (black dots), with three year average as bold line (red). The ice core record of formate obtained by A. Eichler (blue diamonds, 1-year-average based on 2148 measurements [*Eichler*, 2000c]) fits well with the record determined using the 1-year sampling strategy (described in chapter 5.1).

Correlation analysis

Similarities in the concentration data may give hints concerning sources and atmospheric history of the individual compounds. A correlation analysis was performed using the *Pearson Product Moment Correlation*. Three year average values were used and the years affected by the meltwater influx were removed from the record. The resulting correlation coefficient r, which is also called Pearson coefficient, indicates the degree of linear dependence of two compounds and lies in the range of -1 (total negative correlation) to 1 (total positive correlation). To determine whether the coefficient r is significant, a *t*-test was performed, testing the null hypothesis (i.e. no correlation). If the resulting p-value is below a certain level of significance α (usually α=0.05), the null hypothesis is rejected, stating that there is a significant correlation. The calculations were performed using the software IBM® SPSS® Statistics version 22. The entire results of the correlation analysis are presented in the "supporting material" section (Table 7.1). Correlations significant at the 0.05 and 0.01 level are marked. In order to facilitate the detection of similarities and connections between different compounds, a correlation map was generated using MATLAB® (Fig. 5.6). A prominent group of compounds exhibiting strong positive correlations is easily visible in the correlation map. The group is composed of FSS (burned area due to forest fires in southern Switzerland), the biomass burning marker compound PHB, and the compounds MPH, SUB, PIN, PIM, NIT, AMM, SUL, and G. All organic compounds except for G show medium to high correlations to FSS, with correlation coefficients ranging from 0.561 (p=0.030) for PIM to 0.864 (p<0.001) for PHB. This indicates biomass burning to be a possible source for the concentration changes of the organic acids. PIM (C7) and SUB (C8) are strongly correlated, which suggests a similar source for these compounds. SUB and AZE are believed to be formed by photo-oxidation of unsaturated fatty acids [*Stephanou and Stratigakis*, 1993a], such as oleic and linoleic acids. The strong correlation observed for SUB and PIM suggests PIM to be produced either by the same source as SUB, or by further oxidation of SUB, yielding dicarboxylic acids with lower carbon number. All the compounds of the group are negatively correlated to the measured pH of the glacier samples (r=-0.744 in average). Although biomass burning is a general source for highly oxidized, acidic compounds, the observed correlation to the pH value might be rather due to sulfate, as the sulfate level has a high influence on the pH of the aerosol and thus of the ice sample. The organic acids are weak acids and their concentration in the ice is much lower compared to sulfate, therefore their influence on the pH value is of minor importance. G exhibits correlations to all compounds of the group, especially to PIN (r=0.784, p=0.001); however, there is no obvious correlation to the area burned by forest fires.
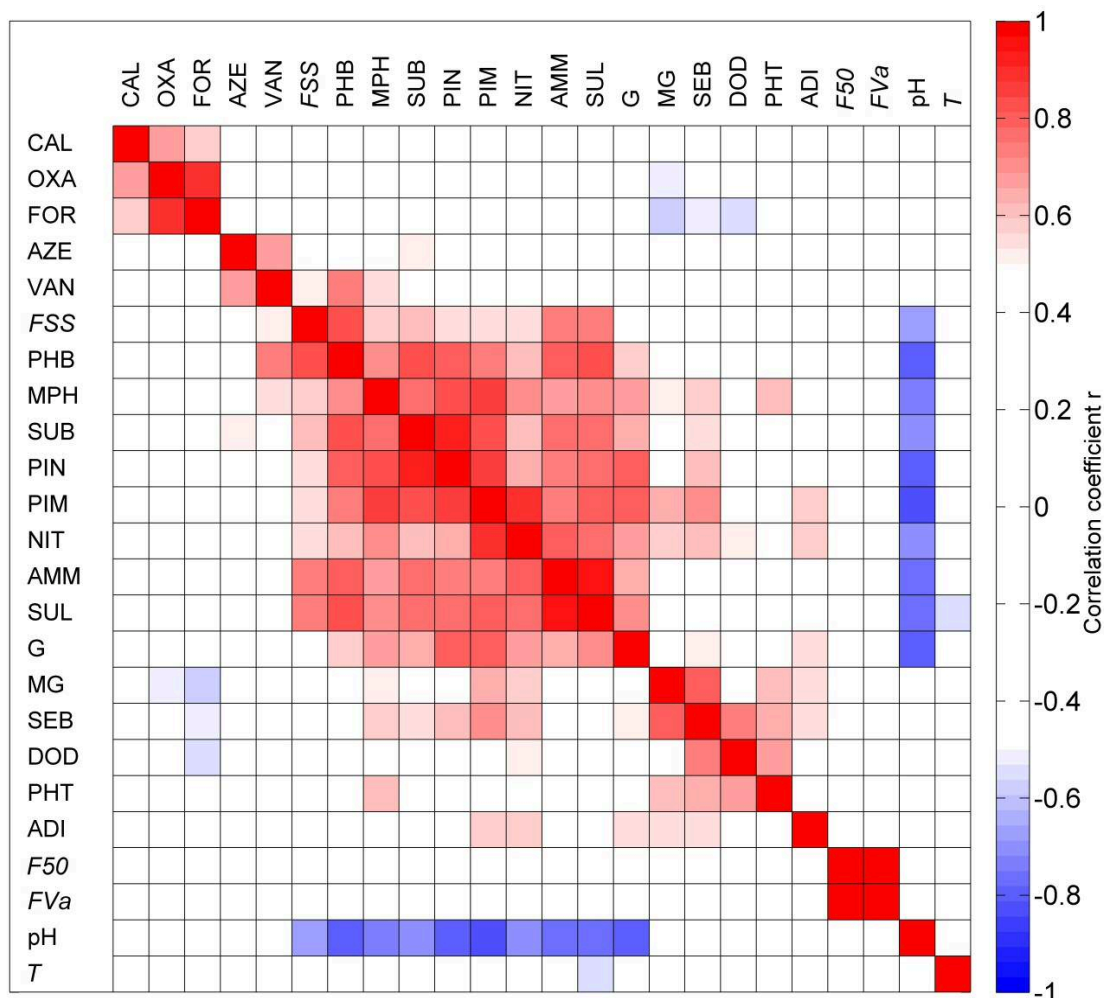
Fig. 5.6 Correlation map of compound concentrations detected in the ice core, pH of the ice core samples, and additional data (italicized, T = temperature in Lugano (Valais), FSS = burned area by forest fires in southern Switzerland, FVa = burned area by forest fires in Valais, $F50$ = burned area by forest fires within a distance of 50 km from sampling site). The color-coded scale gives the value of the correlation coefficient r for each pair of variables. The variables are grouped by similarity. (MATLAB function corrmap.m by Barry M. Wise, Eigenvector Research, Inc., www.eigenvector.com, accessed 2014.05.14).

A second group visible in Fig. 5.6 consists of CAL, OXA, and FOR. OXA and FOR are highly correlated (r=0.886, p<0.001) and they both show correlations to CAL (r=0.633 and 0.465, respectively). As CAL is a constituent of mineral dust particles, the observed correlations might be caused by common transport due to the uptake of the two acids by basic aerosol, containing mineral dust particles.

In addition to the described correlations, a strong correlation is also found among the longer-chained dicarboxylic acids SEB (C10) and DOD (C12) (r=0.769, p=0.001) suggesting a similar source for both compounds. Interestingly, both dicarboxylic acids are correlated to PHT (r=0.545, p=0.036 and r=0.519, p=0.047, respectively), which has been reported to be formed

by photo-oxidation of anthropogenic emissions, such as polycyclic aromatic hydrocarbons and phthalates [*Kautzman et al.*, 2010]. To a minor extend, PHT can also be attributed to primary emissions by biomass burning and vehicle exhaust [*Zhang et al.*, 2010]. Therefore, SEB and DOD might also result from anthropogenic sources.

ADI (C6 dicarboxylic acid) has been reported to be of anthropogenic origin [*Grosjean et al.*, 1978]. It exhibits no significant correlation to PHT, suggesting a different, yet anthropogenic source. Moderate correlations are found to the dicarbonyls G and MG and the diacids PIM (C7) and SEB (C10) with coefficients ranging from 0.514 to 0.577. As PIM and SEB were already linked to biomass burning, but no such correlation is visible for ADI, PIM and SEB may be partly formed from a second, anthropogenically influenced source.

Principal Component Analysis

In order to further elucidate the described connections, a principal component analysis (PCA) was performed (using IBM® SPSS® Statistics version 22). In a PCA, a set of principal components (or factors) is extracted from a dataset. These PCs are orthogonal, i.e. independent of each other, and explain a certain proportion of the variance of the data. In the context of atmospheric chemistry, the PCs could represent independent environmental parameters influencing aerosol composition, for example. Together with the PCs, the PCA computes *loadings* for the given variables. Loadings can be explained as correlations between the original variables and the extracted principal components; therefore, high loadings show the connection of a variable to a certain PC ([*Hervé*, 2003]). The PCA was calculated based on the dataset used for correlation analysis (i.e., three year averages without the period influenced by melting). Concerning the forest fire data, only the dataset for southern Switzerland was used, as no significant correlations were obtained for the fire data from Valais or the 50 km range around the glacier site. For the same reason, the temperature of Lugano was not used either. The results are presented in Table 5.3 and Table 5.4.

Table 5.3 Principal components and explained variance (calculated using SPSS® Statistics)

Principal component	Eigenvalue	Explained variance %	Cumulative %
PC1	9.881	47.052	47.052
PC2	3.976	18.934	65.985
PC3	1.968	9.371	75.356
PC4	1.462	6.964	82.320

Table 5.4 Component matrix

	Components			
Variable	PC1	PC2	PC3	PC4
PIM	**0.967**			
PIN	**0.873**			
MPH	**0.866**			
NIT	**0.863**			
SUB	**0.835**			
pH	**-0.835**			
PHB	**0.816**	0.413		
SUL	**0.801**	0.496		
AMM	**0.781**	0.488		
G	**0.774**			
SEB	**0.725**	-0.442		
FSS	**0.672**	0.481		
MG	0.644	-0.544		
ADI	0.467	-0.435	0.410	
CAL		**0.742**		
FOR	-0.401	**0.683**		0.523
OXA		**0.672**		0.410
PHT		-0.595		
DOD	0.513	-0.587		
VAN	0.549		**-0.783**	
AZE			-0.509	0.618

Factor loadings ≤|0.4| are not shown for reasons of clarity.

Four principal components were found to account for 82.3 % of the variability of the data in total. PIM, PIN, MPH, NIT, SUB, PHB, SUL, AMM, G, SEB, and FSS load positively on PC1 with loadings higher than 0.65, and pH loads negatively on PC1. All those compounds (except for SEB) have already been grouped by the correlation analysis. PC1 might therefore be connected to biomass burning, explaining 47.1 % of the data variability. Biomass burning is thus suggested to be the most important parameter influencing the composition of organic aerosol deposited at the glacier site.

The second principal component (PC2), which accounts for 18.9 % of the data variability, is dominated by high positive loadings of CAL, OXA, and FOR, all above 0.65. These correlations have also been observed in the correlation map (Fig. 5.6), and were explained by a possible link to mineral dust, which is the major source of CAL being transported to the glacier. Interestingly, the compounds SEB, ADI, MG, DOD, and PHT load negatively on PC2, indicating a link between these species. Indeed, the five compounds show medium to good correlations among each other. As ADI and PHT are reported to be of anthropogenic origin [*Hatakeyama et al.*, 1987; *Koch et al.*, 2000; *Zhang et al.*, 2010], this group may be influenced by anthropogenic emissions. PC3 is dominated by a negative loading of VAN, PC4 by a positive loading of AZE. VAN and AZE are well correlated (r=0.601, p=0.018), however, as they load on different principal components, they may be partly assigned to different sources. VAN is reported to be a conifer biomass burning marker, while AZE is formed by photo-oxidation of oleic acid, for example. Therefore, PC3 may be linked to a second type of biomass burning. A source assignment was not possible for PC4, as the compounds loading on PC4 (AZE, OXA, and FOR) showed no significant correlation except for the already discussed link between OXA and FOR. In order to facilitate the interpretation of the resulting principal components, a *Varimax* rotation was applied. The goal of a *Varimax* rotation is the assignment of a small number of large loadings and a large number of small (or zero) loadings to a PC. Formally, the *Varimax* algorithm searches for a rotation (i.e. linear combination) of the original principal components that yields maximum variance of the loadings ([*Hervé*, 2003]).

The resulting rotated component matrix is given in Table 5.5. After the rotation, only eight components load on more than one component, leaving the matrix more structured. Furthermore, only three variables, including the pH, exhibit a negative loading, which also facilitates interpretation. PC1 is still suggested to be linked to biomass burning. In contrast to the original component matrix, all compounds loading on PC1 – except for G – show a significant correlation to the burned area (FSS). PC2 is dominated by high positive loadings of PHT, SEB, MG, ADI, and DOD, revealing a possible connection to anthropogenic emissions. CAL, OXA, and FOR load positively on PC3, supporting the suggested link to mineral dust transport. Finally, AZE and VAN exhibit high positive loadings on PC4, which may have biomass burning and/or biogenic background.

The correlation and principal component analyses of the concentration changes suggest that the major sources influencing the organic composition of the historic glacier samples were (in order of decreasing importance) i) biomass burning, ii) anthropogenic emissions, iii) mineral

dust, and iv) biomass burning/biogenic emission. In the following, these source assignments of organic species deposited at the Grenzgletscher are discussed in more detail.

Table 5.5 Rotated component matrix

Variable	Components			
	PC1	PC2	PC3	PC4
SUL	**0.959**			
AMM	**0.936**			
PHB	**0.892**			
pH	**-0.854**			
FSS	**0.848**			
PIN	**0.811**	0.411		
PIM	**0.793**	0.565		
SUB	**0.776**			0.434
NIT	**0.729**	0.454		
MPH	**0.693**	0.433		
G	**0.692**	0.471		
MG		**0.852**		
SEB		**0.816**		
PHT		**0.750**		
ADI		**0.697**		
DOD		**0.629**		
FOR			**0.899**	
OXA			**0.899**	
CAL			**0.516**	-0.433
AZE				**0.859**
VAN	0.426		-0.558	**0.643**

Varimax rotation converged in 7 iterations. Factor loadings <|0.4| are not shown for reasons of clarity.

Biomass burning

The main factor influencing the composition of organic species in the ice core from upper Grenzgletscher is suggested to be biomass burning. PIN is found to exhibit a good correlation (r=0.609, p=0.016) to the burned area in southern Switzerland and a strong correlation (r=0.864, p<0.001) to the biomass burning marker compound PHB, which both indicates

biomass burning to be a source for PIN deposited at the glacier. This was not expected in the first place, since PIN is unlikely to be emitted directly through biomass burning, as it is formed in the atmosphere as an oxidation product of biogenic VOCs. However, its precursors, α- and β-pinene, are formed and emitted by a wide range of plant species, especially monoterpene storing conifers, like Scots pine (*pinus sylvestris* L.) [*Bäck et al.*, 2012], and to a minor extend also deciduous trees (e.g., European beech (*fagus sylvatica* L.) [*Dindorf et al.*, 2006] or English oak (*quercus robur* L.*)* [*Pérez-Rial et al.*, 2009]). Indeed, several studies report enhanced emissions of α- and β-pinene through biomass burning [*Cheng et al.*, 2011; *Kahnt et al.*, 2013; *Lee et al.*, 2005; *Simpson et al.*, 2011]. As the emission rate of α-pinene increases exponentially with temperature [*Janson*, 1993; *Komenda*, 2002; *Martin et al.*, 1999], the heat wave associated with forest fires may cause the emission of large amounts of terpenes from the needles of the surrounding softwood trees. Alternatively, pinenes could be emitted directly from the burning trees, provided that not all of the emitted terpenes are oxidized in the flames. Emissions from smoldering are generally found to be higher than from flaming [*Lee et al.*, 2005]. Pinenes can also be emitted from wood burning in fireplaces and stoves, although at much lower emission levels compared to active prescribed burning [*Cheng et al.*, 2011; *Lee et al.*, 2005]. This is possibly due to the much lower concentration levels of monoterpenes in trunks and logs compared to leaves of softwood, as terpenes are mainly formed in chloroplasts in the leaves. Once emitted into smoke plumes, α- and β-pinene are likely to be oxidized by ozone or OH-radicals to form less volatile products leading to SOA. The formation of pinonic acid associated with wood burning is reported by Cheng et al. [*Cheng et al.*, 2011]; hence, the formation of pinic acid in wood burning plumes is also likely, as both pinonic acid and pinic acid are major products of pinene oxidation [*Hoffmann et al.*, 1998; *O'Dowd et al.*, 2002; *Yu et al.*, 1999]. In addition to the described enhanced emission of precursors, a second factor leading to high concentrations of PIN in connection with biomass burning might be the presence of a larger aerosol phase. As biomass burning is a source of primary particles, the increase in aerosol phase might lead to enhanced partitioning of the newly formed pinic acid into the particle phase, preventing its further degradation. PIN is often used as a marker for biogenic emissions. However, the results of this study indicate that the concentration of PIN detected in the ice core from Grenzgletscher is dominated by biomass burning origin, compared to natural biogenic emissions.

G is a secondary oxidation product formed from biogenic as well as anthropogenic precursors, but has also been reported as a primary emission product by biomass burning. However, no significant correlation among G and the burned area in southern Switzerland was observed.

The connection to biomass burning may therefore differ from other investigated compounds by source region or other unknown aspects.

VAN is a biomass burning marker for conifer species (see chapter 1.1.5) and exhibits a good correlation to PHB (r=0.694, p=0.004) and medium correlations to FSS and AZE (r=0.524 and 0.601, p=0.045 and 0.018, respectively). As VAN is also loading on PC1, but shows no significant correlation to the other dicarboxylic acids and ions grouped by the correlation analysis, VAN might result from a different source, which is at the same time also related to biomass burning.

For certain years, pronounced peaks are visible in the historic records. The largest peak is visible in all records except for those of G, MG, and PHT, in the year 1974. Within the limits of dating accuracy (which is ± 1 year [*Eichler et al.*, 2000b]), the observed concentration maximum might be assigned to biomass burning aerosol from the historic fire season in 1973. With forest fires especially occurring during winter, the burned area in southern Switzerland reached a century maximum of about 7300 ha, which is ten times the mean annual area burned between 1942 and 1993.

Anthropogenic emissions

Volatile organic compounds are emitted by anthropogenic activities, such as industrial production and traffic. The results of this study suggest anthropogenic VOCs to contribute significantly to the organic species detected in the ice core. This is consistent with the sampling site being located in proximity to several highly industrialized countries in Central Europe. PHT, SEB, MG, ADI, and DOD are suggested to be formed by the atmospheric oxidation of anthropogenic emissions. Their direct emission is also possible (e.g., vehicular exhaust), yet reported to be of minor importance compared to secondary formation from VOCs [*Wang et al.*, 2006a]. The emission levels of non-methane(NM)-VOCs and SO_2 in France, Italy, and Switzerland from 1970 to 2000 are shown in Fig. 5.7. In all three countries, SO_2 emissions are reduced significantly starting around 1975-1980, whereas NM-VOC emissions do not decrease significantly until the early 1990s. Actually, this trend is also indicated in the ice core records, as the maximum concentration levels of major VOC oxidation products PHT, ADI, and DOD are found to occur only in the late 1970s to early 1980s and the concentrations are still high in the early 1990s. Unfortunately, the concentration trend could not be investigated thoroughly during this time because of the period influenced by meltwater percolation.
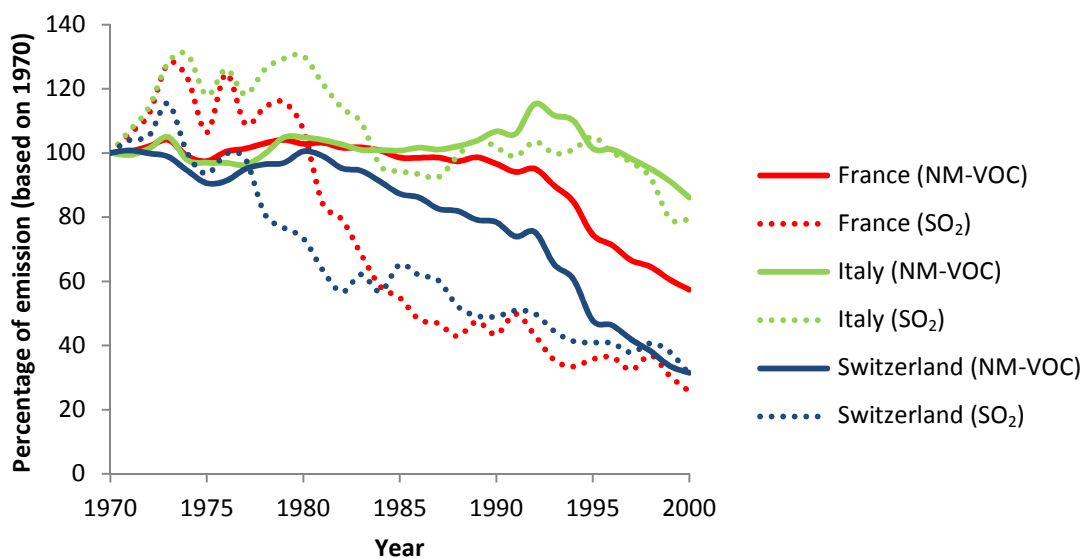
Fig. 5.7 Anthropogenic emissions of non-methane volatile organic compounds (NM-VOC) and SO_2 in France, Italy, and Switzerland from 1970 (basis) to 2000. The data was extracted from the Emission database for Global Atmospheric Research (EDGAR) database (http://edgar.jrc.ec.europa.eu, accessed 04-28-2014).

Mineral dust

A third important parameter influencing the composition of chemical species found in the ice is mineral dust. The observed correlations among OXA, FOR, and CAL are due to common transport. OXA and FOR are taken up by the basic mineral dust during transport to the glacier by acid-base reaction. This could be explained by the high acidity and volatility of the small acids OXA and FOR. Larger (di)carboxylic acids are not found to be correlated to CAL. This is consistent with their lower volatility and lower acidity compared to OXA and FOR.

The known Saharan dustfall of 1949 is visible in both the records of CAL and OXA, but is not included in the record of FOR. Therefore, sources of OXA and FOR might be similar but not identical over the whole time period covered by the glacier. An alternative explanation for the link of OXA to mineral dust containing Ca^{2+} is the stabilization of oxalate due to the formation of calcium oxalate, thus preventing photo-induced decomposition of oxalate ions (which is reported to occur in the presence of iron oxides [*Kim et al.*, 2010; *Rodríguez et al.*, 2009]).

5.2.2.2 Seasonal variation of organic compounds in 1992 and 1993

Ten ice core samples covering the years 1992 and 1993 (dating by A. Eichler, personal communication) were measured to examine the seasonal variation of organic species. The resulting records are presented in Fig. 5.8.
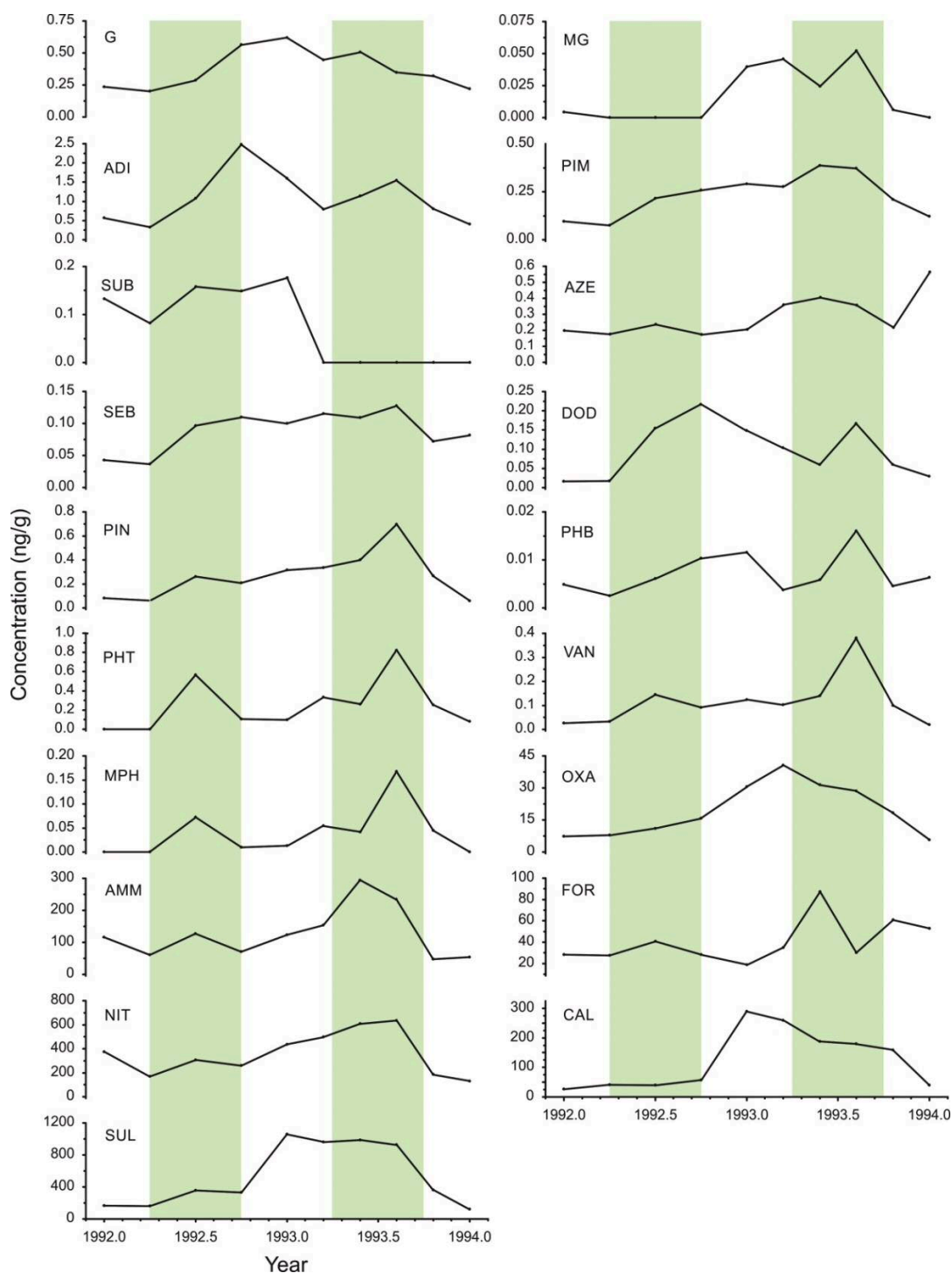
Fig. 5.8 Seasonal variation of α-dicarbonyls, (di)carboxylic acids and ions measured in the glacier ice core from upper Grenzgletscher. The vegetation periods (approx. May – October) are highlighted in green.

The resulting records show the seasonal variation of organic trace compounds and major ions during the year. The vegetation period from May to October is highlighted in green. Many of the targeted compounds exhibit distinct maxima during this period, for example PIN, PHT, MPH, AMM, and VAN. Higher concentrations during summertime can be explained on the one hand, by the enhanced transport to the glacier due to convection-dominated processes in summer, on the other hand, by enhanced emission rates of the respective compounds or their precursors. For PIN, concentration maxima during the vegetation period were expected as a consequence of the enhanced emission of its precursors α- and β-pinene from vegetation at higher temperatures. For the anthropogenic compounds PHT and MPH, for example, the obtained summer maxima might be caused by effective transport. As summer concentrations are suggested to reveal the regional influence of air pollution, the link to the regional industry and traffic as VOC emitting sources is also consistent. However, some compounds show different seasonal variations with maxima shifted to winter. CAL, SUL, and OXA, for example, exhibit concentration maxima at the beginning of 1993. As the transport to the glacier in winter is dominated by advective processes and free tropospheric conditions, compounds deposited in winter might be assigned to long distance transport. This supports the assignment of CAL and OXA to mineral dust, which is brought to the glacier by long distance transport of air masses from North Africa. Another reason for enhanced concentrations of organic compounds in wintertime is biomass burning, as almost all the forest fires take place during the cold and dry season from December to April [*Swissfire database; Pezzatti et al.*, 2005]. Indeed, the biomass burning marker compound PHB as well as the dicarboxylic acids PIM, PIN, SUB, and SEB, which were suggested to be assigned to biomass burning exhibit concentration maxima or at least elevated concentrations during winter. Due to the limited time resolution, it is not possible to explain the seasonal variation of the compounds detected in the ice in more detail. However, the described seasonal variation is in good agreement with the source assignment presented in this work.

5.2.3 Conclusion

For the first time, long-term measurements of organic trace components, such as di- and monocarboxylic acids and α-dicarbonyls, have been reported in an Alpine glacier ice core from upper Grenzgletscher, Switzerland. Correlation analysis and PCA revealed that the obtained concentration changes represent changes in the area affected by forest fires. Thus, biomass burning is suggested to be the most important parameter influencing the composition of the organic compounds present in the ice. When investigating biomass burning aerosol

constituents, it is important to notice that biomass burning is not only contributing to atmospheric aerosol by primary emissions during the burning process but also by the formation of secondary organic aerosol after the enhanced emission of biogenic VOCs at elevated temperature. According to this, PIN quantified in the ice core is suggested to be formed as secondary oxidation product of monoterpenes emitted during biomass burning. Concentration trends of some organic compounds also represent changes in anthropogenic emissions. The anthropogenic emission of VOCs, leading to polar oxidation products being deposited at the glacier site, is therefore considered to be a second parameter influencing the composition of organic species in the ice.

These observations are in contrast to the results obtained for the small carboxylic acids OXA and FOR. A strong correlation of OXA and FOR to CAL was observed, indicating the uptake of small acids by basic, calcareous aerosol. The concentration records of OXA and FOR are thus mainly affected by changing dust transport to the drilling site. No such connection was detected for larger dicarboxylic acids.

5.3 Non-target analysis

As discussed in chapter 1.2, organic matter present in ice cores is a mixture of immense complexity comprising thousands of different compounds. Studies focusing on the analysis of ice samples on a molecular level (including the work presented in this thesis) have already provided valuable information on the chemical composition of the ice. However, as with organic aerosol currently present in the atmosphere, a major part of the organic carbon preserved in the ice is still unknown. Furthermore, certain knowledge about the type of chemical species present in the ice is essential for studies on a molecular level – including compound specific method development. Therefore, a non-target analysis of the ice core samples from Grenzgletscher was performed using high resolution accurate mass spectrometry. Since many organic compounds are only present in trace amounts, the glacier samples were enriched using SPE prior to mass spectrometric analysis.

5.3.1 Sample preparation and MS

Aliquots of the melted glacier samples were enriched by a factor of about 200 using SPE with C18 stationary phase. As the available sample volume was less for samples of higher age and

generally limited, samples were combined for certain years to yield a total volume for SPE of at least 80 mL per sample.

SPE cartridges (3 mL) were equilibrated with 4x2.5 mL ACN and 4x2.5 mL ultrapure water using a vacuum manifold. The melted ice core samples (or ultrapure water for blank assessment) were applied to the cartridges using a flow rate of 1-2 mL/min. After retention, the cartridges were sucked dry for about 1 min before elution. Elution was performed manually by applying 5x1 mL ACN at a flow rate of less than 1 mL/min to ensure complete elution. The solvent was evaporated using a gentle stream of N_2 at 30 °C. The residue was dissolved in 500 µL of eluent solution (H_2O/ACN 90/10, v/v) and the solution was provided for UHPLC-HRMS analysis.

To perform a non-target analysis using HRMS, the sample solution can either be injected directly into the ESI source, or be separated by (U)HPLC prior to mass spectrometric analysis. The direct approach is less time and solvent consuming compared to the procedure including chromatographic separation. However, as all compounds enter the ion source at the same time, ionization suppression may occur, especially impeding the ionization of trace compounds present in the sample. Therefore, the samples were separated by a C18 analytical column before entering the ionization source.

The measurements were conducted using the UHPLC-HRMS system described in Section 2.3.3 and 4.2.4. The UHPLC flow rate was 500 µL/min, the injection volume was 20 µL. The optimized gradient was 1 % B at 0 min, 1 % B at 1 min, 20 % B at 2 min, 20 % B at 5 min, 30 % B at 6 min, 50 % B at 7 min, 99 % B at 7.5 min, and 99 % B at 8 min. As the gradient started with a high water content, heated electrospray ionization (HESI) was applied to enhance vaporization of the solution. The HESI temperature (heating the LC flow before it enters the spray needle in the ESI source) was set to 120 °C. ESI was conducted in the negative ionization mode.

To extend the calibration range of the instrument to lower masses, an additional calibration standard (4-hydroxybutanoic-acid) with *m/z* 103.04007 ([M-H]⁻) was added to the commercially available calibration mix before performing the mass calibration. All samples were measured in quadruplicate. The resulting data were assessed using commercially available software (SIEVE® and XCalibur®, Thermo Scientific). The data analysis workflow was conducted as follows: By measuring 26 samples and a blank sample four times each, with 1086 mass spectra per chromatographic run, a two dimensional space of retention time (0.7-7 min) vs. mass to charge ratio (*m/z* 80-500) of the UHPLC-MS analyses of all samples was created. Sieve was used to search the dataset for peaks above a threshold value of 1e05 counts, which

differ significantly from the blank chromatogram. The resulting list contains *m/z* ratios with corresponding retention time. As the measurement was performed in the negative ion mode, the *m/z* ratios were attributed to molecular ions [M-H]$^-$ of the compounds present in the ice samples. Besides, the software is able to assign signals from adduct and cluster ions, as well as isotopic signals with the same retention time and exact mass difference to the molecular ion. This prevents those ions to be falsely listed as independent molecular ions. The assignment of possible elemental compositions for each compound was done manually using XCalibur® 2.2. Molecular formulas were assigned using carbon (C), hydrogen (H), oxygen (O), nitrogen (N), and sulfur (S) with the following constraints: #^{12}C: 1 to 45, #^{1}H: 1 to 60, #^{14}N: 0 to 10, #^{16}O: 2 to 45, and #^{32}S: 0 to 4. Formulas with a mass tolerance of more than ±2.5 ppm, and a non-integer or negative double bond equivalent (DBE) were removed. Chemically unreasonable formulas involving several heteroatoms in one molecule or chemically impossible O/C and H/C-ratios were sorted out as well. Additionally, the abundance and intensity height of the ^{13}C isotopic peak was checked to finally verify the attributed elemental formula.

5.3.2   Results and discussion

Over 1,000 *m/z* ratios were detected in the glacier samples, of which 409 were assigned a molecular formula with a mass tolerance <|2.5| ppm. The resulting list of *m/z* ratios was divided into CHO, CHNO, CHOS and CHNOS containing compounds.

5.3.2.1   CHO and CHNO containing compounds

The majority of *m/z* ratios measured in the ice core samples were assigned molecular formulas containing CHO and CHNO (see Table 7.2 and Table 7.3 in the supporting material section). Depending on their O/C and H/C ratios, the complex mixture of organic compounds present in environmental samples can be visualized using a *van-Krevelen* diagram (Fig. 5.9). In this diagram, different ranges of O/C vs. H/C are associated with certain compound classes. Kim et al., 2003 [*Kim et al.*, 2003] assigned the areas A, B, and C (blue ellipses) to the compound classes lipids, condensed hydrocarbons, and lignins, respectively. Some of the detected compounds lie in the range of condensed hydrocarbons and lignins, however the major part of the compounds exhibit an O/C value between 0.2 and 0.5 and H/C value between 1.4 and 2.2. This location is within the area D, which was assigned to aliphatic species in a recent study focusing on the analysis of urban aerosol using ultrahigh resolution mass spectrometry

[*Kourtchev et al.*, 2014]. In the same study, the areas labeled E and F are associated with SOA and aromatic species, respectively.
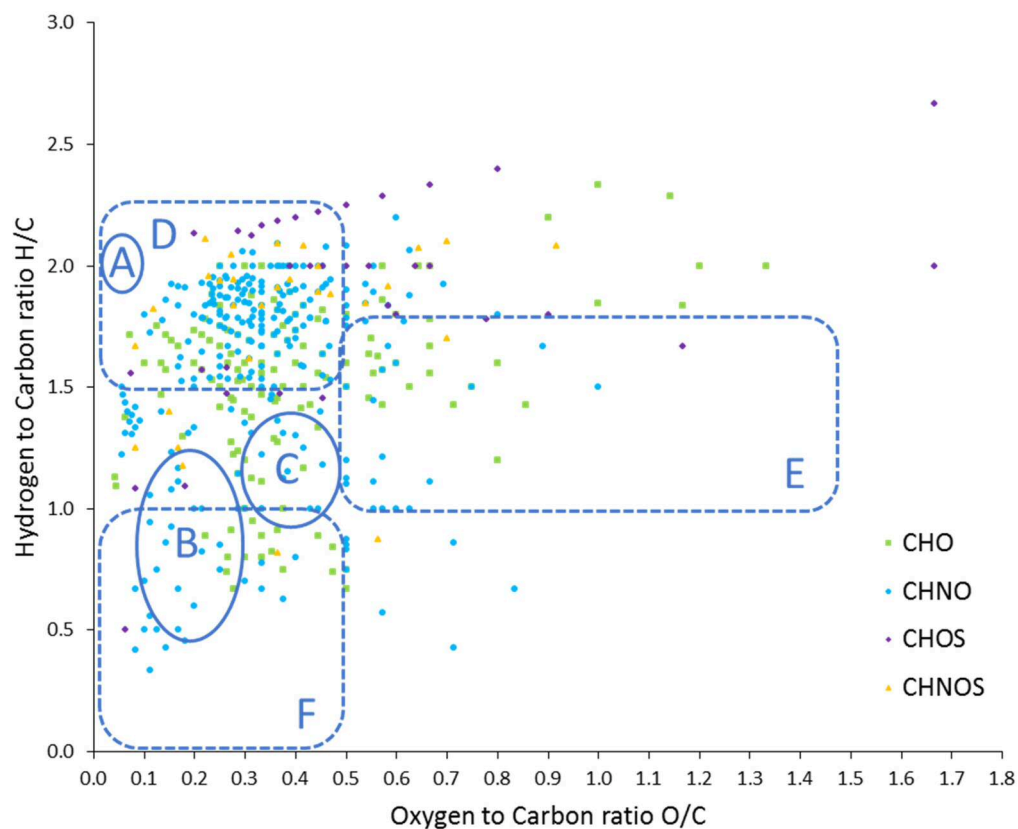
 Fig. 5.9 *Van Krevelen* diagram of CHO, CHNO, CHOS, and CHNOS containing compounds detected in the ice core samples from Grenzgletscher. Areas A, B, and C are assigned to the compound classes lipids, condensed hydrocarbons, and lignins [*Kim et al.*, 2003], D, E, and F to aliphatic species, SOA, and aromatic species, respectively [*Kourtchev et al.*, 2014].

Kroll et al., 2011, suggested the carbon oxidation state to be a valuable metric for describing chemical properties of complex atmospheric organic aerosol. For compounds composed of only carbon, hydrogen, and oxygen, the average carbon oxidation state $\overline{OS}_C$ can be estimated using Equ. 5.1.

$$\overline{OS}_C \approx 2\,O/C - H/C \tag{5.1}$$

As nitrogen atoms are not included in the calculation, the use of $\overline{OS}_C$ is discussed here only for CHO containing compounds. The plot of the resulting $\overline{OS}_C$ values against the number of carbon atoms for the CHO containing compounds detected in the ice core is depicted in Fig. 5.10. Several studies describe ranges of $\overline{OS}_C$ for certain aerosol classes, such as biomass burning

organic aerosol (BBOA), semi-volatile oxidized organic aerosol (SV-OOA), and low-volatile oxidized organic aerosol (LV-OOA), the last two corresponding to fresh and aged secondary aerosol produced by atmospheric oxidation processes ([*Kroll et al.*, 2011] and references cited there). The position of these individual groups in the $\overline{OS}_C$-n plane is marked by blue ellipses. Most of the observed compounds in this work lie in the range associated with biomass burning aerosol. This supports the results of the target analysis described in section 5.2.2, which suggest biomass burning to be the major source of organic species present in the ice core from Grenzgletscher. The importance of secondary organic aerosol as a source for organics in ice is also indicated, as many compounds lay in the range attributed to SV-OOA and LV-OOA.
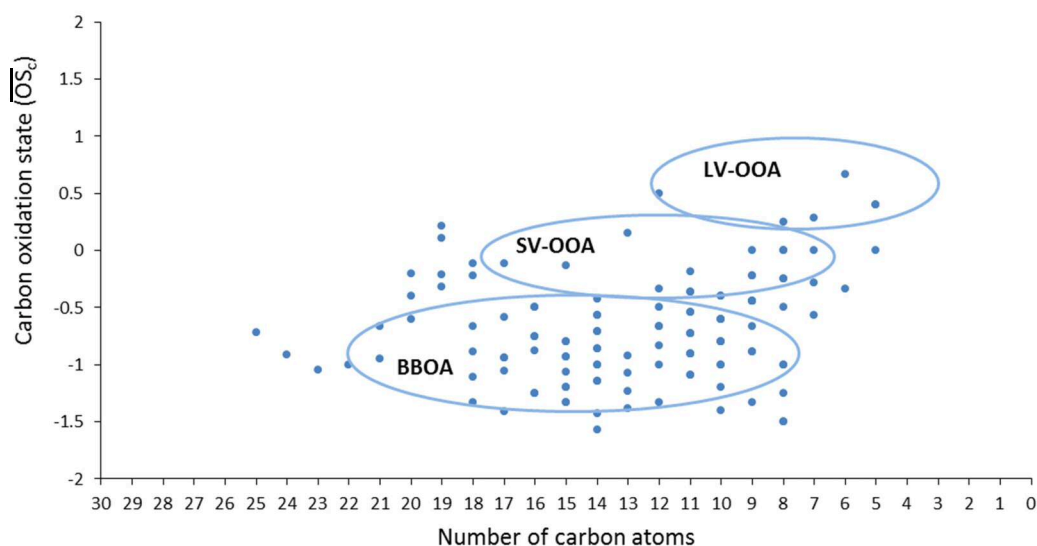
Fig. 5.10 Carbon oxidation state ($\overline{\mathbf{OS}}_\mathbf{C}$) versus number of carbon atoms for CHO-containing compounds present in the ice core samples.

5.3.2.2 CHOS and CHNOS containing compounds

Several organic compounds containing sulfur or both sulfur and nitrogen were found in the ice core samples. The lists of CHOS and CHNOS containing compounds are presented in Table 5.6 and Table 5.7, respectively. Among these compounds, organosulfates and nitrooxy organosulfates constitute an important compound class, as they are found to be a major fraction of ABSOA (see section 1.1.6). To the author's best knowledge, this work is the first to report the investigation of OS and NOS in ice core samples. To be identified as OS or NOS, the number of oxygen atoms in an organic molecule has to be at least four times the number of sulfur atoms. More than 20 possible OS or NOS species were found in the ice core from

Grenzgletscher, including prominent examples extensively described in the literature, e.g., organosulfate *m/z* 153 and nitrooxy organosulfates *m/z* 294. The latter were identified also through the presence of all five isomers reported in the literature, as well as MS/MS experiments, resulting in the same fragments as reported by Surratt et al. [*Surratt et al.*, 2007]. The obtained fragment mass spectrum of *m/z* 294 is given in the "supporting material" section.

Table 5.6 CHOS and containing compounds in the Grenzgletscher ice core

measured *m/z* [M-H]⁻	formula	mass deviation (ppm)	DBE	RT (min)	possible compound, literature
152.9864	$C_3H_6O_5S$	0.083	1	0.39	[*Hansen et al.*, 2014; *Stone et al.*, 2012; *Surratt et al.*, 2008; *Surratt et al.*, 2007] (aerosol), [*Altieri et al.*, 2009] (rain)
155.0020	$C_3H_8O_5S$	0.017	0	0.37	2-hydroxypropyl hydrogen sulfate
167.0384	$C_5H_{12}O_4S$	0.043	0	1.90; 2.22	pentyl hydrogen sulfate
181.0541	$C_6H_{14}O_4S$	0.426	0	2.40; 2.54	hexyl hydrogen sulfate
195.0700	$C_7H_{16}O_4S$	0.19	0	3.11; 3.47	[*Vogel* 2014] heptyl hydrogen sulfat
209.0858	$C_8H_{18}O_4S$	-1.114	0	5.88; 6.68	[*Vogel* 2014] octyl hydrogen sulfat
223.1014	$C_9H_{20}O_4S$	0.121	0	6.66; 6.75; 6.87; 6.30; 7.17	[*Lin et al.*, 2012a] nonyl hydrogen sulfat
225.0080	$C_6H_{10}O_7S$	1.037	2	2.14; 2.50	[*Lin et al.*, 2012a]
237.1171	$C_{10}H_{22}O_4S$	0.282	0	6.97; 7.11	[*Lin et al.*, 2012a]
251.0964	$C_{10}H_{20}O_5S$	0.328	1	2.82; 3.03; 3.23; 3.30	[*Lin et al.*, 2012a]
259.0646	$C_{11}H_{16}O_5S$	0.164	4	2.73	[*Lin et al.*, 2012a]
265.1120	$C_{11}H_{22}O_5S$	0.65	1	3.63; 3.85; 4.94; 5.96	[*Lin et al.*, 2012a]
265.1486	$C_{12}H_{26}O_4S$	0.855	0	7.64	
269.1219	$C_{14}H_{22}O_3S$	0.526	4	7.12	
278.9955	$C_{16}H_8OS_2$	1.650	13	2.14; 2.50	
297.0474	$C_{10}H_{18}O_6S_2$	0.125	2	7.13; 7.78	
299.0266	$C_9H_{16}O_7S_2$	0.075	2	3.58; 7.17; 4.98	
313.0788	$C_{11}H_{22}O_6S_2$	0.054	1	7.78	
337.2058	$C_{16}H_{34}O_5S$	0.628	0	7.76	[*Lin et al.*, 2012a]
345.0320	$C_{10}H_{18}O_9S_2$	-0.077	2	6.45; 7.69	
367.1590	$C_{19}H_{28}O_5S$	0.033	6	6.76	
369.1750	$C_{19}H_{30}O_5S$	0.195	5	6.96	
377.1588	$C_{24}H_{26}O_2S$	0.413	12	7.49	
388.0975	$C_{14}H_{28}O_6S_3$	-0.667	0		
395.2114	$C_{18}H_{36}O_7S$	-0.217	1	7.94	[*Lin et al.*, 2012a]
399.1483	$C_{19}H_{28}O_7S$	-0.12	1	7.54	
401.1489	$C_{15}H_{30}O_{10}S$	-0.945	6	7.97	
461.2556	$C_{27}H_{42}O_2S_2$	0.421	1	7.60	

Table 5.7 CHNOS containing compounds in the Grenzgletscher ice core

measured m/z [M-H]$^-$	MW	formula	mass deviation (ppm)	DBE	RT (min)	literature
220.0802	221	$C_{12}H_{15}NOS$	0.099	6	7.74	
236.0752	237	$C_{12}H_{15}NO_2S$	0.200	6	6.89	
294.0659*	295a	$C_{10}H_{17}NO_7S$	0.967	3	4.10; 5.81; 6.08; 6.37; 6.53	[*Gao et al.*, 2006; *Gómez-González et al.*, 2012; *Hansen et al.*, 2014; *Iinuma et al.*, 2007; *Kristensen and Glasius*, 2011; *Lin et al.*, 2012a; *Surratt et al.*, 2007; *Surratt et al.*, 2008; *Vogel* 2014; *Yttri et al.*, 2011] (aerosol) and [*Altieri et al.*, 2009] (rain)
294.1386	295b	$C_{12}H_{25}NO_5S$	1.031	1	3.86	
298.0973	299	$C_{10}H_{21}NO_7S$	0.282	1	7.00; 7.23	[*Lin et al.*, 2012a]
331.1122	332	$C_{17}H_{20}N_2O_3S$	-0.291	9	0.39	
350.0556	351	$C_{13}H_{21}NO_4S_3$	-0.324	4	7.78	
351.1233	352	$C_{13}H_{24}N_2O_7S$	-0.014	3	6.82	
364.1622	365	$C_{16}H_{31}NO_4S_2$	-0.668	2	7.97	
368.2128	369	$C_{17}H_{31}N_5O_2S$	0.871	5	7.91	
374.2012	375	$C_{18}H_{33}NO_5S$	0.462	3	6.71	[*Vogel* 2014] aerosol
376.2166	377	$C_{18}H_{35}NO_5S$	0.300	2	6.95; 7.08	[*Vogel* 2014] aerosol
390.1961	391	$C_{18}H_{33}NO_6S$	0.944	3	6.00; 6.76	[*Vogel* 2014] aerosol
408.2062	409	$C_{18}H_{35}NO_7S$	0.229	2	7.49	[*Vogel* 2014] aerosol
416.0626	417	$C_{12}H_{23}N_3O_7S_3$	0.059	3	2.49; 3.33	
423.1810	424	$C_{17}H_{32}N_2O_8S$	0.733	3	2.81	
432.2794	433	$C_{22}H_{43}NO_5S$	-0.040	2	7.54	
437.0413	438a	$C_{16}H_{14}N_4O_9S$	0.339	12	7.88	
437.1969	438b	$C_{18}H_{34}N_2O_8S$	0.298	3	3.38	
439.2133	440	$C_{18}H_{36}N_2O_8S$	0.182	2	7.73	
450.2903	451	$C_{22}H_{45}NO_6S$	0.417	1	7.73	
451.2461	452	$C_{24}H_{40}N_2O_2S_2$	-0.051	6	7.84	
454.0522	455a	$C_{12}H_{25}NO_{11}S_3$	0.009	1	6.82; 7.16; 7.35	
454.1299	455b	$C_{20}H_{28}N_3O_3S_3$	-0.148	8	7.88	
461.2669	462	$C_{18}H_{38}N_8O_4S$	-0.554	4	7.83	
493.2600	494	$C_{22}H_{42}N_2O_8S$	0.689	3	6.91	

*Five isomers were separated by UHPLC, which is the same number of isomers described in the literature (e.g. [*Gómez-González et al.*, 2012]).

The presence of (nitrooxy) organosulfates in the ice core indicates the influence of both anthropogenic and biogenic emissions at the sampling site in the Alps. This observation is consistent with the results of the target analysis presented in the previous chapters.

5.3.3 Conclusion and outlook

A non-target-screening analysis of ice core samples from Grenzgletscher was performed using high-resolution mass spectrometry. More than 400 compounds were observed and assigned a molecular formula, many of which have already been described to be present in aerosol-related environmental samples. Using a *van Krevelen* diagram, most of the compounds were suggested to be aliphatic species. By comparison of the carbon oxidation state with data from the literature, a major part of the CHO-containing organic compounds in the ice was suggested to originate from biomass burning processes.

Further studies should investigate the effect of compounds containing nitrogen and other heteroatoms on measured OS_C, as many of the detected molecules contain nitrogen and/or sulfur. While the work presented in this thesis is focused on the organic compounds present in all measured ice core samples in total, a time-resolved synopsis of chemical species in the glacier ice core will be object of future study.

For the first time, several organosulfates and nitrooxy organosulfates, including the ubiquitous nitrooxy organosulfates *m/z* 294, have been found in the ice core from Grenzgletscher. While this study reported OS and NOS on a qualitative level, a quantitative analysis of OS and NOS in future ice core studies may provide new insights into the interplay of biogenic and anthropogenic compounds in SOA formation over time. Especially concerning the Alps as a region influenced by biogenic emissions as well as anthropogenic emissions from the surrounding industry in Central Europe, the investigation of ABSOA in glaciers might be beneficial. Additionally, ice core studies focusing on OS and NOS in polar regions could reveal new information on the long range transport of anthropogenically enhanced SOA components and their abundance in connection to human activity. The nitrooxy organosulfates *m/z* 294 have already been reported in arctic aerosol, indicating their potential presence in polar ice cores.

Concerning method development for non-target screening analysis of ice, the sample enrichment is a crucial step as the compounds are only present in trace amounts in the ice. However, the applied enrichment technique determines the range of compounds accessible for analysis. Therefore, additional optimization of the extraction procedure, such as fractionated extraction, could prove useful for the analysis of non-polar and polar compounds in the same ice sample, especially in case of limited sample volume.

6 SUMMARY AND OUTLOOK

The development and validation of two methods for the quantification of small, polar organic compounds in snow and ice samples was a major part of the thesis work. The first method comprised stir bar sorptive extraction and HPLC-ESI-MS analysis, targeting α-dicarbonyls glyoxal and methylglyoxal. The focus of the method development lay on the prevention or reduction of background contamination from the ubiquitous analytes. A clean-up procedure of the derivatization reagent as well as additional heating of all glassware used during the sample preparation was applied, effectively minimizing blank concentrations. The developed method was well suited for the sensitive and selective analysis of glyoxal and methylglyoxal in molten ice and snow samples. As a proof of principle, snow samples from Hohenpeissenberg (Germany) and ice core samples from a Swiss glacier were analyzed.

The second method targeting organic compound in ice comprises SPE and UHPLC-ESI-MS with high resolution accurate mass detection for the analysis of dicarboxylic acids and monocarboxylic acids. SPE with strong anion exchange was applied, followed by a derivatization step employing esterification. The developed method proved to be well-suited for dicarboxylic acids (≥ C6); however, for small dicarboxylic acids, especially oxalic acid, high initial contamination levels were found on SPE cartridges and the extraction showed poor efficiency. A cleaning procedure was developed, combined with exchange of the counter ion to enhance retention of especially small dicarboxylic acids during SPE. This led to a significant reduction of blank concentrations; however, the extraction efficiency could not be enhanced. Further optimization is needed to extend the applicability range of the method to small dicarboxylic acids, possibly through the use of new, polymer-based sorbent materials. As small dicarboxylic acids exhibit chemical properties differing significantly from their homologues, an additional method might be necessary. Oxalic acid can be analyzed using ion chromatography, as done in the glacier field study described in chapter 5.

Both methods were used to analyze ice samples from a glacier ice core from upper Grenzgletscher in the Swiss Alps in collaboration with PSI in Villigen, Switzerland. Forty-nine ice core samples covering the time period from 1942 to 1993 were prepared at PSI and analyzed in Mainz. Data analysis was performed using correlation and principal component analysis. Biomass burning, emission of anthropogenic VOCs, as well as mineral dust transport to the glacier were identified to be the three major parameters influencing the observed

concentrations of organic compounds in the ice. Future studies should include the application of the methods to snow and ice samples from polar regions, to evaluate differences in atmospheric transport and sources of organic matter compared to those found in the mid-latitude glacier. Additionally, samples of much higher age are accessible by analyzing ice cores from polar regions like Antarctica or Greenland. This is very interesting, as naturally occurring changes in the chemical composition of the ice (and hence the atmosphere) could be investigated and compared to anthropogenically caused changes observed after the time of industrialization. However, a compromise between available sample volume and time resolution has to be found when analyzing ice cores from polar regions. By using volumes of 50-80 mL, which is the range applied for the analysis of the Grenzgletscher samples, time resolution would decrease due to the limited amount of sample per year. By analyzing less sample volume to maintain high temporal resolution, the concentration of some trace compounds may fall below the detection limit.

Besides the determination of historic records, the analysis of small, polar organic compounds in snow and ice may also be beneficial concerning the investigation of processes occurring in the ice during and after deposition. Upon exposure to sunlight, chemical species present in the ice may be object to photochemistry. For example, the enhanced photo-dissociation of iron oxides to form bioavailable Fe(II) involving oxalic and formic acids as electron donors in iron complexes has been observed in laboratory and outdoor experiments [*Kim et al.*, 2010]. Analysis of polar, acidic compounds in snow and ice may help to improve the understanding of complex photochemical processes happening in ice, for they are believed to be quite different from aqueous photochemistry.

Concerning further analysis of biomass burning marker compounds in ice cores, it would be beneficial to also quantify levoglucosan in ice cores, as it can account for up to 5 % of smoke particle mass [*Reid et al.*, 2005] and is a specific tracer for wood burning. However, the analysis of levoglucosan requires the application of an additional method.

Furthermore, the methods developed during the doctoral work could also be applied to different matrices in the context of atmospheric chemistry. As the methods have been optimized for molten snow and ice samples, they might be easily transferable to the analysis other aqueous environmental matrices such as rain, fog, and surface water. With modifications in the extraction procedure (filter extraction instead of SPE) the method for dicarboxylic acids can be used for the analysis of aerosol samples. Initial experiments have already been carried out as a proof of principle.

7 APPENDIX

7.1 Supporting material
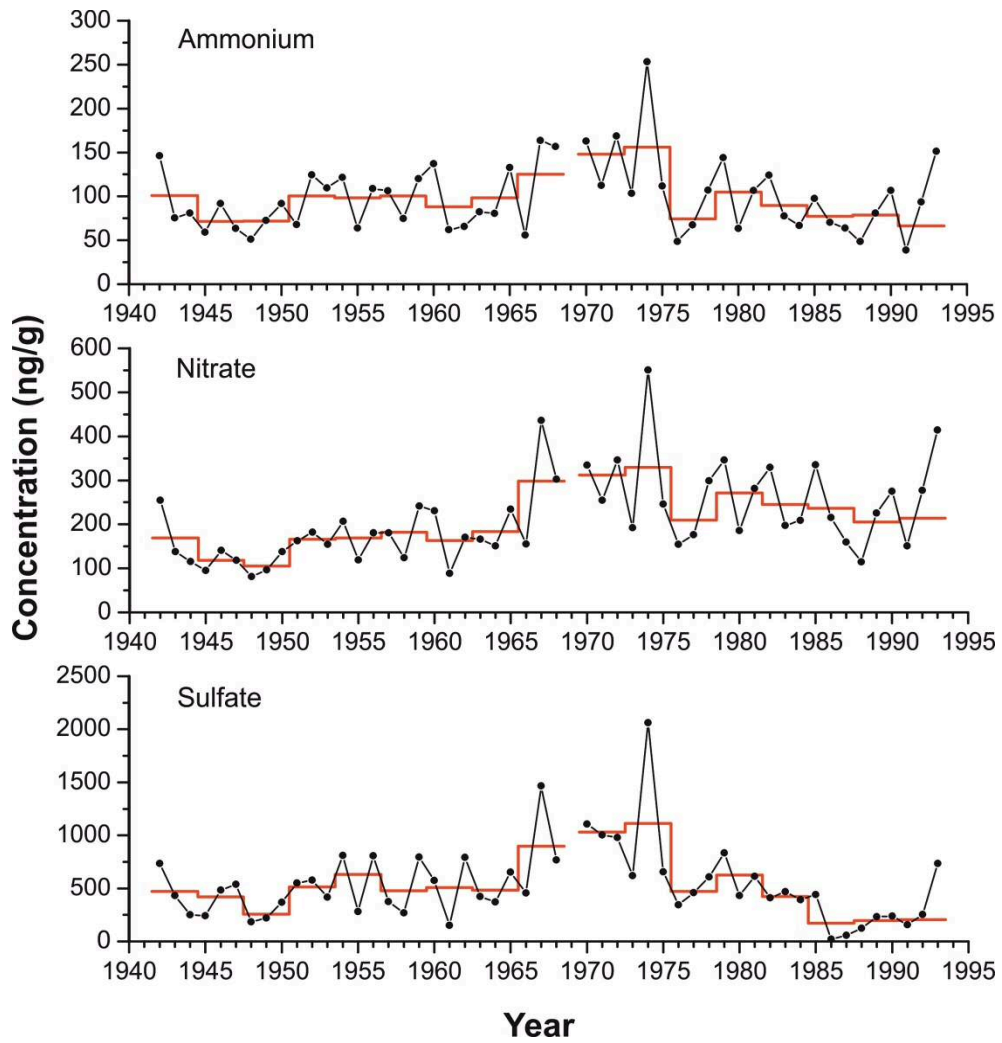

Fig. 7.1 Ice core records of ions ammonium (AMM), nitrate (NIT), and sulfate (SUL) in the alpine ice core from upper Grenzgletscher (with three year average as bold line).
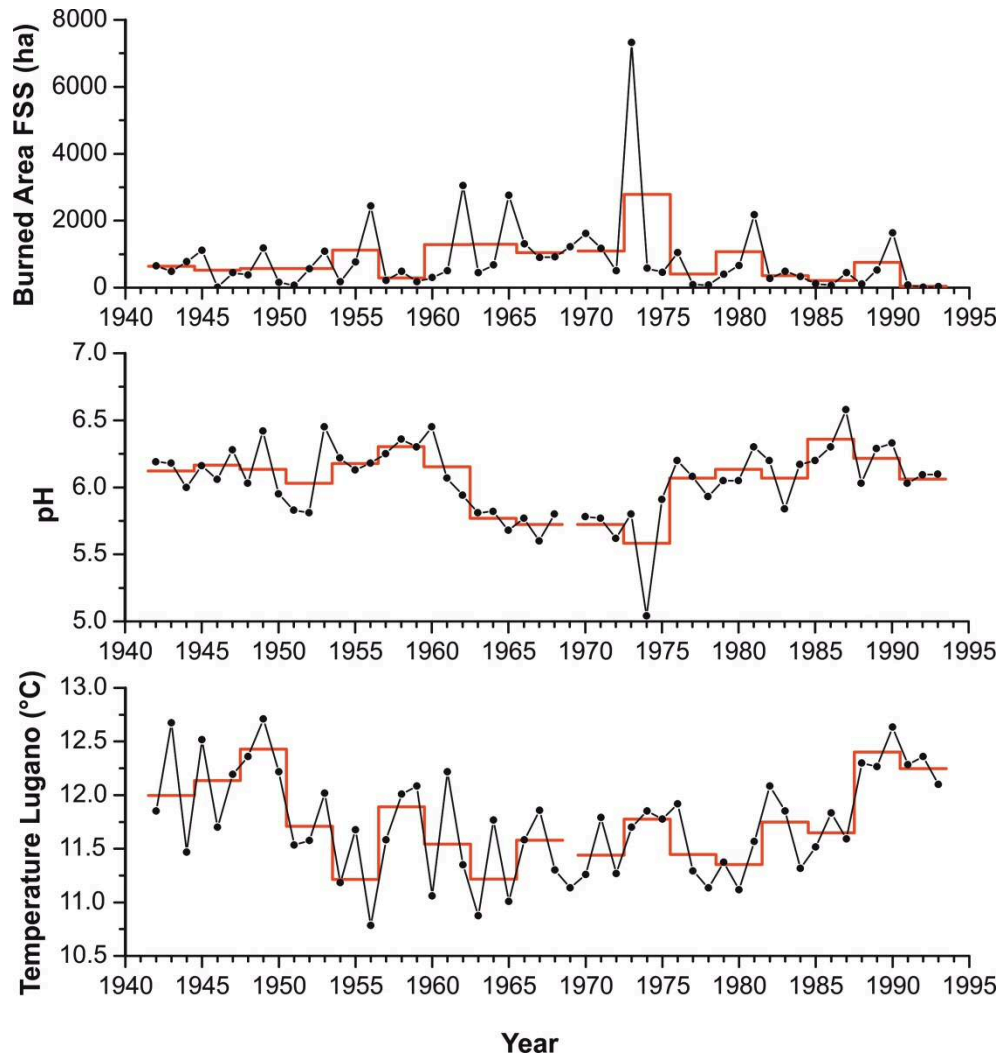
Fig. 7.2 Burned area by forest fires in southern Switzerland (FSS), pH of the ice core samples and mean annual temperature in Lugano (Valais, Switzerland) from 1942 to 1993 (with three year average as bold line).

Table 7.1 Correlation matrix with correlation coefficient r (Pearson) and corresponding p-value (*correlations significant at the 0.05 level, **correlations significant at the 0.01 level)

Correlation matrix - part 1

		G	MG	ADI	PIM	SUB	AZE	SEB	DOD	PIN	PHT	MPH	VAN
G	r		0.534*	0.514	0.784**	0.640*	0.029	0.561*	0.364	0.784**	0.153	0.541*	0.162
	p-value		0.041	0.050	0.001	0.010	0.918	0.029	0.183	0.001	0.586	0.037	0.565
MG	r	0.534*		0.560*	0.691**	0.384	0.139	0.793**	0.500	0.555*	0.669**	0.621*	0.216
	p-value	0.041		0.030	0.004	0.157	0.621	0.000	0.058	0.032	0.006	0.013	0.439
ADI	r	0.514	0.560*		0.577*	0.255	0.190	0.537*	0.449	0.279	0.303	0.208	-0.090
	p-value	0.050	0.030		0.024	0.359	0.497	0.039	0.093	0.314	0.272	0.458	0.749
PIM	r	0.784**	0.691**	0.577*		0.821**	0.315	0.717**	0.444	0.873**	0.379	0.849**	0.386
	p-value	0.001	0.004	0.024		0.000	0.253	0.003	0.098	0.000	0.164	0.000	0.155
SUB	r	0.640*	0.384	0.255	0.821**		0.514*	0.574*	0.229	0.933**	0.203	0.716**	0.426
	p-value	0.010	0.157	0.359	0.000		0.050	0.025	0.412	0.000	0.467	0.003	0.114
AZE	r	0.029	0.139	0.190	0.315	0.514*		0.332	0.311	0.299	0.157	0.257	0.601*
	p-value	0.918	0.621	0.497	0.253	0.050		0.226	0.260	0.278	0.576	0.354	0.018
SEB	r	0.561*	0.793**	0.537*	0.717**	0.574*	0.332		0.769**	0.662**	0.545*	0.570*	0.261
	p-value	0.029	0.000	0.039	0.003	0.025	0.226		0.001	0.007	0.036	0.026	0.347
DOD	r	0.364	0.500	0.449	0.444	0.229	0.311	0.769**		0.245	0.519*	0.396	0.259
	p-value	0.183	0.058	0.093	0.098	0.412	0.260	0.001		0.378	0.047	0.144	0.352
PIN	r	0.784**	0.555*	0.279	0.873**	0.933**	0.299	0.662**	0.245		0.215	0.748**	0.356
	p-value	0.001	0.032	0.314	0.000	0.000	0.278	0.007	0.378		0.442	0.001	0.193
PHT	r	0.153	0.669**	0.303	0.379	0.203	0.157	0.545*	0.519*	0.215		0.573*	0.122
	p-value	0.586	0.006	0.272	0.164	0.467	0.576	0.036	0.047	0.442		0.025	0.664
MPH	r	0.541*	0.621*	0.208	0.849**	0.716**	0.257	0.570*	0.396	0.748**	0.573*		0.512
	p-value	0.037	0.013	0.458	0.000	0.003	0.354	0.026	0.144	0.001	0.025		0.051
VAN	r	0.162	0.216	-0.090	0.386	0.426	0.601*	0.261	0.259	0.356	0.122	0.512	
	p-value	0.565	0.439	0.749	0.155	0.114	0.018	0.347	0.352	0.193	0.664	0.051	
PHB	r	0.577*	0.185	0.087	0.733**	0.829**	0.461	0.379	0.198	0.785**	-0.099	0.659**	0.694**
	p-value	0.024	0.508	0.757	0.002	0.000	0.084	0.163	0.479	0.001	0.727	0.007	0.004
AMM	r	0.605*	0.166	0.131	0.735**	0.732**	0.169	0.272	0.141	0.722**	0.054	0.663**	0.398
	p-value	0.017	0.554	0.641	0.002	0.002	0.546	0.327	0.615	0.002	0.849	0.007	0.142
FOR	r	-0.188	-0.547*	-0.396	-0.319	0.058	0.014	-0.458	-0.578*	-0.022	-0.374	-0.310	-0.455
	p-value	0.501	0.035	0.144	0.247	0.838	0.961	0.086	0.024	0.938	0.170	0.260	0.088
OXA	r	-0.226	-0.489	-0.416	-0.324	-0.019	-0.151	-0.336	-0.471	-0.036	-0.282	-0.326	-0.535*
	p-value	0.419	0.065	0.123	0.239	0.946	0.591	0.221	0.076	0.898	0.309	0.235	0.040
NIT	r	0.607*	0.592*	0.558*	0.853**	0.563*	0.147	0.556*	0.465	0.605*	0.443	0.748**	0.365
	p-value	0.016	0.020	0.030	0.000	0.029	0.601	0.031	0.081	0.017	0.098	0.001	0.181
SUL	r	0.644**	0.225	0.259	0.787**	0.737**	0.192	0.281	0.129	0.741**	0.033	0.660**	0.367
	p-value	0.010	0.421	0.350	0.001	0.002	0.493	0.310	0.647	0.002	0.908	0.007	0.178
CAL	r	-0.042	-0.277	-0.236	-0.069	0.011	-0.272	-0.363	-0.471	0.069	-0.409	-0.154	-0.326
	p-value	0.881	0.318	0.398	0.806	0.970	0.326	0.183	0.077	0.806	0.130	0.585	0.236
pH	r	-0.746**	-0.459	-0.297	-0.825**	-0.666**	-0.105	-0.483	-0.220	-0.783**	-0.083	-0.724**	-0.375
	p-value	0.001	0.086	0.282	0.000	0.007	0.708	0.068	0.430	0.001	0.770	0.002	0.168
T	r	-0.301	-0.006	-0.286	-0.273	-0.284	-0.414	0.094	0.005	-0.190	-0.101	-0.210	-0.412
	p-value	0.276	0.984	0.301	0.324	0.306	0.125	0.740	0.985	0.497	0.721	0.453	0.127
F50	r	0.187	0.026	0.167	0.014	-0.168	-0.282	-0.032	0.359	-0.152	0.454	0.162	-0.110
	p-value	0.503	0.926	0.551	0.962	0.549	0.309	0.910	0.188	0.589	0.090	0.565	0.696
FVa	r	0.168	0.000	0.125	-0.042	-0.164	-0.329	-0.021	0.330	-0.146	0.432	0.093	-0.174
	p-value	0.551	1.000	0.658	0.881	0.559	0.231	0.942	0.230	0.604	0.107	0.742	0.534
FSS	r	0.473	-0.030	-0.022	0.561*	0.637*	0.171	0.216	0.192	0.609*	-0.120	0.587*	0.524*
	p-value	0.075	0.917	0.938	0.030	0.011	0.541	0.440	0.493	0.016	0.669	0.022	0.045

Correlation matrix - part 2

		PHB	AMM	FOR	OXA	NIT	SUL	CAL	pH	T	F50	FVa	FSS
G	r	0.577*	0.605*	-0.188	-0.226	0.607*	0.644**	-0.042	-0.746**	-0.301	0.187	0.168	0.473
	p-value	0.024	0.017	0.501	0.419	0.016	0.010	0.881	0.001	0.276	0.503	0.551	0.075
MG	r	0.185	0.166	-0.547*	-0.489	0.592*	0.225	-0.277	-0.459	-0.006	0.026	0.000	-0.030
	p-value	0.508	0.554	0.035	0.065	0.020	0.421	0.318	0.086	0.984	0.926	1.000	0.917
ADI	r	0.087	0.131	-0.396	-0.416	0.558*	0.259	-0.236	-0.297	-0.286	0.167	0.125	-0.022
	p-value	0.757	0.641	0.144	0.123	0.030	0.350	0.398	0.282	0.301	0.551	0.658	0.938
PIM	r	0.733**	0.735**	-0.319	-0.324	0.853**	0.787**	-0.069	-0.825**	-0.273	0.014	-0.042	0.561*
	p-value	0.002	0.002	0.247	0.239	0.000	0.001	0.806	0.000	0.324	0.962	0.881	0.030
SUB	r	0.829**	0.732**	0.058	-0.019	0.563*	0.737**	0.011	-0.666**	-0.284	-0.168	-0.164	0.637*
	p-value	0.000	0.002	0.838	0.946	0.029	0.002	0.970	0.007	0.306	0.549	0.559	0.011
AZE	r	0.461	0.169	0.014	-0.151	0.147	0.192	-0.272	-0.105	-0.414	-0.282	-0.329	0.171
	p-value	0.084	0.546	0.961	0.591	0.601	0.493	0.326	0.708	0.125	0.309	0.231	0.541
SEB	r	0.379	0.272	-0.458	-0.336	0.556*	0.281	-0.363	-0.483	0.094	-0.032	-0.021	0.216
	p-value	0.163	0.327	0.086	0.221	0.031	0.310	0.183	0.068	0.740	0.910	0.942	0.440
DOD	r	0.198	0.141	-0.578*	-0.471	0.465	0.129	-0.471	-0.220	0.005	0.359	0.330	0.192
	p-value	0.479	0.615	0.024	0.076	0.081	0.647	0.077	0.430	0.985	0.188	0.230	0.493
PIN	r	0.785**	0.722**	-0.022	-0.036	0.605*	0.741**	0.069	-0.783**	-0.190	-0.152	-0.146	0.609*
	p-value	0.001	0.002	0.938	0.898	0.017	0.002	0.806	0.001	0.497	0.589	0.604	0.016
PHT	r	-0.099	0.054	-0.374	-0.282	0.443	0.033	-0.409	-0.083	-0.101	0.454	0.432	-0.120
	p-value	0.727	0.849	0.170	0.309	0.098	0.908	0.130	0.770	0.721	0.090	0.107	0.669
MPH	r	0.659**	0.663**	-0.310	-0.326	0.748**	0.660**	-0.154	-0.724**	-0.210	0.162	0.093	0.587*
	p-value	0.007	0.007	0.260	0.235	0.001	0.007	0.585	0.002	0.453	0.565	0.742	0.022
VAN	r	0.694**	0.398	-0.455	-0.535*	0.365	0.367	-0.326	-0.375	-0.412	-0.110	-0.174	0.524*
	p-value	0.004	0.142	0.088	0.040	0.181	0.178	0.236	0.168	0.127	0.696	0.534	0.045
PHB	r		0.795**	-0.129	-0.184	0.566*	0.813**	0.080	-0.758**	-0.371	-0.207	-0.253	0.864**
	p-value		0.000	0.648	0.511	0.028	0.000	0.778	0.001	0.173	0.459	0.363	0.000
AMM	r	0.795**		-0.067	-0.004	0.780**	0.952**	0.289	-0.742**	-0.399	0.066	0.030	0.742**
	p-value	0.000		0.811	0.989	0.001	0.000	0.297	0.002	0.141	0.817	0.914	0.002
FOR	r	-0.129	-0.067		0.886**	-0.539*	-0.063	0.465	0.208	0.057	-0.232	-0.190	-0.107
	p-value	0.648	0.811		0.000	0.038	0.823	0.081	0.457	0.841	0.405	0.498	0.705
OXA	r	-0.184	-0.004	0.886**		-0.415	-0.011	0.633*	0.176	0.150	-0.213	-0.154	-0.090
	p-value	0.511	0.989	0.000		0.124	0.969	0.011	0.530	0.595	0.445	0.583	0.749
NIT	r	0.566*	0.780**	-0.539*	-0.415		0.787**	0.010	-0.714**	-0.393	0.227	0.160	0.506
	p-value	0.028	0.001	0.038	0.124		0.000	0.971	0.003	0.148	0.416	0.568	0.054
SUL	r	0.813**	0.952**	-0.063	-0.011	0.787**		0.394	-0.740**	-0.476	0.078	0.026	0.766**
	p-value	0.000	0.000	0.823	0.969	0.000		0.146	0.002	0.073	0.783	0.926	0.001
CAL	r	0.080	0.289	0.465	0.633*	0.010	0.394		-0.072	-0.104	-0.173	-0.164	0.175
	p-value	0.778	0.297	0.081	0.011	0.971	0.146		0.798	0.712	0.537	0.560	0.534
pH	r	-0.758**	-0.742**	0.208	0.176	-0.714**	-0.740**	-0.072		0.285	0.155	0.228	-0.673**
	p-value	0.001	0.002	0.457	0.530	0.003	0.002	0.798		0.303	0.581	0.413	0.006
T	r	-0.371	-0.399	0.057	0.150	-0.393	-0.476	-0.104	0.285		-0.291	-0.212	-0.386
	p-value	0.173	0.141	0.841	0.595	0.148	0.073	0.712	0.303		0.293	0.448	0.155
F50	r	-0.207	0.066	-0.232	-0.213	0.227	0.078	-0.173	0.155	-0.291		0.983**	0.102
	p-value	0.459	0.817	0.405	0.445	0.416	0.783	0.537	0.581	0.293		0.000	0.717
FVa	r	-0.253	0.030	-0.190	-0.154	0.160	0.026	-0.164	0.228	-0.212	0.983**		0.064
	p-value	0.363	0.914	0.498	0.583	0.568	0.926	0.560	0.413	0.448	0.000		0.821
FSS	r	0.864**	0.742**	-0.107	-0.090	0.506	0.766**	0.175	-0.673**	-0.386	0.102	0.064	
	p-value	0.000	0.002	0.705	0.749	0.054	0.001	0.534	0.006	0.155	0.717	0.821	

Table 7.2 CHO containing compounds detected in the Grenzgletscher ice core.

measured m/z [M-H]⁻	formula	mass deviation (ppm)	DBE	RT (min)	literature
125.0972	$C_8H_{14}O$	-0.067	2	3.11; 4.13; 6.67	[*Lin et al.*, 2012a]
129.0195	$C_5H_6O_4$	0.372	3	0.71	[*Lin et al.*, 2012a]
131.0350	$C_5H_8O_4$	-0.092	2	1.28	[*Altieri et al.*, 2009; *Mazzoleni et al.*, 2010; *Müller et al.*, 2009]
139.0765	$C_8H_{12}O_2$	0.267	3	2.11	[*Lin et al.*, 2012a; *Mazzoleni et al.*, 2010; *Zhao et al.*, 2013]
141.0558	$C_7H_{10}O_3$	0.302	3	2.43	[*Lin et al.*, 2012a; *Mazzoleni et al.*, 2010]
141.0921	$C_8H_{14}O_2$	0.333	2	2.58; 2.91	[*Mazzoleni et al.*, 2010]
143.1078	$C_8H_{16}O_2$	-0.161	1	7.58	[*Mazzoleni et al.*, 2010]
147.0452	$C_9H_8O_2$	0.321	6	2.31; 2.47	[*Mazzoleni et al.*, 2010]
149.0244	$C_8H_6O_3$	-0.251	6	2.00; 2.24	[*Lin et al.*, 2012a; *Mazzoleni et al.*, 2010]
151.0401	$C_8H_8O_3$	0.017	5	3.08	[*Mazzoleni et al.*, 2010]
151.1129	$C_{10}H_{16}O$	0.01	3	4.16	[*Lin et al.*, 2012a]
155.1079	$C_9H_{16}O_2$	0.303	2	3.97	[*Mazzoleni et al.*, 2010]
157.0506	$C_7H_{10}O_4$	0.05	3	1.62	[*Gómez-González et al.*, 2012; *Lin et al.*, 2012a; *Mazzoleni et al.*, 2010; *Vogel* 2014]
157.0871	$C_8H14_4O_3$	-0.176	2	2.55; 2.75; 2.97; 3.21	[*Kourtchev et al.*, 2013; *Mazzoleni et al.*, 2010; *Vogel* 2014]
163.0403	$C_9H_8O_3$	0.323	6	2.49; 2.76	[*Mazzoleni et al.*, 2010]
165.0193	$C_8H_6O_4$	-0.375	6	1.98	[*Lin et al.*, 2012a; *Mazzoleni et al.*, 2010]
165.0409	$C_5H_{10}O_6$	2.052	1	2.71; 7.94	[*Zhao et al.*, 2013]
165.0557	$C_9H_{10}O_3$	-0.409	5	2.82	[*Lin et al.*, 2012a; *Mazzoleni et al.*, 2010]
167.1079	$C_{10}H_{16}O_2$	-0.078	3	4.89	[*Lin et al.*, 2012a; *Zhao et al.*, 2013]
169.0871	$C_9H_{14}O_3$	0.133	3	2.45	[*Kourtchev et al.*, 2013; *Lin et al.*, 2012a; *Mazzoleni et al.*, 2010; *Müller et al.*, 2009]
171.0664	$C_8H_{12}O_4$	0.104	3	1.93	[*Claeys et al.*, 2009; *Hoffmann et al.*, 1998; *Kourtchev et al.*, 2013; *Kristensen and Glasius*, 2011; *Mazzoleni et al.*, 2010; *Müller et al.*, 2009; *Vogel* 2014]
173.0456	$C_7H_{10}O_5$	-0.154	3	0.91; 1.09	[*Bateman et al.*, 2012; *Lin et al.*, 2012a; *Mazzoleni et al.*, 2010; *Vogel* 2014]
177.0560	$C_{10}H_{10}O_3$	-0.155	6	2.97; 3.18	[*Lin et al.*, 2012a; *Mazzoleni et al.*, 2010]
179.0351	$C_9H_8O_4$	0.212	6	2.08; 2.56; 2.82	[*Mazzoleni et al.*, 2010]
179.0715	$C_{10}H_{12}O_3$	0.237	5	6.87	[*Lin et al.*, 2012a; *Mazzoleni et al.*, 2010]
181.0719	$C_6H_{14}O_6$	0.324	0	0.32	
181.0871	$C_{10}H_{14}O_3$	0.289	4	2.59	[*Lin et al.*, 2012a; *Mazzoleni et al.*, 2010]
183.0666	$C_9H_{12}O_4$	-0.23	4	2.11; 2.47	[*Lin et al.*, 2012a; *Mazzoleni et al.*, 2010; *Müller et al.*, 2009; *Vogel* 2014]
183.1027	$C_{10}H_{16}O_3$	-0.26	3	2.84; 2.92; 3.18; 7.10	[*Kourtchev et al.*, 2013; *Lin et al.*, 2012a; *Mazzoleni et al.*, 2010]
185.0821	$C_9H_{14}O_4$	-0.12	3	2.19; 3.72; 2.92	[*Chan et al.*, 2011; *Kourtchev et al.*, 2013; *Mazzoleni et al.*, 2010; *Mazzoleni et al.*, 2012; *Müller et al.*, 2009; *Vogel* 2014; *Yu et al.*, 1998]
187.0614	$C_8H_{12}O_5$	0.285	3	1.42; 1.65; 1.86	[*Claeys et al.*, 2009; *Müller et al.*, 2009], [*Gómez-González et al.*, 2012; *Kourtchev et al.*, 2013; *Lin et al.*, 2012a; *Mazzoleni et al.*, 2010; *Vogel* 2014]
187.0977	$C_9H_{16}O_4$	-0.279	2	3.11	[*Kourtchev et al.*, 2013; *Mazzoleni et al.*, 2010; *Müller et al.*, 2009]

189.0408	$C_7H_{10}O_6$	0.258	3	0.39	[*Altieri et al.*, 2009; *Lin et al.*, 2012a; *Mazzoleni et al.*, 2010; *Vogel* 2014]
189.0560	$C_{11}H_{10}O_3$	0.542	7	3.50	[*Lin et al.*, 2012a; *Mazzoleni et al.*, 2010]
193.0871	$C_{11}H_{14}O_3$	0.012	5	2.77	[*Lin et al.*, 2012a; *Mazzoleni et al.*, 2010]
195.1030	$C_{11}H_{16}O_3$	-0.039	4	2.73	[*Lin et al.*, 2012a; *Mazzoleni et al.*, 2010; *Zhao et al.*, 2013]
197.1185	$C_{11}H_{18}O_3$	0.468	3	7.58	[*Kourtchev et al.*, 2013; *Lin et al.*, 2012a; *Mazzoleni et al.*, 2010]
199.0978	$C_{10}H_{16}O_4$	0.441	3	2.13; 2.43; 3.98	[*Müller et al.*, 2009], [*Lin et al.*, 2012a; *Mazzoleni et al.*, 2010; *Mazzoleni et al.*, 2012]
201.0770	$C_9H_{14}O_5$	0.513	3	1.97;	[*Iinuma et al.*, 2013; *Müller et al.*, 2009], [*Kahnt et al.*, 2014; *Lin et al.*, 2012a; *Mazzoleni et al.*, 2010 *Vogel* 2014]
201.1134	$C_{10}H_{18}O_4$	0.386	2	4.57; 4.37; 6.96; 6.28; 7.58;	[*Mazzoleni et al.*, 2010]
203.0565	$C_8H_{12}O_6$	0.437	3	0.39; 1.76	[*Altieri et al.*, 2009; *Kourtchev et al.*, 2013; *Kristensen and Glasius*, 2011; *Lin et al.*, 2012a; *Mazzoleni et al.*, 2010; *Müller et al.*, 2009; *Szmigielski et al.*, 2007; *Vogel* 2014]
205.0509	$C_{11}H_{10}O_4$	0.136	7	2.39; 2.55; 2.71	[*Lin et al.*, 2012a; *Mazzoleni et al.*, 2010]
207.1759	$C_{14}H_{24}O$	0.199	3	7.79	
209.0820	$C_{11}H_{14}O_4$	0.037	5	6.88	[*Mazzoleni et al.*, 2010]
209.1549	$C_{13}H_{22}O_2$	0.224	3	7.11	[*Lin et al.*, 2012a; *Mazzoleni et al.*, 2010; *Zhao et al.*, 2013]
211.0465	$C_6H_{12}O_8$	2.035	1	2.72	[*Zhao et al.*, 2013]
211.0978	$C_{11}H_{16}O_4$	0.131	4	3.08; 4.90	[*Lin et al.*, 2012a; *Mazzoleni et al.*, 2010]
213.1135	$C_{11}H_{18}O_4$	0.458	3	3.18; 2.57; 4.03; 3.79; 2.88; 2.73; 3.28	[*Lin et al.*, 2012a; *Mazzoleni et al.*, 2010]
213.1498	$C_{12}H_{22}O_3$	0.479	2	7.32	[*Mazzoleni et al.*, 2010]
215.0928	$C_{10}H_{16}O_5$	-0.264	3	2.39; 2.67	[*Iinuma et al.*, 2013; *Müller et al.*, 2009], [*Kahnt et al.*, 2014], [*Lin et al.*, 2012a; *Mazzoleni et al.*, 2010; *Mazzoleni et al.*, 2012; *Vogel* 2014]
215.1290	$C_{11}H_{20}O_4$	-0.336	2	2.87	[*Lin et al.*, 2012a; *Mazzoleni et al.*, 2010]
217.0719	$C_9H_{14}O_6$	-0.052	3	1.98	[*Müller et al.*, 2009] Iinuma 2009; [*Lin et al.*, 2012a; *Mazzoleni et al.*, 2010; *Vogel* 2014]
217.1084	$C_{10}H_{18}O_5$	-0.032	2	1.80; 2.17; 2.45	[*Lin et al.*, 2012a; *Mazzoleni et al.*, 2010; *Müller et al.*, 2009; *Zhao et al.*, 2013]
223.1708	$C_{14}H_{24}O_2$	0.344	3	7.83	[*Lin et al.*, 2012a; *Mazzoleni et al.*, 2010]
225.1499	$C_{13}H_{22}O_3$	0.454	3	7.36; 7.07	[*Lin et al.*, 2012a; *Mazzoleni et al.*, 2010]
229.1086	$C_{11}H_{18}O_5$	-0.248	3	2.60	[*Lin et al.*, 2012a; *Mazzoleni et al.*, 2010; *Müller et al.*, 2009; *Vogel* 2014*; Zhao et al.*, 2013]
229.1597	$C_{16}H_{22}O$	-1.39	6	7.66	
231.1242	$C_{11}H_{20}O_5$	-0.073	2	2.50	[*Lin et al.*, 2012a; *Mazzoleni et al.*, 2010; *Zhao et al.*, 2013]
233.1033	$C_{10}H_{18}O_6$	0.165	2	2.08	[*Lin et al.*, 2012a; *Mazzoleni et al.*, 2010; *Müller et al.*, 2009; *Vogel* 2014]
233.1547	$C_{15}H_{22}O_2$	0.158	5	7.87	[*Lin et al.*, 2012a; *Mazzoleni et al.*, 2010]
235.1706	$C_{15}H_{24}O_2$	0.496	4	7.70; 7.93	[*Lin et al.*, 2012a]
237.0773	$C_{12}H_{14}O_5$	0.52	6	6.43	[*Lin et al.*, 2012a; *Mazzoleni et al.*, 2010; *Müller et al.*, 2009]

241.1087	C$_{12}$H$_{18}$O$_{5}$	0.469	4	2.25; 2.47; 2.60; 2.92; 3.28; 3.53	[*Lin et al.*, 2012a; *Mazzoleni et al.*, 2010; *Vogel* 2014; *Zhao et al.*, 2013]
241.1448	C$_{13}$H$_{22}$O$_{4}$	0.488	3	6.98	[*Mazzoleni et al.*, 2010]
243.0875	C$_{11}$H$_{16}$O$_{6}$	-0.047	4	2.00; 2.43	[*Lin et al.*, 2012a; *Mazzoleni et al.*, 2010; *Vogel* 2014]
243.1242	C$_{12}$H$_{20}$O$_{5}$	-0.07	3	2.41; 2.98; 2.66; 3.24	[*Lin et al.*, 2012a; *Mazzoleni et al.*, 2010; *Müller et al.*, 2009; *Zhao et al.*, 2013]
245.1034	C$_{11}$H$_{18}$O$_{6}$	-0.333	3	2.89; 3.15	[*Müller et al.*, 2009], [*Lin et al.*, 2012a; *Mazzoleni et al.*, 2010; *Mazzoleni et al.*, 2012; *Vogel* 2014]
245.1396	C$_{12}$H$_{22}$O$_{5}$	0.094	2	3.68; 4.00; 3.19; 2.54	[*Lin et al.*, 2012a; *Mazzoleni et al.*, 2010; *Zhao et al.*, 2013]
247.0977	C$_{14}$H$_{16}$O$_{4}$	-0.009	7	7.77	[*Lin et al.*, 2012a; *Mazzoleni et al.*, 2010]
253.1447	C$_{14}$H$_{22}$O$_{4}$	-0.168	4	7.27	[*Chan et al.*, 2011; *Mazzoleni et al.*, 2010; *Mazzoleni et al.*, 2012]
253.1812	C$_{15}$H$_{26}$O$_{3}$	0.324	3	7.77	[*Lin et al.*, 2012a; *Mazzoleni et al.*, 2010]
255.1605	C$_{14}$H$_{24}$O$_{4}$	0.656	3	6.73	[*Chan et al.*, 2011; *Lin et al.*, 2012a; *Mazzoleni et al.*, 2010; *Mazzoleni et al.*, 2012]
257.1037	C$_{12}$H$_{18}$O$_{6}$	0.694	4	2.76; 3.03; 2.24; 2.42; 2.29	[*Lin et al.*, 2012a; *Mazzoleni et al.*, 2010]
257.1400	C$_{13}$H$_{22}$O$_{5}$	0.789	3	5.95	[*Lin et al.*, 2012a; *Mazzoleni et al.*, 2010; *Vogel* 2014; *Zhao et al.*, 2013]
265.1086	C$_{14}$H$_{18}$O$_{5}$	-0.102	6	7.18	[*Lin et al.*, 2012a; *Mazzoleni et al.*, 2010]
267.1606	C$_{15}$H$_{24}$O$_{4}$	0.365	4	7.52; 7.83	[*Lin et al.*, 2012a; *Mazzoleni et al.*, 2010; *Mazzoleni et al.*, 2012]
269.1398	C$_{14}$H$_{22}$O$_{5}$	0.531	4	2.81; 3.13	[*Mazzoleni et al.*, 2012], [*Chan et al.*, 2011; *Lin et al.*, 2012a; *Mazzoleni et al.*, 2010; *Zhao et al.*, 2013]
269.1763	C$_{15}$H$_{26}$O$_{4}$	0.473	3	6.99	[*Chan et al.*, 2011; *Lin et al.*, 2012a; *Mazzoleni et al.*, 2010]
271.0618	C$_{15}$H$_{12}$O$_{5}$	0.639	10	6.10	[*LeClair et al.*, 2012; *Lin et al.*, 2012a; *Mazzoleni et al.*, 2010; *Zhao et al.*, 2013]
271.1556	C$_{14}$H$_{24}$O$_{5}$	0.638	3	7.58; 6.53	[*Chan et al.*, 2011; *LeClair et al.*, 2012; *Lin et al.*, 2012a; *Mazzoleni et al.*, 2010; *Mazzoleni et al.*, 2012; *Vogel* 2014; *Zhao et al.*, 2013]
273.1502	C$_{17}$H$_{22}$O$_{3}$	0.813	7	7.65	[*LeClair et al.*, 2012; *Lin et al.*, 2012a; *Mazzoleni et al.*, 2010]
273.1713	C$_{14}$H$_{26}$O$_{5}$	0.45	2	3.51; 4.01; 3.80; 5.22	[*LeClair et al.*, 2012; *Lin et al.*, 2012a; *Mazzoleni et al.*, 2010; *Zhao et al.*, 2013]
281.1396	C$_{15}$H$_{22}$O$_{5}$	0.509	5	7.70	[*Lin et al.*, 2012a; *Mazzoleni et al.*, 2010]
283.1557	C$_{15}$H$_{24}$O$_{5}$	0.399	4	6.80	[*Chan et al.*, 2011; *Lin et al.*, 2012a; *Mazzoleni et al.*, 2010; *Mazzoleni et al.*, 2012; *Vogel* 2014; *Zhao et al.*, 2013]
285.1194	C$_{10}$H$_{22}$O$_{9}$	0.542	0	0.39	
289.1086	C$_{16}$H$_{18}$O$_{5}$	0.668	8	6.99	[*LeClair et al.*, 2012; *Lin et al.*, 2012a; *Mazzoleni et al.*, 2010]
293.1400	C$_{16}$H$_{22}$O$_{5}$	0.999	6	7.79	[*LeClair et al.*, 2012; *Lin et al.*, 2012a; *Mazzoleni et al.*, 2010]
293.1761	C$_{17}$H$_{26}$O$_{4}$	0.025	5	7.54	[*Chan et al.*, 2011; *LeClair et al.*, 2012; *Mazzoleni et al.*, 2010]
295.1404	C$_{12}$H$_{24}$O$_{8}$	1.42	1	7.80	[*LeClair et al.*, 2012]
295.1555	C$_{16}$H$_{24}$O$_{5}$	0.383	5	6.69; 6.84; 7.35	[*LeClair et al.*, 2012; *Lin et al.*, 2012a; *Mazzoleni et al.*, 2010]
299.1504	C$_{15}$H$_{24}$O$_{6}$	0.262	4	7.56	[*Lin et al.*, 2012a; *Mazzoleni et al.*, 2010; *Vogel* 2014]
299.2230	C$_{17}$H$_{32}$O$_{4}$	-0.009	2	7.96	[*Lin et al.*, 2012a; *Mazzoleni et al.*, 2010]
301.1659	C$_{15}$H$_{26}$O$_{6}$	0.459	3	7.23; 7.64	[*Lin et al.*, 2012a; *Mazzoleni et al.*, 2010]

301.2025	C$_{16}$H$_{30}$O$_5$	0.54	2	6.08; 6.40	[*Lin et al.*, 2012a; *Mazzoleni et al.*, 2010; *Zhao et al.*, 2013]
303.1759	C$_{22}$H$_{24}$O	1.027	11	6.62	
307.0616	C$_{18}$H$_{12}$O$_5$	0.857	13	7.37	
309.1714	C$_{17}$H$_{26}$O$_5$	0.688	5	7.44; 7.63	[*LeClair et al.*, 2012; *Mazzoleni et al.*, 2010; *Zhao et al.*, 2013]
311.1507	C$_{16}$H$_{24}$O$_6$	0.637	5	7.74	[*LeClair et al.*, 2012; *Lin et al.*, 2012a; *Mazzoleni et al.*, 2010]
313.0725	C$_{17}$H$_{14}$O$_6$	0.73	11	7.54	[*Mazzoleni et al.*, 2010; *Zhao et al.*, 2013]
317.1246	C$_{14}$H$_{22}$O$_8$	0.155	4	3.31	[*Lin et al.*, 2012a; *Mazzoleni et al.*, 2010; *Vogel* 2014]
317.1397	C$_{18}$H$_{22}$O$_5$	0.451	8	7.65	[*Lin et al.*, 2012a; *Mazzoleni et al.*, 2010]
317.1914	C$_{23}$H$_{26}$O	0.824	11	7.10	
321.0770	C$_{19}$H$_{14}$O$_5$	0.571	13	7.86	
321.1561	C$_{14}$H$_{26}$O$_8$	0.277	2	2.31	
321.1714	C$_{18}$H$_{26}$O$_5$	0.85	6	7.75	[*Lin et al.*, 2012a; *Mazzoleni et al.*, 2010]
323.1715	C$_{14}$H$_{28}$O$_8$	1.235	1	7.95	[*Zhao et al.*, 2013]
327.0876	C$_{18}$H$_{16}$O$_6$	0.638	11	7.68	[*LeClair et al.*, 2012; *Mazzoleni et al.*, 2010; *Zhao et al.*, 2013]
339.1452	C$_{17}$H$_{24}$O$_7$	0.276	6	7.50	[*Lin et al.*, 2012a; *Mazzoleni et al.*, 2010]
339.1665	C$_{14}$H$_{28}$O$_9$	-0.017	1	1.99	
341.1031	C$_{19}$H$_{18}$O$_6$	-0.004	11	7.76	[*LeClair et al.*, 2012; *Mazzoleni et al.*, 2010; *Zhao et al.*, 2013]
347.2444	C$_{18}$H$_{36}$O$_6$	0.311	1	6.24; 6.37; 6.52; 6.70	
351.0876	C$_{20}$H$_{16}$O$_6$	0.138	13	7.87	
355.1190	C$_{20}$H$_{20}$O$_6$	0.615	11	7.83	[*LeClair et al.*, 2012; *Mazzoleni et al.*, 2010; *Zhao et al.*, 2013]
361.1512	C$_{16}$H$_{26}$O$_9$	0.621	4	3.44	
361.2239	C$_{18}$H$_{34}$O$_7$	0.647	2	2.66; 2.72; 3.07; 3.25; 3.34	
373.1661	C$_{21}$H$_{26}$O$_6$	0.21	9	7.86	[*Mazzoleni et al.*, 2010; *Zhao et al.*, 2013]
379.2132	C$_{21}$H$_{32}$O$_6$	0.021	6	7.80	[*Mazzoleni et al.*, 2010]
385.0570	C$_{19}$H$_{14}$O$_9$	0.194	13	6.76	
387.0729	C$_{19}$H$_{16}$O$_9$	0.451	12	6.58	
387.1152	C$_{13}$H$_{24}$O$_{13}$	0.3	2	0.34	
389.0938	C$_{12}$H$_{22}$O$_{14}$	0.107	2	7.94	
417.2287	C$_{24}$H$_{34}$O$_6$	0.379	8	7.66	[*Zhao et al.*, 2013]
449.2037	C$_{20}$H$_{34}$O$_{11}$	0.434	4	4.02	[*Zhao et al.*, 2013]
479.2293	C$_{25}$H$_{36}$O$_9$	0.217	8	6.34	

Table 7.3 CHNO containing compounds detected in the Grenzgletscher ice core

measured m/z [M-H]⁻	formula	mass deviation (ppm)	DBE	RT (min)	literature
119.0252	$C_6H_4ON_2$	-0.387	6	2.26	
120.0204	$C_5H_3ON_3$	0.041	6	2.20	
122.0361	$C_5H_5ON_3$	0.122	5	0.45	
124.0153	$C_4H_3O_2N_3$	-0.32	5	0.41	
132.0205	$C_6H_3ON_3$	0.037	7	1.03	
133.0409	$C_7H_6ON_2$	0.179	6	2.37	[*Lin et al.*, 2012a]
136.0405	$C_7H_7O_2N$	-0.087	5	1.79	[*Lin et al.*, 2012a]
136.0518	$C_6H_7ON_3$	-0.112	5	0.58	
138.0197	$C_6H_5O_3N$	0.244	5	3.20	[*Mazzoleni et al.*, 2010]
143.0252	$C_8H_4ON_2$	0.027	8	3.10	
144.0204	$C_7H_3ON_3$	0.034	8	2.85	
144.0668	$C_6H_{11}O_3N$	-0.007	2	0.78	[*Lin et al.*, 2012a]
151.0262	$C_5H_4O_2N_4$	-0.19	6	0.39	
152.0354	$C_7H_7O_3N$	0.484	5	4.61; 5.43	[*Lin et al.*, 2012a; *Mazzoleni et al.*, 2010]
162.0198	$C_8H_5O_3N$	0.393	7	2.01	[*Lin et al.*, 2012a; *Zhao et al.*, 2013]
164.0467	$C_7H_7O_2N_3$	0.306	6	0.69	
165.0417	$C_6H_6O_2N_4$	-0.295	6	0.96	
166.0510	$C_8H_9O_3N$	-0.039	5	7.06	[*Lin et al.*, 2012a; *Mazzoleni et al.*, 2010]
168.0204	$C_9H_3ON_3$	0.148	10	2.33	
168.0305	$C_7H_7O_4N$	0.054	5	2.33	[*Lin et al.*, 2012a; *Mazzoleni et al.*, 2010; *Vogel* 2014]
170.0361	$C_9H_5ON_3$	0.088	9	2.03	
171.0524	$C_5H_8O_3N_4$	0.039	4	0.38	
172.0619	$C_7H_{11}O_4N$	0.575	3	1.61	[*Lin et al.*, 2012a; *Mazzoleni et al.*, 2010]
172.0983	$C_8H_{15}O_3N$	0.368	2	0.38; 1.91	[*Lin et al.*, 2012a]
176.0354	$C_9H_7O_3N$	0.021	7	2.72	[*Lin et al.*, 2012a; *Zhao et al.*, 2013]
178.0512	$C_9H_9O_3N$	0.076	6	1.96	[*Lin et al.*, 2012a; *Mazzoleni et al.*, 2010]
179.0099	$C_7H_4O_4N_2$	0.224	7	2.92	[*Lin et al.*, 2012a]
179.0576	$C_7H_8O_2N_4$	0.174	6	1.64	
180.0304	$C_8H_7O_4N$	0.217	6	3.34	[*Lin et al.*, 2012a; *Mazzoleni et al.*, 2010]
180.0668	$C_9H_{11}O_3N$	0.464	5	7.52	[*Lin et al.*, 2012a; *Mazzoleni et al.*, 2010]
181.1347	$C_{10}H_{18}ON_2$	0.295	3	2.39	
182.0361	$C_{10}H_5ON_3$	0.411	10	2.72	
182.0464	$C_8H_9O_4N$	0.434	5	2.90	[*Lin et al.*, 2012a; *Mazzoleni et al.*, 2010]
183.0048	$C_6H_4O_5N_2$	-0.352	6	3.98	[*Lin et al.*, 2012a; *Mazzoleni et al.*, 2010]
184.0517	$C_{10}H_7ON_3$	0.026	9	2.39	
184.0981	$C_9H_{15}O_3N$	0.018	3	2.77	[*Lin et al.*, 2012a]
194.0461	$C_9H_9O_4N$	0.458	6	2.42	[*Lin et al.*, 2012a; *Mazzoleni et al.*, 2010]
195.0049	$C_7H_3O_5N_2$	0.233	7	2.79; 2.97	
197.0205	$C_7H_6O_5N_2$	0.434	6	6.33; 6.82	[*Lin et al.*, 2012a; *Mazzoleni et al.*, 2010]
200.1294	$C_{10}H_{19}O_3N$	0.216	2	2.81	[*Lin et al.*, 2012a]
202.1086	$C_9H_{17}O_4N$	0.139	2	0.37	[*Zhao et al.*, 2013]
203.1192	$C_{12}H_{16}ON_2$	0.707	6	7.60	

205.0620	$C_{10}H_{10}O_3N_2$	0.12	7	2.13	[*Lin et al.*, 2012a]
206.0361	$C_{12}H_5ON_3$	0.121	12	3.72	
208.1346	$C_{12}H_{19}O_2N$	0.086	4	2.34	
210.0311	$C_{11}H_5O_2N_3$	0.382	11	6.00	
210.0410	$C_9H_9O_5N$	0.164	6	4.87; 3.32	[*Lin et al.*, 2012a; *Mazzoleni et al.*, 2010]
210.0775	$C_{10}H_{13}O_4N$	0.28	5	6.75	[*Lin et al.*, 2012a; *Mazzoleni et al.*, 2010]
211.0362	$C_8H_8O_5N_2$	0.357	6	7.32; 7.56	[*Lin et al.*, 2012a; *Mazzoleni et al.*, 2010]
212.1295	$C_{11}H_{19}O_3N$	0.204	3	4.76	
212.1660	$C_{12}H_{23}O_2N$	0.508	2	6.61	
214.0513	$C_{12}H_9O_3N$	0.577	9	7.57	[*Lin et al.*, 2012a]
214.0724	$C_9H_{13}O_5N$	0.487	4	1.82	[*Lin et al.*, 2012a; *Mazzoleni et al.*, 2010]
214.1086	$C_{10}H_{17}O_4N$	0.274	3	0.37; 1.88; 2.98	[*Lin et al.*, 2012a; *Mazzoleni et al.*, 2010]
214.1450	$C_{11}H_{21}O_3N$	-0.125	2	3.75	[*Lin et al.*, 2012a]
216.0415	$C_{10}H_7O_3N_3$	0.026	9	2.12	
216.1241	$C_{10}H_{19}O_4N$	-0.376	2	0.38; 2.78	
218.1300	$C_{12}H_{17}ON_3$	-0.163	6	4.85; 5.08	
224.0567	$C_{10}H_{11}O_5N$	0.198	6	2.81; 3.41	[*Lin et al.*, 2012a; *Mazzoleni et al.*, 2010]
224.0931	$C_{11}H_{15}O_4N$	0.441	5	7.87	[*Lin et al.*, 2012a; *Mazzoleni et al.*, 2010]
225.0520	$C_9H_{10}O_5N_2$	0.355	6	7.74	[*Lin et al.*, 2012a; *Mazzoleni et al.*, 2010]
225.1613	$C_{12}H_{22}O_2N_2$	0.439	3	1.75	
226.1451	$C_{12}H_{21}O_3N$	0.456	3	4.71; 5.26	[*Zhao et al.*, 2013]
226.1816	$C_{13}H_{25}O_2N$	0.432	2	7.10	
227.0827	$C_{13}H_{12}O_2N_2$	0.524	9	7.65	
228.0881	$C_{10}H_{15}O_5N$	0.588	4	7.37; 7.51	[*Lin et al.*, 2012a; *Mazzoleni et al.*, 2010]
228.1605	$C_{12}H_{23}O_3N$	-0.425	2	6.04	
229.0984	$C_{13}H_{14}O_2N_2$	0.083	8	7.59	
230.1300	$C_{13}H_{17}ON_3$	-0.024	7	6.46	
230.1399	$C_{11}H_{21}O_4N$	0.037	2	3.18; 7.00; 7.25	
231.0624	$C_8H_{12}O_6N_2$	0.003	4	1.82	[*Lin et al.*, 2012a]
231.1350	$C_{10}H_{20}O_4N_2$	-0.002	2	0.37	
232.0943	$C_8H_{15}O_5N_3$	0.371	3	1.61	
233.1143	$C_9H_{18}O_5N_2$	0.151	2	7.79	
238.0723	$C_{11}H_{13}O_5N$	0.27	6	3.83	[*Lin et al.*, 2012a; *Mazzoleni et al.*, 2010]
239.0674	$C_{10}H_{12}O_5N_2$	-0.02	6	7.84	[*Mazzoleni et al.*, 2010]
240.1242	$C_{12}H_{19}O_4N$	-0.006	4	2.75; 3.34	[*Lin et al.*, 2012a; *Mazzoleni et al.*, 2010]
240.1609	$C_{13}H_{23}O_3N$	0.221	3	7.31	
241.0469	$C_9H_{10}O_6N_2$	0.584	6	6.26	[*Lin et al.*, 2012a]
241.1195	$C_{11}H_{18}O_4N_2$	0.413	4	0.37; 1.93	[*Lin et al.*, 2012a]
243.1350	$C_{11}H_{20}O_4N_2$	-0.289	3	1.56; 2.53	[*Zhao et al.*, 2013]
243.1715	$C_{12}H_{24}O_3N_2$	-0.065	2	1.53	
244.1457	$C_{14}H_{19}ON_3$	-0.064	7	7.08	
244.1555	$C_{12}H_{23}O_4N$	-0.006	2	4.73; 2.45; 6.16; 7.63	
245.1410	$C_{13}H_{18}ON_4$	-0.222	7	4.85	
245.1509	$C_{11}H_{22}O_4N_2$	0.08	2	1.95	

246.1098	C$_9$H$_{17}$O$_5$N$_3$	0.187	3	2.09; 6.62	
252.0883	C$_{12}$H$_{15}$O$_5$N	0.374	6	7.74	[*Lin et al.*, 2012a; *Mazzoleni et al.*, 2010]
252.1610	C$_{14}$H$_{23}$O$_3$N	0.647	4	7.83	[*Mazzoleni et al.*, 2010]
253.0472	C$_{10}$H$_{10}$O$_6$N$_2$	0.438	7	6.97	[*Lin et al.*, 2012a]
253.1198	C$_{12}$H$_{18}$O$_4$N$_2$	0.433	5	2.33; 3.64; 6.45	[*Lin et al.*, 2012a; *Zhao et al.*, 2013]
253.1923	C$_{14}$H$_{26}$O$_2$N$_2$	0.429	3	7.10	
254.1400	C$_{13}$H$_{21}$O$_4$N	0.427	4	7.78; 3.18; 3.68	[*Lin et al.*, 2012a]
256.1194	C$_{12}$H$_{19}$O$_5$N	0.484	4	7.66	[*Lin et al.*, 2012a; *Mazzoleni et al.*, 2010]
256.1559	C$_{13}$H$_{23}$O$_4$N	0.58	3	2.86	
257.0934	C$_{14}$H$_{14}$O$_3$N$_2$	0.601	9	7.22	
257.1145	C$_{11}$H$_{18}$O$_5$N$_2$	0.331	4	2.28	
257.1511	C$_{12}$H$_{22}$O$_4$N$_2$	0.426	3	1.86; 3.18	
258.1351	C$_{12}$H$_{21}$O$_5$N	0.015	3	2.94	[*Mazzoleni et al.*, 2010]
258.1613	C$_{15}$H$_{21}$ON$_3$	0.133	7	7.41	
258.1712	C$_{13}$H$_{25}$O$_4$N	-0.006	2	6.61; 7.70	
259.1201	C$_{13}$H$_{16}$O$_2$N$_4$	-0.189	8	3.77	
260.1254	C$_{10}$H$_{19}$O$_5$N$_3$	0.062	3	7.15; 2.54	
261.1457	C$_{11}$H$_{22}$O$_5$N$_2$	-0.096	2	1.84	
264.0727	C$_9$H$_{15}$O$_8$N	0.077	3	2.55	[*Mazzoleni et al.*, 2010; *Vogel* 2014]
264.0878	C$_{13}$H$_{15}$O$_5$N	-0.022	7	2.35	[*Lin et al.*, 2012a; *Mazzoleni et al.*, 2010]
264.1610	C$_{15}$H$_{23}$O$_3$N	0.466	5	7.92	[*Mazzoleni et al.*, 2010]
268.1559	C$_{14}$H$_{23}$O$_4$N	0.33	4	4.43; 5.91	[*Mazzoleni et al.*, 2010; *Zhao et al.*, 2013]
268.1922	C$_{15}$H$_{27}$O$_3$N	0.421	3	7.39	
269.1512	C$_{13}$H$_{22}$O$_4$N$_2$	0.296	4	2.67	
270.1098	C$_{11}$H$_{17}$O$_5$N$_3$	0.504	5	3.65	
270.1615	C$_{16}$H$_{21}$ON$_3$	0.386	8	7.54	
270.1713	C$_{14}$H$_{25}$O$_4$N	0.55	3	4.93; 6.06; 6.60; 4.09; 7.37	
271.1668	C$_{13}$H$_{24}$O$_4$N$_2$	-0.149	3	1.75; 4.76; 1.54; 0.37; 2.13	[*LeClair et al.*, 2012; *Vogel* 2014]
272.1507	C$_{13}$H$_{23}$O$_5$N	0.161	3	2.19	[*LeClair et al.*, 2012; *Mazzoleni et al.*, 2010]
272.1772	C$_{16}$H$_{23}$ON$_3$	0.604	7	7.60	
272.1871	C$_{14}$H$_{27}$O$_4$N	0.362	2	7.10; 7.41; 6.40	[*LeClair et al.*, 2012]
273.1461	C$_{12}$H$_{22}$O$_5$N$_2$	0.677	3	2.22	[*LeClair et al.*, 2012]
274.1412	C$_{11}$H$_{21}$O$_5$N$_3$	0.861	3	7.45	
274.1450	C$_{16}$H$_{21}$O$_3$N	0.668	7	7.97	[*LeClair et al.*, 2012]
274.1566	C$_{15}$H$_{21}$O$_2$N$_3$	0.765	7	5.29	[*LeClair et al.*, 2012]
275.1405	C$_{15}$H$_{20}$O$_3$N$_2$	0.851	7	7.87	[*LeClair et al.*, 2012]
275.1618	C$_{12}$H$_{24}$O$_5$N$_2$	0.708	2	1.99	
276.1564	C$_{11}$H$_{23}$O$_5$N$_3$	-0.123	2	0.37; 1.85	
278.1614	C$_{12}$H$_{25}$O$_6$N	0.249	1	2.28	
280.1560	C$_{15}$H$_{23}$O$_4$N	0.53	5	7.91; 7.45	[*Mazzoleni et al.*, 2010]
280.1923	C$_{16}$H$_{27}$O$_3$N	0.261	4	7.43	
281.1660	C$_{18}$H$_{22}$ON$_2$	0.19	9	7.95	

282.1352	$C_{14}H_{21}O_5N$	0.688	5	7.78	[*Lin et al.*, 2012a; *Mazzoleni et al.*, 2010; *Zhao et al.*, 2013]
282.1714	$C_{15}H_{25}O_4N$	0.526	4	6.44; 6.82	
283.1668	$C_{14}H_{24}O_4N_2$	0.599	4	5.96	
285.1462	$C_{13}H_{22}O_5N_2$	0.543	4	2.93	
285.1823	$C_{14}H_{26}O_4N_2$	0.524	3	3.84; 6.62	
286.1666	$C_{14}H_{25}O_5N$	0.922	3	6.28; 6.60	[*Mazzoleni et al.*, 2010]
286.1929	$C_{17}H_{25}ON_3$	0.609	7	7.70	
288.1455	$C_{13}H_{23}O_6N$	0.206	3	0.37; 2.94	[*LeClair et al.*, 2012; *Mazzoleni et al.*, 2010; *Vogel* 2014; *Zhao et al.*, 2013]
288.1569	$C_{12}H_{23}O_5N_3$	0.853	3	1.75	[*LeClair et al.*, 2012]
289.1775	$C_{13}H_{26}O_5N_2$	0.778	2	7.41	
292.1768	$C_{13}H_{27}O_6N$	0.887	1	1.92	[*Zhao et al.*, 2013]
293.1470	$C_{10}H_{22}O_6N_4$	0.145	2	0.37	
295.1414	$C_{13}H_{20}O_4N_4$	0.31	6	2.00	
296.1506	$C_{15}H_{23}O_5N$	0.351	5	6.74; 7.73	[*Mazzoleni et al.*, 2010]
298.1664	$C_{15}H_{25}O_5N$	-0.021	4	7.71	[*Mazzoleni et al.*, 2010; *Zhao et al.*, 2013]
299.1616	$C_{14}H_{24}O_5N_2$	0.351	4	6.56; 2.71; 3.02	
299.1978	$C_{15}H_{28}O_4N_2$	0.098	3	7.10	
300.1821	$C_{15}H_{27}O_5N$	0.679	3	6.97	
300.2086	$C_{18}H_{27}ON_3$	0.58	7	7.78	
300.2186	$C_{16}H_{31}O_4N$	0.361	2	7.74	
302.1363	$C_{12}H_{21}O_6N_3$	0.567	4	2.93	
302.1612	$C_{14}H_{25}O_6N$	0.329	3	2.25	[*Mazzoleni et al.*, 2010; *Vogel* 2014; *Zhao et al.*, 2013]
302.1724	$C_{13}H_{25}O_5N_3$	0.516	3	6.62; 7.71	
303.1202	$C_{12}H_{20}O_7N_2$	0.415	4	2.76	
305.1357	$C_{12}H_{22}O_7N_2$	0.543	3	2.95; 2.61	[*Zhao et al.*, 2013]
306.1251	$C_{18}H_{17}O_2N_3$	0.261	12	7.53	
306.1351	$C_{16}H_{21}O_5N$	0.634	7	7.64	[*Lin et al.*, 2012a; *Mazzoleni et al.*, 2010]
306.1559	$C_{13}H_{25}O_7N$	0.277	2	0.38	
309.1827	$C_{16}H_{26}O_4N_2$	0.386	5	7.71	
312.1823	$C_{16}H_{27}O_5N$	0.877	4	6.74; 7.01	
313.1772	$C_{15}H_{26}O_5N_2$	0.941	4	6.29	
313.2137	$C_{16}H_{30}O_4N_2$	0.7	3	7.40	
316.1516	$C_{13}H_{23}O_6N_3$	0.257	4	3.02	
318.1563	$C_{14}H_{25}O_7N$	0.172	3	3.22	[*Mazzoleni et al.*, 2010]
319.1515	$C_{13}H_{24}O_7N_2$	-0.139	3	2.25	
320.1355	$C_{13}H_{23}O_8N$	0.219	3	1.57	[*Mazzoleni et al.*, 2010; *Zhao et al.*, 2013]
322.1297	$C_{16}H_{21}O_6N$	0.184	7	7.77	[*Lin et al.*, 2012a; *Mazzoleni et al.*, 2010; *Zhao et al.*, 2013]
326.0883	$C_{14}H_{17}O_8N$	0.277	7	1.94	[*LeClair et al.*, 2012; *Lin et al.*, 2012a; *Mazzoleni et al.*, 2010]
326.2088	$C_{16}H_{29}O_4N_3$	0.369	4	6.58	
326.2345	$C_{18}H_{33}O_4N$	-0.036	3	6.72	
327.1928	$C_{16}H_{28}O_5N_2$	0.351	4	6.97	
327.2292	$C_{17}H_{32}O_4N_2$	0.12	3	7.60	
329.1723	$C_{15}H_{26}O_6N_2$	-0.273	4	2.63	

330.1563	$C_{15}H_{25}O_7N$	0.741	4	7.29; 7.84; 7.54	[*Lin et al.*, 2012a; *Mazzoleni et al.*, 2010]
330.1675	$C_{14}H_{25}O_6N_3$	0.64	4	6.29	[*Zhao et al.*, 2013]
330.2037	$C_{15}H_{29}O_5N_3$	0.502	3	7.40	
330.2291	$C_{17}H_{33}O_5N$	0.677	2	7.68	
332.1465	$C_{13}H_{23}O_7N_3$	0.472	4	2.39	
336.0687	$C_{10}H_{15}O_{10}N_3$	0.396	5	2.57	[*Zhao et al.*, 2013]
336.1470	$C_{18}H_{19}O_2N_5$	0.66	12	6.95; 7.23	
338.1460	$C_{13}H_{25}O_9N$	0.371	2	7.96	[*Zhao et al.*, 2013]
338.1613	$C_{17}H_{25}O_6N$	0.737	6	7.71	[*Mazzoleni et al.*, 2010]
338.1728	$C_{16}H_{25}O_5N_3$	0.727	6	7.57	
339.1465	$C_{18}H_{20}O_3N_4$	0.284	11	6.78	
341.2083	$C_{17}H_{30}O_5N_2$	-0.719	4	7.29	
342.2288	$C_{18}H_{33}O_5N$	-0.048	3	7.27	[*LeClair et al.*, 2012]
343.2242	$C_{17}H_{32}O_5N_2$	0.188	3	3.55	[*LeClair et al.*, 2012]
344.1832	$C_{15}H_{27}O_6N_3$	0.091	4	6.97	
344.2189	$C_{16}H_{32}O_6N_2$	0.231	2	7.60	
350.1037	$C_{20}H_{17}O_5N$	0.355	13	7.67	
356.1721	$C_{17}H_{27}O_7N$	0.518	5	7.54	[*Mazzoleni et al.*, 2010]
358.1985	$C_{16}H_{29}O_6N_3$	0.45	4	7.29	
358.2242	$C_{18}H_{33}O_6N$	0.946	3	7.00	
358.2604	$C_{19}H_{37}O_5N$	-0.269	2	7.68	
364.2866	$C_{22}H_{39}O_3N$	0.803	4	7.94	
369.2036	$C_{18}H_{30}O_6N_2$	-0.135	5	7.54	[*Zhao et al.*, 2013]
369.2399	$C_{19}H_{34}O_5N_2$	0.012	4	7.47	
370.2352	$C_{18}H_{33}O_5N_3$	0.312	4	2.21	
371.2194	$C_{18}H_{32}O_6N_2$	0.539	4	2.45	
376.1770	$C_{20}H_{27}O_6N$	0.131	8	7.95	[*Mazzoleni et al.*, 2010]
376.2712	$C_{19}H_{39}O_6N$	0.449	1	7.69	
378.2142	$C_{17}H_{33}O_8N$	0.819	2	2.42	[*Zhao et al.*, 2013]
383.2559	$C_{20}H_{36}O_5N_2$	0.351	4	7.19	
384.2760	$C_{21}H_{39}O_5N$	0.139	3	7.69	
385.1622	$C_{17}H_{26}O_8N_2$	-0.049	6	2.86	
385.1988	$C_{18}H_{30}O_7N_2$	0.326	5	7.49	
385.2348	$C_{19}H_{34}O_6N_2$	0.312	4	7.67	
386.2301	$C_{18}H_{33}O_6N_3$	0.132	4	7.52	
386.2554	$C_{20}H_{37}O_6N$	0.256	3	7.87	[*Zhao et al.*, 2013]
386.2919	$C_{21}H_{41}O_5N$	0.164	2	7.96	
388.2498	$C_{23}H_{35}O_4N$	0.459	7	7.85	
389.2663	$C_{19}H_{38}O_6N_2$	-0.463	2	7.84	
391.1203	$C_{24}H_{16}O_2N_4$	0.565	19	7.60	
394.1876	$C_{20}H_{29}O_7N$	0.341	7	7.87	
399.2870	$C_{21}H_{40}O_5N_2$	-0.089	3	7.59	
405.2609	$C_{19}H_{38}O_7N_2$	0.359	2	7.88	
410.2916	$C_{23}H_{41}O_5N$	0.155	4	7.94	
414.2616	$C_{20}H_{37}O_6N_3$	0.509	4	3.92	

415.2567	$C_{19}H_{36}O_6N_4$	0.631	4	1.97	
426.2866	$C_{23}H_{41}O_6N$	0.419	4	7.57; 7.88	
428.3022	$C_{23}H_{43}O_6N$	-0.213	3	7.86	[*Zhao et al.*, 2013]
430.0783	$C_{20}H_{17}O_{10}N$	0.003	13	3.80	
430.3183	$C_{23}H_{45}O_6N$	0.067	2	7.76	
434.2549	$C_{24}H_{37}O_6N$	-0.049	7	7.85	
439.1723	$C_{20}H_{28}O_9N_2$	0.015	8	7.95	[*Zhao et al.*, 2013]
443.2778	$C_{22}H_{40}O_7N_2$	0.012	4	7.88	
468.1454	$C_{28}H_{23}O_6N$	-0.065	18	7.98	
478.2567	$C_{24}H_{37}O_7N_3$	0.285	8	7.83	
482.2222	$C_{16}H_{33}O_{10}N_7$	-0.111	4	7.94	
483.3448	$C_{26}H_{48}O_6N_2$	0.765	4	7.09	
488.3392	$C_{29}H_{47}O_5N$	0.355	7	7.54	
496.3289	$C_{27}H_{47}O_7N$	0.552	5	6.68	
497.3348	$C_{25}H_{46}O_6N_4$	-0.097	5	2.46	
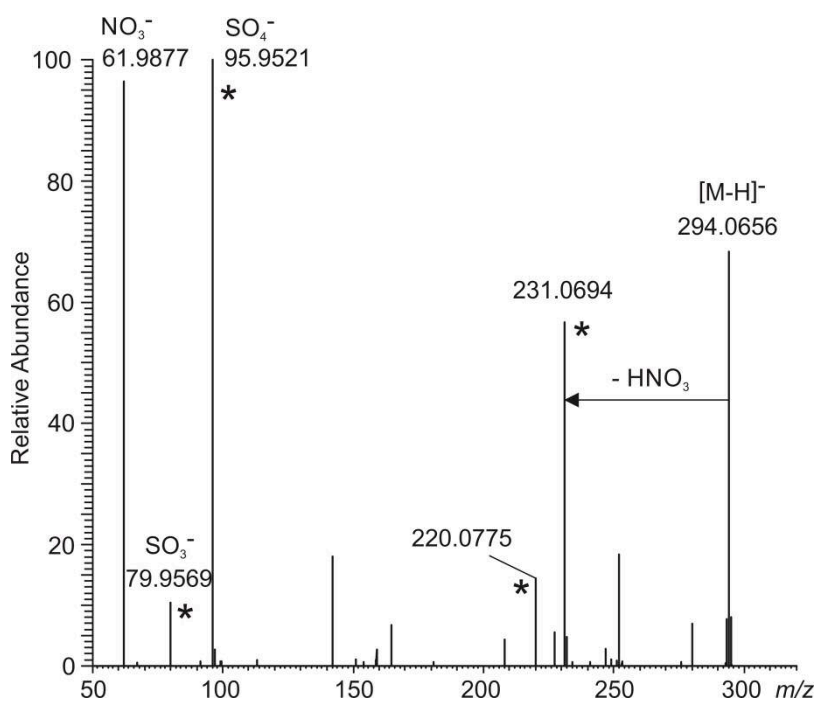
Fig. 7.3 MS²-spectrum of NOS 295 (*m/z* 294, [M-H]⁻). The marked (*) signals are also reported in MS/MS experiments by [*Surratt et al.*, 2007].

7.2   List of abbreviations

a.s.l.	above sea level
a.u.	arbitrary units
ACN	acetonitrile
ADI	adipic acid
AMM	ammonium
APCI	atmospheric pressure chemical ionization
API	atmospheric pressure ionization
APPI	atmospheric pressure photo ionization
BHA	benzyl hydroxylamine
CAL	calcium cation, Ca^{2+}
CDD	Cole du Dome
CDL	Colle del Lys
CG	Colle Gnifetti
CI	chemical ionization
CID	collision-induced dissociation
CRM	charge residue model
DAN	2,3-diaminonaphthalene
DNPH	dinitrophenylhydrazine
DOD	dodecanedioic acid
EI	electron ionization
EIC	extracted ion chromatogram
Equ.	equation
ESI	electrospray ionization
Fig.	figure
FOR	formate
G	glyoxal
GC	gas chromatography
GLU	glutaric acid
HESI	heated electrospray ionization
HPLC	high performance liquid chromatography
HRAM	high resolution accurate mass
HRMS	high resolution mass spectrometry
IEM	ion emission model
IT	ion trap
$K_{O/W}$	octanol-water partitioning coefficient
LC	liquid chromatography
m w.e.	meter water equivalent
m/z	mass to charge ratio

MAL	malonic acid
MeOH	methanol
MG	methylglyoxal
MPH	methylphthalic acid
MS	mass spectrometry
NIT	nitrate
NP	normal Phase
OXA	oxalate
PAH	polycyclic aromatic hydrocarbon
PDMS	polydimethylsiloxane
PFBHA	pentafluorobenzyl hydroxylamine
PHB	*p*-hydroxybenzoic acid
PHT	phthalic acid
PIM	pimelic acid
PIN	pinic acid
POP	persistent organic pollutant
QIT	quadrupole ion trap
RP	reversed phase
SAX	strong anion exchange
SBSE	stir bar sorptive extraction
SEB	sebacic acid
SOA	secondary organic aerosol
SPE	solid phase extraction
SUB	suberic acid
SUC	succinic acid
SUC-d4	succinic acid-2,2,3,3-d4
SUL	sulfate
V	volume
VAN	vanillic acid
VOC	volatile organic compound
WSOC	water-soluble organic compound

7.3   List of figures

7.4   List of tables

7.5   References

Altieri, K. E., A. G. Carlton, H.-J. Lim, B. J. Turpin, and S. P. Seitzinger (2006), Evidence for Oligomer Formation in Clouds: Reactions of Isoprene Oxidation Products, *Environ. Sci. Technol., 40*(16), 4956–4960.

Altieri, K. E., B. J. Turpin, and S. P. Seitzinger (2009), Oligomers, organosulfates, and nitrooxy organosulfates in rainwater identified by ultra-high resolution electrospray ionization FT-ICR mass spectrometry, *Atmos. Chem. Phys., 9*(7), 2533–2542.

Altieri, K., S. P. Seitzinger, A. Carlton, B. J. Turpin, G. C. Klein, and A. G. Marshall (2008), Oligomers formed through in-cloud methylglyoxal reactions: Chemical composition, properties, and mechanisms investigated by ultra-high resolution FT-ICR mass spectrometry, *Atmos. Environ., 42*(7), 1476–1490.

Angelis, M. de, R. Traversi, and R. Udisti (2012), Long-term trends of mono-carboxylic acids in Antarctica: comparison of changes in sources and transport processes at the two EPICA deep drilling sites, *Tellus B, 64*(0), 573.

Ariya, P. A., F. Domine, G. Kos, M. Amyot, V. Côté, H. Vali, T. Lauzier, W. F. Kuhs, K. Techmer, T. Heinrichs et al. (2011), Snow - a photobiochemical exchange platform for volatile and semi-volatile organic compounds with the atmosphere, *Environ. Chem., 8*(1), 62–73.

Atkinson, R., and J. Arey (2003), Gas-phase tropospheric chemistry of biogenic volatile organic compounds: a review, *Atmos. Environ., 37*, 197–219.

Bäck, J., J. Aalto, M. Henriksson, H. Hakola, Q. He, and M. Boy (2012), Chemodiversity of a Scots pine stand and implications for terpene air concentrations, *Biogeosciences, 9*(2), 689–702.

Baltussen, E., P. Sandra, F. David, and C. Cramers (1999), Stir bar sorptive extraction (SBSE), a novel extraction technique for aqueous samples: Theory and principles, *J. Micro. Sep., 11*(10), 737–747.

Bao, M.-l., F. Pantani, O. Griffini, D. Burrini, D. Santianni, and K. Barbieri (1998), Determination of carbonyl compounds in water by derivatization–solid-phase microextraction and gas chromatographic analysis, *J. Chromatogr. A, 809*(1-2), 75–87.

Barbante, C., M. Schwikowski, T. Döring, H. W. Gäggeler, U. Schotterer, L. Tobler, K. van de Velde, C. Ferrari, G. Cozzi, A. Turetta et al. (2004), Historical Record of European Emissions of Heavy Metals to the Atmosphere Since the 1650s from Alpine Snow/Ice Cores Drilled near Monte Rosa, *Environ. Sci. Technol., 38*(15), 4085–4090.

Bateman, A. P., J. Laskin, A. Laskin, and S. A. Nizkorodov (2012), Applications of High-Resolution Electrospray Ionization Mass Spectrometry to Measurements of Average Oxygen to Carbon Ratios in Secondary Organic Aerosols, *Environ. Sci. Technol., 46*(15), 8315–8324.

Blando, J. D., and B. J. Turpin (2000), Secondary organic aerosol formation in cloud and fog droplets: a literature evaluation of plausibility, *Atmospheric Environment, 34*(10), 1623–1632.

Cammann, K. (Ed.) (2001), *Instrumentelle Analytische Chemie. Verfahren, Anwendungen, Qualitätssicherung*, 1st ed., Spektrum Akademischer Verlag, Heidelberg.

Carlton, A. G., B. J. Turpin, K. E. Altieri, S. P. Seitzinger, A. Reff, H.-J. Lim, and B. Ervens (2007), Atmospheric oxalic acid and SOA production from glyoxal: Results of aqueous photooxidation experiments, *Atmos. Environ., 41*(35), 7588–7602.

Carlton, A., C. Wiedinmyer, and J. H. Kroll (2009), A review of Secondary Organic Aerosol (SOA) formation from isoprene, *Atmos. Chem. Phys., 9*, 4987–5005.

Cecil, L. D., J. R. Green, and L. G. Thompson (Eds.) (2004), *Earth Paleoenvironments: Records Preserved in Mid- and Low-Latitude Glaciers*, Kluwer Academic Publishers, New York.

Chan, M. N., J. D. Surratt, A. W. H. Chan, K. Schilling, J. H. Offenberg, M. Lewandowski, E. O. Edney, T. E. Kleindienst, M. Jaoui, E. S. Edgerton et al. (2011), Influence of aerosol acidity on the chemical composition of secondary organic aerosol from β-caryophyllene, *Atmos. Chem. Phys., 11*(4), 1735–1751.

Chebbi, A., and P. Carlier (1996), Carboxylic acids in the troposphere, occurrence, sources, and sinks: A review, *Atmos. Environ., 30*(24), 4233–4249.

Cheng, Y., J. R. Brook, S.-M. Li, and A. Leithead (2011), Seasonal variation in the biogenic secondary organic aerosol tracer cis-pinonic acid: Enhancement due to emissions from regional and local biomass burning, *Atmos. Environ., 45*(39), 7105–7112.

Christoffersen, T., J. Hjorth, O. Horie, N. Jensen, D. Kotzias, L. Molander, P. Neeb, L. Ruppert, R. Winterhalter, A. Virkkula et al. (1998), cis-pinic acid, a possible precursor for organic aerosol formation from ozonolysis of α-pinene, *Atmospheric Environment, 32*(10), 1657–1661.

Claeys, M., Y. Iinuma, R. Szmigielski, J. D. Surratt, F. Blockhuys, C. van Alsenoy, O. Böge, B. Sierau, Y. Gómez-González, R. Vermeylen et al. (2009), Terpenylic Acid and Related Compounds from the Oxidation of α-Pinene: Implications for New Particle Formation and Growth above Forests, *Environ. Sci. Technol., 43*(18), 6976–6982.

Conedera, M., P. Marxer, W. Tinner, C. Hofmann, and B. Ammann (1996), Fire Ecology and History Research in the Southern Part of Switzerland, *International Forest Fire News*(15), 13–21.

Darer, A. I., N. C. Cole-Filipiak, A. E. O'Connor, and M. J. Elrod (2011), Formation and Stability of Atmospherically Relevant Isoprene-Derived Organosulfates and Organonitrates, *Environ. Sci. Technol., 45*(5), 1895–1902.

David, F., and P. Sandra (2007), Stir bar sorptive extraction for trace analysis, *J. Chromatogr. A, 1152*(1-2), 54–69.

Decesari, S., M. C. Facchini, S. Fuzzi, and E. Tagliavini (2000), Characterization of watersoluble organic compounds in atmospheric aerosol: A new approach, *J. Geophys. Res., 105*(D1), 1481–1489.

Dindorf, T., U. Kuhn, L. Ganzeveld, G. Schebeske, P. Ciccioli, C. Holzke, R. Köble, G. Seufert, and J. Kesselmeier (2006), Significant light and temperature dependent monoterpene emissions from European beech (Fagus sylvatica L.) and their potential impact on the European volatile organic compound budget, *J. Geophys. Res., 111*(D16).

Dominé, F., and P. B. Shepson (2002), Air-Snow Interactions and Atmospheric Chemistry, *Science, 297*, 1506–1510.

Doscher, A., H. W. Gäggeler, U. Schotterer, and M. Schwikowski (1996), A historical record of ammonium concentrations from a glacier in the Alps, *Geophys. Res. Lett., 23*(20), 2741–2744.

Douglas, T. A., F. Domine, M. Barret, C. Anastasio, H. J. Beine, J. Bottenheim, A. Grannas, S. Houdier, S. Netcheva, G. Rowland et al. (2012), Frost flowers growing in the Arctic ocean-atmosphere–sea ice–snow interface: 1. Chemical composition, *J. Geophys. Res., 117*.

Duarte, R. M., C. A. Pio, and A. C. Duarte (2005), Spectroscopic study of the water-soluble organic matter isolated from atmospheric aerosols collected under different atmospheric conditions, *Analytica Chimica Acta, 530*(1), 7–14.

Eichler, A., M. Schwikowski, and H. W. Gäggeler (2000a), An Alpine ice-core record of anthropogenic HF and HCl emissions, *Geophys. Res. Lett., 27*(19), 3225–3228.

Eichler, A., M. Schwikowski, H. W. Gäggeler, V. Furrer, H.-A. Synal, J. Beer, M. Saurer, and M. Funk (2000b), Glaciochemical dating of an ice core from upper Grenzgletscher (4200 m a.s.l.), *J. Glaciol., 46*(154), 507–515.

Eichler, A., (2000c), Dissertation Universität Bern.

Eichler, A., M. Schwikowski, and H. W. Gäggeler (2001), Meltwater-induced relocation of chemical species in Alpine firn, *Tellus, 53B*, 192–203.

Elgstoen, K. B. P. (2008), Liquid chromatography–tandem mass spectrometry method for routine measurement of oxalic acid in human plasma, *J. Chromatogr. B, 873*(1), 31–36.

Ervens, B., G. Feingold, G. J. Frost, and S. M. Kreidenweis (2004), A modeling study of aqueous production of dicarboxylic acids: 1. Chemical pathways and speciated organic mass production, *J. Geophys. Res., 109*(D15).

Ervens, B., B. J. Turpin, and R. J. Weber (2011), Secondary organic aerosol formation in cloud droplets and aqueous particles (aqSOA): a review of laboratory, field and model studies, *Atmos. Chem. Phys., 11*(21), 11069–11102.

Ervens, B., and R. Volkamer (2010), Glyoxal processing by aerosol multiphase chemistry: towards a kinetic modeling framework of secondary organic aerosol formation in aqueous particles, *Atmos. Chem. Phys., 10*(17), 8219–8244.

Fischer, H., D. Wagenbach, and J. Kipfstuhl (1998a), Sulfate and nitrate firn concentrations on the Greenland ice sheet 1. Largescale geographical deposition changes, *J. Geophys. Res., 103*, 21927–21934.

Fischer, H., M. Werner, D. Wagenbach, M. Schwager, Thorsteinnson T., Wilhelms F., J. Kipfstuhl, and S. Sommer (1998b), Little Ice Age clearly recorded in northern Greenland ice cores, *Geophys. Res. Lett., 25*(10), 1749–1752.

Froyd, K. D., S. M. Murphy, D. M. Murphy, J. A. de Gouw, N. C. Eddingsaas, and P. O. Wennberg (2010), Contribution of isoprene-derived organosulfates to free tropospheric aerosol mass, *Proceedings of the National Academy of Sciences, 107*(50), 21360–21365.

Fu, P., K. Kawamura, K. Usukura, and K. Miura (2013), Dicarboxylic acids, ketocarboxylic acids and glyoxal in the marine aerosols collected during a round-the-world cruise, *Marine Chemistry, 148*, 22–32.

Fu, T., D. J. Jacob, F. Wittrock, J. Burrows, M. Vrekoussis, and D. Henze (2008), Global budgets of atmospheric glyoxal and methylglyoxal, and implications for formation of secondary organic aerosols, *J. Geophys. Res., 113*(D15), D15303.

Fuzzi, S., M. C. Facchini, S. Decesari, E. Matta, and M. Mircea (2002), Soluble organic compounds in fog and cloud droplets: what have we learned over the past few years?, *Atmospheric Research, 64*(1-4), 89–98.

Gabrieli, J., P. Vallelonga, G. Cozzi, P. Gabrielli, A. Gambaro, M. Sigl, F. Decet, M. Schwikowski, H. Gäggeler, C. Boutron et al. (2010), Post 17th-Century Changes of European PAH Emissions Recorded in High-Altitude Alpine Snow and Ice, *Environ. Sci. Technol., 44*(9), 3260–3266.

Gabrielli, P., C. Barbante, C. Boutron, G. Cozzi, V. Gaspari, F. Planchon, C. Ferrari, C. Turetta, S. Hong, and P. Cescon (2005), Variations in atmospheric trace elements in Dome C (East Antarctica) ice over the last two climatic cycles, *Atmos. Environ., 39*(34), 6420–6429.

Gao, S., J. D. Surratt, E. M. Knipping, E. S. Edgerton, M. Shahgholi, and J. H. Seinfeld (2006), Characterization of polar organic components in fine aerosols in the southeastern United States: Identity, origin, and evolution, *J. Geophys. Res., 111*(D14).

Gómez-González, Y., W. Wang, R. Vermeylen, X. Chi, J. Neirynck, I. A. Janssens, W. Maenhaut, and M. Claeys (2012), Chemical characterisation of atmospheric aerosols during a 2007 summer field campaign at Brasschaat, Belgium: sources and source processes of biogenic secondary organic aerosol, *Atmos. Chem. Phys., 12*(1), 125–138.

Griffin, R. J., D. Dabdub, and J. H. Seinfeld (2002), Secondary organic aerosol 1. Atmospheric chemical mechanism for production of molecular constituents, *J. Geophys. Res., 107*(D17), 4332.

Grosjean, D., K. van Cauwenberghe, J. P. Schmid, P. E. Kelley, and J. N. Pitts (1978), Identification of C3-C10 aliphatic dicarboxylic acids in airborne particulate matter, *Environ. Sci. Technol., 12*(3), 313–317.

Gross, J. H. (2013), *Massenspektrometrie. Ein Lehrbuch*, 1st ed., Springer, Heidelberg.

Guilhermet, J., S. Preunkert, D. Voisin, C. Baduel, and M. Legrand (2013), Major 20th century changes of water-soluble humic-like substances (HULIS WS) aerosol over Europe inferred from Alpine ice cores, *J. Geophys. Res. Atmos., 118*(9), 3869–3878.

Gunz, D. W., and M. R. Hoffmann (1990), Field investigations on the snow chemistry in central and southern California - II. Carbonyls and carboxylic acids, *Atmos. Environ., 24A*(7), 1673–1684.

Hansen, A. M. K., K. Kristensen, Q. T. Nguyen, A. Zare, F. Cozzi, J. K. Nøjgaard, H. Skov, J. Brandt, J. H. Christensen, J. Ström et al. (2014), Organosulfates and organic acids in Arctic aerosols: speciation, annual variation and concentration levels, *Atmos. Chem. Phys. Discuss., 14*(4), 4745–4785.

Hatakeyama, S., M. Ohno, J. Weng, H. Takagi, and H. Akimoto (1987), Mechanism for the formation of gaseous and particulate products from ozone-cycloalkene reactions in air, *Environ. Sci. Technol., 21*, 52–57.

Hatch, L. E., J. M. Creamean, A. P. Ault, J. D. Surratt, M. N. Chan, J. H. Seinfeld, E. S. Edgerton, Y. Su, and K. A. Prather (2011), Measurements of Isoprene-Derived Organosulfates in Ambient Aerosols by Aerosol Time-of-Flight Mass Spectrometry - Part 1: Single Particle Atmospheric Observations in Atlanta, *Environ. Sci. Technol., 45*(12), 5105–5111.

Hennion, M.-C. (1999), Solid-phase extraction: method development, sorbents, and coupling with liquid chromatography, *J. Chromatogr. A, 856*(1-2), 3–54.

Hervé, A. (2003), Factor Rotations in Factor Analysis, in *Encyclopedia of Social Sciences Research Methods*, edited by M. Lewis-Beck, A. Bryman, and T. Futing, Thousand Oaks (CA): Sage.

Hoffmann, T., R. Bandur, U. Marggraf, and M. Linscheid (1998), Molecular composition of organic aerosols formed in the α-pinene/O 3 reaction: Implications for new particle formation processes, *J. Geophys. Res., 103*(D19), 25569.

Ho, K., S. Lee, J. Cao, K. Kawamura, T. Watanabe, Y. Cheng, and J. C. Chow (2006), Dicarboxylic acids, ketocarboxylic acids and dicarbonyls in the urban roadside area of Hong Kong, *Atmospheric Environment, 40*(17), 3030–3040.

Houdier, S., M. Barret, F. Dominé, T. Charbouillot, L. Deguillaume, and D. Voisin (2011), Sensitive determination of glyoxal, methylglyoxal and hydroxyacetaldehyde in environmental water samples by using dansylacetamidooxyamine derivatization and liquid chromatography/fluorescence, *Anal Chim Acta, 704*(1-2), 162–173.

Hsieh, L.-Y., S.-C. Kuo, C.-L. Chen, and Y. I. Tsai (2007), Origin of low-molecular-weight dicarboxylic acids and their concentration and size distribution variation in suburban aerosol, *Atmos. Environ., 41*(31), 6648–6661.

Hyder, M., J. Genberg, M. Sandahl, E. Swietlicki, and J. Å. Jönsson (2012), Yearly trend of dicarboxylic acids in organic aerosols from south of Sweden and source attribution, *Atmos. Environ., 57*, 197–204.

Iinuma, Y., O. Böge, A. Kahnt, and H. Herrmann (2009), Laboratory chamber studies on the formation of organosulfates from reactive uptake of monoterpene oxides, *Phys. Chem. Chem. Phys., 11*(36), 7985.

Iinuma, Y., A. Kahnt, A. Mutzel, O. Böge, and H. Herrmann (2013), Ozone-Driven Secondary Organic Aerosol Production Chain, *Environ. Sci. Technol., 47*(8), 3639–3647.

Iinuma, Y., C. Müller, T. Berndt, O. Böge, M. Claeys, and H. Herrmann (2007), Evidence for the Existence of Organosulfates from β-Pinene Ozonolysis in Ambient Secondary Organic Aerosol, *Environ. Sci. Technol., 41*(19), 6678–6683.

IPCC 2013a: Summary for Policymakers. In: Climate Change 2013: The Physical Science Basis. Contribution of Working Group I to the Fifth Assessment Report of the Intergovernmental Panel on Climate Change [Stocker, T.F., D. Qin, G.-K. Plattner, M. Tignor, S.K. Allen, J. Boschung, A. Nauels, Y. Xia, V. Bex and P.M. Midgley (eds.)]. Cambridge University Press, Cambridge, United Kingdom and New York, NY, USA, page 14.

IPCC 2013b: Vaughan, D.G., J.C. Comiso, I. Allison, J. Carrasco, G. Kaser, R. Kwok, P. Mote, T. Murray, F. Paul, J. Ren, E. Rignot, O. Solomina, K. Steffen and T. Zhang, 2013: Observations: Cryosphere. In: Climate Change 2013: The Physical Science Basis. Contribution of Working Group I to the Fifth Assessment Report of the Intergovernmental Panel on Climate Change [Stocker, T.F., D. Qin, G.-K. Plattner, M. Tignor, S.K. Allen, J. Boschung, A. Nauels, Y. Xia, V. Bex and P.M. Midgley (eds.)]. Cambridge University Press, Cambridge, United Kingdom and New York, NY, USA

Jang, M. (2002), Heterogeneous Atmospheric Aerosol Production by Acid-Catalyzed Particle-Phase Reactions, *Science, 298*(5594), 814–817.

Janson, R. W. (1993), Monoterpene emissions from Scots pine and Norwegian spruce, *J. Geophys. Res., 98*(D2), 2839.

Jimenez, J. L., M. R. Canagaratna, N. M. Donahue, A. S. H. Prevot, Q. Zhang, J. H. Kroll, P. F. DeCarlo, J. D. Allan, H. Coe, N. L. Ng et al. (2009), Evolution of Organic Aerosols in the Atmosphere, *Science, 326*(5959), 1525–1529.

Johnson, D., and G. Marston (2008), The gas-phase ozonolysis of unsaturated volatile organic compounds in the troposphere, *Chem. Soc. Rev., 37*(4), 699.

K. Rasmussen (1989), Solid-phase sample extraction for rapid determination of methylmalonic acid in serum and urine by a stable-isotope-dilution method, *Clinical Chemistry, 35*(2), 260–264.

Kahnt, A., S. Behrouzi, R. Vermeylen, M. Safi Shalamzari, J. Vercauteren, E. Roekens, M. Claeys, and W. Maenhaut (2013), One-year study of nitro-organic compounds and their relation to wood burning in PM10 aerosol from a rural site in Belgium, *Atmos. Environ., 81*, 561–568.

Kahnt, A., Y. Iinuma, A. Mutzel, O. Böge, M. Claeys, and H. Herrmann (2014), Campholenic aldehyde ozonolysis: a mechanism leading to specific biogenic secondary organic aerosol constituents, *Atmos. Chem. Phys., 14*(2), 719–736.

Kampf, C. J., B. Bonn, and T. Hoffmann (2011), Development and validation of a selective HPLC-ESI-MS/MS method for the quantification of glyoxal and methylglyoxal in atmospheric aerosols (PM2.5), *Anal Bioanal Chem, 401*(10), 3115–3124.

Kampf, C. J., A. L. Corrigan, A. M. Johnson, W. Song, P. Keronen, R. Königstedt, J. Williams, L. M. Russell, T. Petäjä, H. Fischer et al. (2012), First measurements of reactive α-dicarbonyl concentrations on $PM_{2.5}$ aerosol over the Boreal forest in Finland during HUMPPA-COPEC 2010 – source apportionment and links to aerosol aging, *Atmos. Chem. Phys., 12*(14), 6145–6155.

Kanakidou, M., J. H. Seinfeld, S. N. Pandis, I. Barnes, F. J. Dentener, M. C. Facchini, R. van Dingenen, B. Ervens, A. Nenes, C. J. Nielsen et al. (2005), Organic aerosol and global climate modelling: a review, *Atmos. Chem. Phys., 5*(4), 1053–1123.

Kautzman, K. E., J. D. Surratt, M. N. Chan, A. W. H. Chan, S. P. Hersey, P. S. Chhabra, N. F. Dalleska, P. O. Wennberg, R. C. Flagan, and J. H. Seinfeld (2010), Chemical Composition of Gas- and Aerosol-Phase Products from the Photooxidation of Naphthalene, *J. Phys. Chem. A, 114*(2), 913–934.

Kawamura, K. (1993), Identification of C2-C10 w-Oxocarboxylic Acids, Pyruvic Acid, and alpha-Dicarbonyls in Wet Precipitation and Aerosol Samples by Capillary GC and GC/MS, *Anal. Chem., 65*, 3505–3511.

Kawamura, K., and K. Ikushima (1993), Seasonal changes in the distribution of dicarboxylic acids in the urban atmosphere, *Environ. Sci. Technol., 27*, 2227–2235.

Kawamura, K., Y. Izawa, M. Mochida, and T. Shiraiwa (2012), Ice core records of biomass burning tracers (levoglucosan and dehydroabietic, vanillic and p-hydroxybenzoic acids) and total organic carbon for past 300years in the Kamchatka Peninsula, Northeast Asia, *Geochimica et Cosmochimica Acta, 99*, 317–329.

Kawamura, K., and I. R. Kaplan (1987), Motor Exhaust Emissions as a Primary Source for Dicarboxylic Acids in Los Angeles Ambient Air, *Environ. Sci. Technol., 21*, 105–110.

Kawamura, K., H. Kasukabe, and L. Barrie (1996a), Source and reaction pathways of dicarboxylic acids, ketoacids and dicarbonyls in arctic aerosols: One year of observations, *Atmos. Environ., 30*(10), 1709-1722.

Kawamura, K., and Sakaguchi F. (1999), Molecular distributions of water soluble dicarboxylic acids in marine aerosols over the Pacific Ocean including tropics, *J. Geophys. Res., 104*, 3501–3509.

Kawamura, K., S. Steinberg, and I. R. Kaplan (1985), Capillary GC Determination of Short-Chain Dicarboxylic Acids in Rain, Fog, and Mist, *International Journal of Environmental Analytical Chemistry, 19*(3), 175–188.

Kawamura, K., S. Steinberg, and I. R. Kaplan (1996b), Concentrations of monocarboxylic and dicarboxylic acids and aldehydes in southern California wet precipitations: Comparison of urban and nonurban samples and compositional changes during scavenging, *Atmos. Environ., 30*(7), 1035–1052.

Kawamura, K., S. Steinberg, L. Ng, and I. R. Kaplan (2001a), Wet deposition of low molecular weight mono- and di-carboxylic acids, aldehydes and inorganic species in Los Angeles, *Atmospheric Environment, 35*(23), 3917–3926.

Kawamura, K., I. Suzuki, Y. Fujii, and O. Watanabe (1996c), Ice core record of fatty acids over the past 450 years in Greenland, *Geophys. Res. Lett., 23*(19), 2665–2668.

Kawamura, K., and O. Yasui (2005), Diurnal changes in the distribution of dicarboxylic acids, ketocarboxylic acids and dicarbonyls in the urban Tokyo atmosphere, *Atmos. Environ., 39*(10), 1945–1960.

Kawamura, K., K. Yokoyama, O. Fujii, and O. Watanabe (2001b), A Greenland ice core record of low molecular weight dicarboxylic acids, ketocarboxylic acids, and alpha-dicarbonyls: A trend from Little Ice Age to the present (1540 to 1989 A.D.), *J. Geophys. Res., 106*(D1), 1331–1345.

Keene, W. C., B. W. Mosher, D. J. Jacob, J. W. Munger, R. W. Talbot, R. S. Artz, J. R. Maben, B. C. Daube, and J. N. Galloway (1995), Carboxylic acids in clouds at a high-elevation forested site in central Virginia, *J. Geophys. Res., 100*(D5), 9345.

Kehrwald, N., R. Zangrando, P. Gabrielli, J.-L. Jaffrezo, C. Boutron, C. Barbante, and A. Gambaro (2012), Levoglucosan as a specific marker of fire events in Greenland snow, *Tellus B, 64*(0), 573.

Kehrwald, N., R. Zangrando, A. Gambaro, P. Cescon, and C. Barbante (2010), Specific molecular markers in ice cores provide large-scale patterns in biomass burning, *PAGES news, 18*(2), 59–61.

Khwaja, H. A. (1995), Atmospheric concentrations of carboxylic acids and related compounds at a semiurban site, *Atmospheric Environment, 29*(1), 127–139.

Kim, K., W. Choi, M. R. HOFFMANN, H.-I. Yoon, and B.-K. Park (2010), Photoreductive Dissolution of Iron Oxides Trapped in Ice and Its Environmental Implications, *Environ. Sci. Technol., 44*(11), 4142–4148.

Kim, S., R. W. Kramer, and P. G. Hatcher (2003), Graphical Method for Analysis of Ultrahigh-Resolution Broadband Mass Spectra of Natural Organic Matter, the Van Krevelen Diagram, *Anal. Chem., 75*(20), 5336–5344.

Kippenberger, M., R. Winterhalter, and G. K. Moortgat (2008), Determination of higher carboxylic acids in snow samples using solid-phase extraction and LC/MS-TOF, *Anal Bioanal Chem, 392*(7-8), 1459–1470.

Koch, S., R. Winterhalter, E. Uherek, A. Kolloff, P. Neeb, and G. K. Moortgat (2000), Formation of new particles in the gas-phase ozonolysis of monoterpenes, *Atmos. Environ., 34*(23), 4031–4042.

Komenda, M. (2002), Monoterpene emissions from Scots pine (Pinus sylvestris): Field studies of emission rate variabilities, *J. Geophys. Res., 107*(D13).

Kourtchev, I., S. Fuller, J. Aalto, T. M. Ruuskanen, M. W. McLeod, W. Maenhaut, R. Jones, M. Kulmala, and M. Kalberer (2013), Molecular Composition of Boreal Forest Aerosol from Hyytiälä, Finland, Using Ultrahigh Resolution Mass Spectrometry, *Environ. Sci. Technol., 47*(9), 4069–4079.

Kourtchev, I., I. O'Connor, C. Giorio, S. Fuller, K. Kristensen, W. Maenhaut, J. Wenger, J. Sodeau, M. Glasius, and M. Kalberer (2014), Effects of anthropogenic emissions on the molecular composition of urban organic aerosols: An ultrahigh resolution mass spectrometry study, *Atmospheric Environment, 89*, 525–532.

Kristensen, K., K. L. Enggrob, S. M. King, D. R. Worton, S. M. Platt, R. Mortensen, T. Rosenoern, J. D. Surratt, M. Bilde, A. H. Goldstein et al. (2013), Formation and occurrence of dimer esters of pinene oxidation products in atmospheric aerosols, *Atmos. Chem. Phys., 13*(7), 3763–3776.

Kristensen, K., and M. Glasius (2011), Organosulfates and oxidation products from biogenic hydrocarbons in fine aerosols from a forest in North West Europe during spring, *Atmospheric Environment, 45*(27), 4546–4556.

Kroll, J. H., N. M. Donahue, J. L. Jimenez, S. H. Kessler, M. R. Canagaratna, K. R. Wilson, K. E. Altieri, L. R. Mazzoleni, A. S. Wozniak, H. Bluhm et al. (2011), Carbon oxidation state as a metric for describing the chemistry of atmospheric organic aerosol, *Nature Chem, 3*(2), 133–139.

Kroll, J. H., and J. H. Seinfeld (2008), Chemistry of secondary organic aerosol: Formation and evolution of low-volatility organics in the atmosphere, *Atmos. Environ., 42*(16), 3593–3624.

Kundu, S., K. Kawamura, T. W. Andreae, A. Hoffer, and M. O. Andreae (2010), Molecular distributions of dicarboxylic acids, ketocarboxylic acids and α-dicarbonyls in biomass burning aerosols: implications for photochemical production and degradation in smoke layers, *Atmos. Chem. Phys., 10*, 2209–2225.

Kundu, S., T. A. Quraishi, G. Yu, C. Suarez, F. N. Keutsch, and E. A. Stone (2013), Evidence and quantitation of aromatic organosulfates in ambient aerosols in Lahore, Pakistan, *Atmos. Chem. Phys., 13*(9), 4865–4875.

Lacorte, S., J. Quintana, R. Tauler, F. Ventura, A. Tovar-Sánchez, and C. Duarte (2009), Ultra-trace determination of Persistent Organic Pollutants in Arctic ice using stir bar sorptive extraction and gas chromatography coupled to mass spectrometry, *J. Chromatogr. A, 1216*(49), 8581–8589.

Largiuni, O. (2003), Formaldehyde record from Lys glacier firn core, Monte Rosa massif (Italy), *Atmos. Environ., 37*(27), 3849–3860.

LeClair, J. P., J. L. Collett, and L. R. Mazzoleni (2012), Fragmentation Analysis of Water-Soluble Atmospheric Organic Matter Using Ultrahigh-Resolution FT-ICR Mass Spectrometry, *Environ. Sci. Technol., 46*(8), 4312–4322.

Lee, S., K. Baumann, J. J. Schauer, R. J. Sheesley, L. P. Naeher, S. Meinardi, D. R. Blake, E. S. Edgerton, A. G. Russell, and M. Clements (2005), Gaseous and Particulate Emissions from Prescribed Burning in Georgia, *Environ. Sci. Technol., 39*(23), 9049–9056.

Legrand, M., and M. de Angelis (1995), Origins and variations of light carboxylic acids in polar precipitation, *J. Geophys. Res., 100*(D1), 1445.

Legrand, M., and M. de Angelis (1996), Light carboxylic acids in Greenland ice: A record of past forest fires and vegetation emissions from the boreal zone, *J. Geophys. Res. Atmos., 101*(D2), 4129–4145.

Legrand, M., M. de Angelis, T. Staffelbach, A. Neftel, and B. Stauffer (1992), Large perturbations of ammonium and organic acids content in the summit-Greenland Ice Core. Fingerprint from forest fires?, *19*(5), 473–475.

Legrand, M., S. Preunkert, B. Jourdain, J. Guilhermet, X. Fa{ï}n, I. Alekhina, and J. R. Petit (2013a), Water-soluble organic carbon in snow and ice deposited at Alpine, Greenland, and Antarctic sites: a critical review of available data and their atmospheric relevance, *Clim. Past, 9*(5), 2195–2211.

Legrand, M., S. Preunkert, B. May, J. Guilhermet, H. Hoffman, and D. Wagenbach (2013b), Major 20th century changes of the content and chemical speciation of organic carbon archived in Alpine ice cores: Implications for the long-term change of organic aerosol over Europe, *J. Geophys. Res. Atmos., 118*(9), 3879–3890.

Legrand, M., S. Preunkert, T. Oliveira, C. A. Pio, S. Hammer, A. Gelencsér, A. Kasper-Giebl, and P. Laj (2007a), Origin of C 2 –C 5 dicarboxylic acids in the European atmosphere inferred from year-round aerosol study conducted at a west-east transect, *J. Geophys. Res., 112*(D23).

Legrand, M., S. Preunkert, M. Schock, M. Cerqueira, A. Kasper-Giebl, J. Afonso, C. Pio, A. Gelencsér, and I. Dombrowski-Etchevers (2007b), Major 20th century changes of carbonaceous aerosol components (EC, WinOC, DOC, HULIS, carboxylic acids, and cellulose) derived from Alpine ice cores, *J. Geophys. Res., 112*(D23).

Legrand, M., S. Preunkert, D. Wagenbach, H. Cachier, and H. Puxbaum (2003), A historical record of formate and acetate from a high-elevation Alpine glacier: Implications for their natural versus anthropogenic budgets at the European scale, *J. Geophys. Res. Atmos., 108*(D24).

Legrand, M., S. Preunkert, D. Wagenbach, and H. Fischer (2002), Seasonally resolved Alpine and Greenland ice core records of anthropogenic HCl emissions over the 20th century, *J. Geophys. Res., 107*(D12), 4139.

Li, N., T.-M. Fu, J. Cao, S. Lee, X.-F. Huang, L.-Y. He, K.-F. Ho, J. S. Fu, and Y.-F. Lam (2013), Sources of secondary organic aerosols in the Pearl River Delta region in fall: Contributions from the aqueous reactive uptake of dicarbonyls, *Atmospheric Environment, 76*, 200–207.

Lin, P., A. G. Rincon, M. Kalberer, and J. Z. Yu (2012a), Elemental Composition of HULIS in the Pearl River Delta Region, China: Results Inferred from Positive and Negative Electrospray High Resolution Mass Spectrometric Data, *Environ. Sci. Technol., 46*(14), 7454–7462.

Lin, P., J. Z. Yu, G. Engling, and M. Kalberer (2012b), Organosulfates in Humic-like Substance Fraction Isolated from Aerosols at Seven Locations in East Asia: A Study by Ultra-High-Resolution Mass Spectrometry, *Environ. Sci. Technol., 46*(24), 13118–13127.

Liška, I. (2000), Fifty years of solid-phase extraction in water analysis – historical development and overview, *J. Chromatogr. A, 885*(1-2), 3–16.

Li, Y.-C., and J. Z. Yu (2005), Simultaneous Determination of Mono- and Dicarboxylic Acids, ω-Oxo-carboxylic Acids, Midchain Ketocarboxylic Acids, and Aldehydes in Atmospheric Aerosol Samples, *Environ. Sci. Technol., 39*(19), 7616–7624.

Lohmann, U., and J. Feichter (2005), Global indirect aerosol effects: a review, *Atmos. Chem. Phys.*(5), 715–737.

Maggi, V., S. Villa, A. Finizio, B. Delmonte, P. Casati, and F. Marino (2006), Variability of Anthropogenic and Natural Compounds in High Altitude–high Accumulation Alpine Glaciers, *Hydrobiologia, 562*(1), 43–56.

Mahowald, N., D. S. Ward, S. Kloster, M. G. Flanner, C. L. Heald, N. G. Heavens, P. G. Hess, J.-F. Lamarque, and P. Y. Chuang (2011), Aerosol Impacts on Climate and Biogeochemistry, in *Annual Review of Environment and Resources, Annual Review of Environment and Resources*, edited by A. Gadgil, and D. M. Liverman, pp. 45–74.

Martin, R. S., I. Villanueva, J. Zhang, and C. J. Popp (1999), Nonmethane Hydrocarbon, Monocarboxylic Acid, and Low Molecular Weight Aldehyde and Ketone Emissions from Vegetation in Central New Mexico, *Environ. Sci. Technol., 33*(13), 2186–2192.

Matsunaga, S. N., A. B. Guenther, Y. Izawa, C. Wiedinmyer, J. P. Greenberg, and K. Kawamura (2007), Importance of wet precipitation as a removal and transport process for atmospheric water soluble carbonyls, *Atmos. Environ., 41*(4), 790–796.

Matsunaga, S., and K. Kawamura (2000), Determination of α- and β-Hydroxycarbonyls and Dicarbonyls in Snow and Rain Samples by GC/FID and GC/MS Employing Benzyl Hydroxyl Oxime Derivatization, *Anal. Chem., 72*(19), 4742–4746.

May, B., D. Wagenbach, H. Hoffmann, M. Legrand, S. Preunkert, and P. Steier (2013), Constraints on the major sources of dissolved organic carbon in Alpine ice cores from radiocarbon analysis over the bomb-peak period, *J. Geophys. Res. Atmos., 118*(8), 3319–3327.

Mayewski, P. A., W. B. Lyons, M. J. Spencer, M. Twickler, W. Dansgaard, B. Koci, C. I. Davidson, and R. E. Honrath (1986), Sulfate and Nitrate Concentrations from a South Greenland Ice Core, *Science, 232*(4753), 975–977.

Mayol-Bracero, O. L. (2002), Water-soluble organic compounds in biomass burning aerosols over Amazonia 2. Apportionment of the chemical composition and importance of the polyacidic fraction, *J. Geophys. Res., 107*(D20).

Mazzoleni, L. R., B. M. Ehrmann, X. Shen, A. G. Marshall, and J. L. Collett (2010), Water-Soluble Atmospheric Organic Matter in Fog: Exact Masses and Chemical Formula Identification by Ultrahigh-Resolution Fourier Transform Ion Cyclotron Resonance Mass Spectrometry, *Environ. Sci. Technol., 44*(10), 3690–3697.

Mazzoleni, L. R., P. Saranjampour, M. M. Dalbec, V. Samburova, A. G. Hallar, B. Zielinska, D. H. Lowenthal, and S. Kohl (2012), Identification of water-soluble organic carbon in non-urban aerosols using ultrahigh-resolution FT-ICR mass spectrometry: organic anions, *Environ. Chem., 9*(3), 285.

McConnell, J. R., R. Edwards, G. L. Kok, M. G. Flanner, C. S. Zender, E. S. Saltzman, J. R. Banta, D. R. Pasteris, M. M. Carter, and J. D. W. Kahl (2007), 20th-Century Industrial Black Carbon Emissions Altered Arctic Climate Forcing, *Science, 317*(5843), 1381–1384.

Meyer, V. R. (2009), *Praxis der Hochleistungs-Flüssigkeitschromatographie*, 10th ed., Wiley-VCH, Weinheim.

Mkoma, S. L., and K. Kawamura (2013), Molecular composition of dicarboxylic acids, ketocarboxylic acids, α-dicarbonyls and fatty acids in atmospheric aerosols from Tanzania, East Africa during wet and dry seasons, *Atmos. Chem. Phys., 13*(4), 2235–2251.

Mochida, M., A. Kawabata, K. Kawamura, H. Hatsushika, and K. Yamazaki (2003), Seasonal variation and origins of dicarboxylic acids in the marine atmosphere over the western North Pacific, *J. Geophys. Res., 108*(D6).

Moglioni, A. G., E. García-Expósito, G. P. Aguado, T. Parella, V. Branchadell, G. Y. Moltrasio, and R. M. Ortuño (2000), Divergent Routes to Chiral Cyclobutane Synthons from (−)-α-Pinene and Their Use in the Stereoselective Synthesis of Dehydro Amino Acids, *J. Org. Chem., 65*(13), 3934–3940.

Müller, L., M.-C. Reinnig, H. Hayen, and T. Hoffmann (2009), Characterization of oligomeric compounds in secondary organic aerosol using liquid chromatography coupled to electrospray ionization Fourier transform ion cyclotron resonance mass spectrometry, *Rapid Commun. Mass Spectrom., 23*(7), 971–979.

Munger, J. W., J. COLLETT, B. C. Daube, and M. R. HOFFMANN (1989), Carboxylic acids and carbonyl compounds in southern California clouds and fogs, *Tellus B, 41*(3), 230–242.

Narukawa, M., K. Kawamura, N. Takeuchi, and T. Nakajima (1999), Distribution of dicarboxylic acids and carbon isotopic compositions in aerosols from 1997 Indonesian forest fires, *Geophys. Res. Lett., 26*(20), 3101–3104.

Neng, N. R., C. Cordeiro, A. Freire, and J. M. F. Nogueira (2007), Determination of glyoxal and methylglyoxal in environmental and biological matrices by stir bar sorptive extraction with in-situ derivatization, *J. Chromatogr. A, 1169*(1-2), 47–52.

Neusüß, C., T. Gnauk, A. Plewka, and H. Herrmann (2002), Carbonaceous aerosol over the Indian Ocean: OC/EC fractions and selected specifications from size-segregated onboard samples, *J. Geophys. Res., 107*(D19).

Nolte, C. G., J. J. Schauer, G. R. Cass, and B. R. T. Simoneit (1999), Highly Polar Organic Compounds Present in Meat Smoke, *Environ. Sci. Technol., 33*(19), 3313–3316.

O'Dowd, C. D., P. Aalto, K. Hmeri, M. Kulmala, and T. Hoffmann (2002), Aerosol formation: Atmospheric particles from organic vapours, *Nature, 416*(6880), 497–498.

Pavuluri, C. M., K. Kawamura, and T. Swaminathan (2010), Water-soluble organic carbon, dicarboxylic acids, ketoacids, and α -dicarbonyls in the tropical Indian aerosols, *J. Geophys. Res., 115*(D11).

Pérez-Rial, D., J. Peñuelas, P. López-Mahía, and J. Llusià (2009), Terpenoid emissions from Quercus robur. A case study of Galicia (NW Spain), *J. Environ. Monit., 11*(6), 1268.

Pezzatti, B., M. Conedera, and A. Kaltenbrunner (2005), Die neue Waldbranddatenbank, *Bündnerwald, 58*(6), 37–39.

Pio, C. A., M. Legrand, C. Alves, T. Oliveira, J. Afonso, A. Caseiro, H. Puxbaum, A. Sanchez-Ochoa, and A. Gelencsér (2008), Chemical composition of atmospheric aerosols during the 2003 summer intense forest fire period, *Atmos. Environ., 42*(32), 7530–7543.

Plewka, A., T. Gnauk, E. Brüggemann, and H. Herrmann (2006), Biogenic contributions to the chemical composition of airborne particles in a coniferous forest in Germany, *Atmos. Environ., 40*, 103–115.

Poole, C. F. (2003), New trends in solid-phase extraction, *TrAC Trends in Analytical Chemistry, 22*(6), 362–373.

Poole, C. F., A. D. Gunatilleka, and R. Sethuraman (2000), Contributions of theory to method development in solid-phase extraction, *J. Chromatogr. A, 885*(1-2), 17–39.

Pöschl, U. (2005), Atmospheric Aerosols: Composition, Transformation, Climate and Health Effects, *Angew. Chem. Int. Ed., 44*(46), 7520–7540.

Pratt, K. A., M. N. Fiddler, P. B. Shepson, A. G. Carlton, and J. D. Surratt (2013), Organosulfates in cloud water above the Ozarks' isoprene source region, *Atmos. Environ., 77*, 231–238.

Preunkert, S., and M. Legrand (2013), Towards a quasi-complete reconstruction of past atmospheric aerosol load and composition (organic and inorganic) over Europe since 1920 inferred from Alpine ice cores, *Clim. Past, 9*(4), 1403–1416.

Preunkert, S., M. Legrand, and D. Wagenbach (2001), Sulfate trends in a Col du Dome French Alps ice core: A record of anthropogenic sulfate levels in the European midtroposphere over the twentieth century, *J. Geophys. Res. Atmos., 106*(D23), 31,991-32,004.

Preunkert, S., D. Wagenbach, and M. Legrand (2003), A seasonally resolved alpine ice core record of nitrate: Comparison with anthropogenic inventories and estimation of preindustrial emissions of NO in Europe, *J. Geophys. Res. Atmos., 108*(D21).

Prieto, A., O. Basauri, R. Rodil, A. Usobiaga, L. Fernández, N. Etxebarria, and O. Zuloaga (2010), Stir-bar sorptive extraction: A view on method optimisation, novel applications, limitations and potential solutions, *J. Chromatogr. A, 1217*(16), 2642–2666.

Reemtsma, T., A. These, P. Venkatachari, X. Xia, P. K. Hopke, A. Springer, and M. Linscheid (2006), Identification of Fulvic Acids and Sulfated and Nitrated Analogues in Atmospheric Aerosol by Electrospray Ionization Fourier Transform Ion Cyclotron Resonance Mass Spectrometry, *Anal. Chem., 78*(24), 8299–8304.

Reid, J. S., R. Koppmann, T. F. Eck, and D. P. Eleuterio (2005), A review of biomass burning emissions part II: intensive physical properties of biomass burning particles, *Atmos. Chem. Phys., 5*(3), K799–825.

Rodríguez, E., G. Fernández, B. Ledesma, P. Álvarez, and F. J. Beltrán (2009), Photocatalytic degradation of organics in water in the presence of iron oxides: Influence of carboxylic acids, *Applied Catalysis B: Environmental, 92*(3-4), 240–249.

Rosenberg, E. (2003), The potential of organic (electrospray- and atmospheric pressure chemical ionisation) mass spectrometric techniques coupled to liquid-phase separation for speciation analysis, *J. Chromatogr. A, 1000*(1-2), 841–889.

Safi Shalamzari, M., O. Ryabtsova, A. Kahnt, R. Vermeylen, M.-F. Hérent, J. Quetin-Leclercq, P. van der Veken, W. Maenhaut, and M. Claeys (2013), Mass spectrometric characterization of organosulfates related to secondary organic aerosol from isoprene, *Rapid Commun. Mass Spectrom., 27*(7), 784–794.

Samy, S., L. R. Mazzoleni, S. Mishra, B. Zielinska, and A. G. Hallar (2010), Water-soluble organic compounds at a mountain-top site in Colorado, USA, *Atmos. Environ., 44*(13), 1663–1671.

Sánchez-Rojas, F., C. Bosch-Ojeda, and J. M. Cano-Pavón (2009), A Review of Stir Bar Sorptive Extraction, *Chromatographia, 69*(S1), 79–94.

Saxena, P., and L. M. Hildemann (1996), Water-soluble organics in atmospheric particles: A critical review of the literature and application of thermodynamics to identify candidate compounds, *Journal of Atmospheric Chemistry, 24*, 57–109.

Schauer, J. J., M. J. Kleeman, G. R. Cass, and B. R. T. Simoneit (1999), Measurement of Emissions from Air Pollution Sources. 1. C 1 through C 29 Organic Compounds from Meat Charbroiling, *Environ. Sci. Technol., 33*(10), 1566–1577.

Schauer, J. J., W. F. Rogge, L. M. Hildemann, M. A. Mazurek, G. R. Cass, and B. R. T. Simoneit (1996), Source apportionment of airborne particulate matter using organic compounds as tracers, *Atmos. Environ., 30*(22), 3837–3855.

Schindelka, J., Y. Iinuma, D. Hoffmann, and H. Herrmann (2013), Sulfate radical-initiated formation of isoprene-derived organosulfates in atmospheric aerosols, *Faraday Discuss., 165*, 237.

Schwikowski, M. (2004), Reconstruction of European Air Pollution from Alpine Ice Cores, in *Earth Paleoenvironments: Records Preserved in Mid- and Low-Latitude Glaciers*, edited by L. D. Cecil, J. R. Green, and L. G. Thompson, pp. 95–120, Kluwer Academic Publishers. New York.

Schwikowski, M., C. Barbante, T. Doering, H. W. Gaeggeler, C. Boutron, U. Schotterer, L. Tobler, K. van de Velde, C. Ferrari, G. Cozzi et al. (2004), Post-17th-Century Changes of European Lead Emissions Recorded in High-Altitude Alpine Snow and Ice, *Environ. Sci. Technol., 38*(4), 957–964.

Schwikowski, M., S. Brütsch, H. W. Gäggeler, and U. Schotterer (1999), A high-resolution air chemistry record from an Alpine ice core: Fiescherhorn glacier, Swiss Alps, *J. Geophys. Res., 104*(D11), 13,709-13,719.

Scigelova, M., and A. Makarov (2006), Orbitrap Mass Analyzer – Overview and Applications in Proteomics, *Proteomics, 6*(S2), 16–21.

Seinfeld, J. H., and S. N. Pandis (2006), *Atmospheric Chemistry and Physics: From Air Pollution to Climate Change*, John Wiley & Sons Inc., Hoboken, USA.

Seinfeld, J. H., and J. F. Pankow (2003), Organic Atmospheric Particulate Material, *Annu. Rev. Phys. Chem., 54*(1), 121–140.

Sempére, R., and K. Kawamura (1994), Comparative distributions of dicarboxylic acids and related polar compounds in snow, rain and aerosols from urban atmosphere, *Atmospheric Environment, 28*(3), 449–459.

Sempéré, R., and K. Kawamura (1996), Low molecular weight dicarboxylic acids and related polar compounds in the remote marine rain samples collected from Western Pacific, *Atmospheric Environment, 30*(10-11), 1609–1619.

Sieg, K., E. Fries, and W. Püttmann (2008), Analysis of benzene, toluene, ethylbenzene, xylenes and n-aldehydes in melted snow water via solid-phase dynamic extraction combined with gas chromatography/mass spectrometry, *J. Chromatogr. A, 1178*(1-2), 178–186.

Simoneit, B. R. T. (2002), Biomass burning — a review of organic tracers for smoke from incomplete combustion, *Applied Geochemistry, 17*(3), 129–162.

Simoneit, B. R. T., W. F. Rogge, M. A. Mazurek, L. J. Standley, L. M. Hildemann, and G. R. Cass (1993), Lignin Pyrolysis Products, Lignans, and Resin Acids as Specific Tracers of Plant Classes in Emissions from Biomass Combustion, *Environ. Sci. Technol., 27*, 2533–2541.

Simpson, I. J., S. K. Akagi, B. Barletta, N. J. Blake, Y. Choi, G. S. Diskin, A. Fried, H. E. Fuelberg, S. Meinardi, F. S. Rowland et al. (2011), Boreal forest fire emissions in fresh Canadian smoke plumes: C_1-C_{10} volatile organic compounds (VOCs), CO_2, CO, NO_2, NO, HCN and CH_3CN, *Atmos. Chem. Phys., 11*(13), 6445–6463.

Staffelbach, T., A. Neftel, B. Stauffer, and D. Jacob (1991), A record of the atmospheric methane sink from formaldehyde in polar ice cores, *Nature, 349*, 603–605.

Steinberg, S., K. Kawamura, and I. R. Kaplan (1985), The Determination of α-Keto Acids and Oxalic Acid in Rain, Fog and Mist by HPLC, *International Journal of Environmental Analytical Chemistry, 19*(4), 251–260.

Stephanou, E. G., and N. Stratigakis (1993a), Oxocarboxylic and .alpha.,.omega.-dicarboxylic acids: photooxidation products of biogenic unsaturated fatty acids present in urban aerosols, *Environ. Sci. Technol., 27*(7), 1403–1407.

Stephanou, E. G., and N. Stratigakis (1993b), Oxocarboxylic and a,w-Dicarboxylic Acids: Photooxidation Products of Biogenic Unsaturated Fatty Acids Present in Urban Aerosols, *Environ. Sci. Technol., 27*, 1403–1407.

Stone, E. A., L. Yang, L. E. Yu, and M. Rupakheti (2012), Characterization of organosulfates in atmospheric aerosols at Four Asian locations, *Atmospheric Environment, 47*, 323–329.

Sun, J., and P. Ariya (2006), Atmospheric organic and bio-aerosols as cloud condensation nuclei (CCN): A review, *Atmos. Environ., 40*(5), 795–820.

Surratt, J. D., Y. Gómez-González, A. W. H. Chan, R. Vermeylen, M. Shahgholi, T. E. Kleindienst, E. O. Edney, J. H. Offenberg, M. Lewandowski, M. Jaoui et al. (2008), Organosulfate Formation in Biogenic Secondary Organic Aerosol, *J. Phys. Chem. A, 112*(36), 8345–8378.

Surratt, J. D., J. H. Kroll, T. E. Kleindienst, E. O. Edney, M. Claeys, A. Sorooshian, N. L. Ng, J. H. Offenberg, M. Lewandowski, M. Jaoui et al. (2007), Evidence for Organosulfates in Secondary Organic Aerosol, *Environ. Sci. Technol., 41*(2), 517–527.

Surratt, J. D., S. M. Murphy, J. H. Kroll, N. L. Ng, L. Hildebrandt, A. Sorooshian, R. Szmigielski, R. Vermeylen, W. Maenhaut, M. Claeys et al. (2006), Chemical Composition of Secondary Organic Aerosol Formed from the Photooxidation of Isoprene, *J. Phys. Chem. A, 110*(31), 9665–9690.

Swissfire, forest fire database of Switzerland, M. Conedera, and B. Pezzatti, Swiss Federal Institute for Forest, Snow and Landscape Research WSL, extracted from the Swissfire database, 2014.04.29

Szmigielski, R., J. D. Surratt, Y. Gómez-González, P. van der Veken, I. Kourtchev, R. Vermeylen, F. Blockhuys, M. Jaoui, T. E. Kleindienst, M. Lewandowski et al. (2007), 3-methyl-1,2,3-butanetricarboxylic acid: An atmospheric tracer for terpene secondary organic aerosol, *Geophys. Res. Lett., 34*(24).

Tedetti, M., K. Kawamura, B. Charrière, N. Chevalier, and R. Sempéré (2006), Determination of Low Molecular Weight Dicarboxylic and Ketocarboxylic Acids in Seawater Samples, *Anal. Chem., 78*(17), 6012–6018.

Tetko, I. V., J. Gasteiger, R. Todeschini, A. Mauri, D. Livingstone, P. Ertl, V. A. Palyulin, E. V. Radchenko, N. S. Zefirov, A. S. Makarenko et al. (2005), Virtual Computational Chemistry Laboratory – Design and Description, *J Comput Aided Mol Des, 19*(6), 453–463.

Thermo Fisher Scientific, *Planet Orbitrap*, available at www.planetorbitrap.com, accessed 2014.03.01

Tinner, W., B. Ammann, M. Conedera, H. Gaggeler, B. Sagesser, S. Gedye, and R. Jones (1998), Pollen and charcoal in lake sediments compared with historically documented forest fires in southern Switzerland since AD 1920, *The Holocene, 8*(1), 31–42.

van de Velde, K., C. F. Boutron, C. P. Ferrari, A. Moreau, R. J. Delmas, C. Barbante, T. Bellomi, G. Capodaglio, and P. Cescon (2000), A two hundred years record of atmospheric cadmium, copper and zinc concentrations in high altitude snow and ice from the FrenchItalian Alps, *Geophys. Res. Lett., 27*(2), 249–252.

van Pinxteren, D., C. Neusüß, and H. Herrmann (2014), On the abundance and source contributions of dicarboxylic acids in size-resolved aerosol particles at continental sites in central Europe, *Atmos. Chem. Phys., 14*(8), 3913–3928.

van Pinxteren, M., and H. Herrmann (2013), Glyoxal and methylglyoxal in Atlantic seawater and marine aerosol particles: method development and first application during the Polarstern cruise ANT XXVII/4, *Atmos. Chem. Phys., 13*(23), 11791–11802.

VCCLAB *Virtual Computational Chemistry Laboratory* (2005), available at http://www.vcclab.org. accessed 2013.08.01

Villa, S., C. Negrelli, V. Maggi, A. Finizio, and M. Vighi (2006), Analysis of a firn core for assessing POP seasonal accumulation on an Alpine glacier, *Ecotoxicology and Environmental Safety, 63*(1), 17–24.

Villa, S., M. Vighi, V. Maggi, A. Finizio, and E. Bolzacchini (2003), Historical Trends of Organochlorine Pesticides in an Alpine Glacier, *Journal of Atmospheric Chemistry, 46*, 295–311.

Vogel, A. L., Dissertation 2014, Johannes Gutenberg-Universität Mainz.

Wang, H., K. Kawamura, K. F. Ho, and S. C. Lee (2006a), Low Molecular Weight Dicarboxylic Acids, Ketoacids, and Dicarbonyls in the Fine Particles from a Roadway Tunnel: Possible Secondary Production from the Precursors, *Environ. Sci. Technol., 40*(20), 6255–6260.

Wang, H., K. Kawamura, and D. Shooter (2006b), Wintertime Organic Aerosols in Christchurch and Auckland, New Zealand: Contributions of Residential Wood and Coal Burning and Petroleum Utilization, *Environ. Sci. Technol., 40*(17), 5257–5262.

Wang, H., X. Zhang, and Z. Chen (2009), Development of DNPH/HPLC method for the measurement of carbonyl compounds in the aqueous phase: applications to laboratory simulation and field measurement, *Environ. Chem., 6*, 389–397.

Wang, X. P., B. Q. Xu, S. C. Kang, Z. y. Cong, and T. D. Yao (2008), The historical residue trends of DDT, hexachlorocyclohexanes and polycyclic aromatic hydrocarbons in an ice core from Mt. Everest, central Himalayas, China, *Atmos. Environ., 42*(27), 6699–6709.

Winterhalter, R., M. Kippenberger, J. Williams, E. Fries, K. Sieg, and G. K. Moortgat (2009), Concentrations of higher dicarboxylic acids C-5-C-13 in fresh snow samples collected at the High Alpine Research Station Jungfraujoch during CLACE 5 and 6, *Atmos. Chem. Phys., 9*(6), 2097–2112.

Wozniak, A. S., J. E. Bauer, R. L. Sleighter, R. M. Dickhut, and P. G. Hatcher (2008), Technical Note: Molecular characterization of aerosol-derived water soluble organic carbon using ultrahigh resolution electrospray ionization Fourrier transform ion cyclotron resonance mass spectrometry, *Atmos. Chem. Phys., 8*, 5099–5111.

Xu, F., L. Zou, Y. Liu, Z. Zhang, and C. N. Ong (2011), Enhancement of the capabilities of liquid chromatography-mass spectrometry with derivatization: General principles and applications, *Mass Spectrom. Rev., 30*(6), 1143–1172.

Yoshinari, K. (2000), Theoretical and numerical analysis of the behavior of ions injected into a quadrupole ion trap mass spectrometer, *Rapid Commun. Mass Spectrom., 14*, 215–223.

Yttri, K. E., D. Simpson, J. K. Nøjgaard, K. Kristensen, J. Genberg, K. Stenström, E. Swietlicki, R. Hillamo, M. Aurela, H. Bauer et al. (2011), Source apportionment of the summer time carbonaceous aerosol at Nordic rural background sites, *Atmos. Chem. Phys., 11*(24), 13339–13357.

Yu, J., D. R. Cocker, R. J. Griffin, R. C. Flagan, and J. H. Seinfeld (1999), Gas-Phase Ozone Oxidation of Monoterpenes: Gaseous and Particulate Products, *Journal of Atmospheric Chemistry, 34*, 207–258.

Yu, J., R. C. Flagan, and J. H. Seinfeld (1998), Identification of Products Containing −COOH, −OH, and −CO in Atmospheric Oxidation of Hydrocarbons, *Environ. Sci. Technol., 32*(16), 2357–2370.

Zangrando, R., E. Barbaro, P. Zennaro, S. Rossi, N. M. Kehrwald, J. Gabrieli, C. Barbante, and A. Gambaro (2013), Molecular Markers of Biomass Burning in Arctic Aerosols, *Environ. Sci. Technol.*, 130716103911002.

Zhang, H., D. R. Worton, M. Lewandowski, J. Ortega, C. L. Rubitschun, J.-H. Park, K. Kristensen, P. Campuzano-Jost, D. A. Day, J. L. Jimenez et al. (2012), Organosulfates as Tracers for Secondary Organic Aerosol (SOA) Formation from 2-Methyl-3-Buten-2-ol (MBO) in the Atmosphere, *Environ. Sci. Technol., 46*(17), 9437–9446.

Zhang, Y. Y., L. Müller, R. Winterhalter, G. K. Moortgat, T. Hoffmann, and U. Pöschl (2010), Seasonal cycle and temperature dependence of pinene oxidation products, dicarboxylic acids and nitrophenols in fine and coarse air particulate matter, *Atmos. Chem. Phys., 10*(16), 7859–7873.

Zhao, Y., A. G. Hallar, and L. R. Mazzoleni (2013), Atmospheric organic matter in clouds: exact masses and molecular formula identification using ultrahigh-resolution FT-ICR mass spectrometry, *Atmos. Chem. Phys., 13*(24), 12343–12362.

Zuo, Y., K. Zhang, J. Wu, B. Men, and M. He (2011), Determination of o-phthalic acid in snow and its photochemical degradation by capillary gas chromatography coupled with flame ionization and mass spectrometric detection, *Chemosphere, 83*(7), 1014–1019.

8 POSTER PRESENTATIONS, TALKS, AND JOURNAL ARTICLES

not included in the electronic version

9 ACKNOWLEDGMENT

not included in the electronic version

10 Curriculum vitae

not included in the electronic version